Thermosetting polymer-matrix composites for structural repair applications

by

William Kirby Goertzen

A dissertation submitted to the graduate faculty

in partial fulfillment of the requirements for the degree of

DOCTOR OF PHILOSOPHY

Major: Materials Science and Engineering

Program of Study Committee:
Michael R. Kessler, Major Professor
Mufit Akinc
David Grewell
Zhiqun Lin
Pranav Shrotriya

Iowa State University

Ames, Iowa

2007

Copyright © William Kirby Goertzen, 2007. All rights reserved.

TABLE OF CONTENTS

LIST OF TABLES

LIST OF FIGURES

ACKNOWLEDGEMENTS

I would like to sincerely thank my advisor, Dr. Michael R. Kessler, for his guidance, technical support, and encouragement throughout the research process. I would also like to thank Dr. Mufit Akinc, Dr. David Grewell, Dr. Zhiqun Lin, and Dr. Pranav Shrotriya for serving on my advisory committee and providing additional technical guidance.

This material is based upon work supported under a National Science Foundation Graduate Research Fellowship. This generous support from the federal government is greatly appreciated.

Additional funding has been provided by Iowa State University, a NASA EPSCoR Research Initiation Grant (NCC5-586), and a grant from the Oklahoma Center for the Advancement of Science and Technology (OARS AR03(1)-050).

Additional support from the Strategic Environmental Research and Development Program (SERDP), under the "Environmentally Benign Repair of Composites Using High Temperature Cyanate Ester Nanocomposites" project (Project Number WP-1580, administered through Ames Laboratory, U. S. Department of Energy) is gratefully acknowledged.

The United States Government has assigned the DOE report IS-T 2861 to this dissertation. Notice: This document has been authored under contract by the Iowa State University of Science and Technology under Contract No. DE-AC02007CH11358 with the U.S. Department of Energy. The U.S. Government retains a non-exclusive, paid-up, irrevocable, world-wide license to publish or reproduce the published form of this document, or allow others to do so, for United States Government purposes.

I would like to thank Ben Mac Murray for his help in preparing samples for the current cyanate ester research project, and I would like to thank current and former members of the polymer composites research group—Xia Sheng, Wonje Jeong, Louis Charles, Xing Liu, and Dr.

Jong Lee—for their valuable technical expertise and helpful discussions. I would also like to extend thanks to Phillip Henna, Jun Xu, Jun Wang, and Suck Won Hong for their technical advice and help.

I would like to sincerely thank former researchers on the carbon/epoxy pipe repair project, Jeff Wilson and Josh Duell. I would also like to thank Scott Heaton, an undergraduate research assistant who did much of the work involved in preparing specimens and performing testing for the carbon/epoxy research.

Finally, I would to thank my wonderful wife, Abi, for her unwavering love, support, and encouragement throughout this whole process.

IS-T 2861

ABSTRACT

Several classes of thermosetting polymer matrix composites were evaluated for use in structural repair applications. Initial work involved the characterization and evaluation of woven carbon fiber/epoxy matrix composites for structural pipeline repair. Cyanate ester resins were evaluated as a replacement for epoxy in composites for high-temperature pipe repair applications, and as the basis for adhesives for resin infusion repair of high-temperature composite materials. Carbon fiber/cyanate ester matrix composites and fumed silica/cyanate ester nanocomposites were evaluated for their thermal, mechanical, viscoelastic, and rheological properties as they relate to their structure, chemistry, and processing characteristics. The bisphenol E cyanate ester under investigation possesses a high glass transition temperature, excellent mechanical properties, and unique ambient temperature processability. The incorporation of fumed silica served to enhance the mechanical and rheological properties of the polymer and reduce thermal expansion without sacrificing glass transition or drastically altering curing kinetics. Characterization of the composites included dynamic mechanical analysis, thermomechanical analysis, differential scanning calorimetry, thermogravimetric analysis, rheological and rheokinetic evaluation, and transmission electron microscopy.

CHAPTER 1: GENERAL INTRODUCTION

1.1 Introduction

Thermosetting polymers are often combined with reinforcements, such as fibers, particles, or nanoparticles, to form composite materials, which have enhanced properties in comparison to the neat polymer. This work covers several classes of composite materials based on two thermosetting polymers: epoxy and cyanate ester. These polymers are reinforced with continuous carbon fiber or fumed silica nanoparticles to form composite materials that have applicability for a wide variety of structural repair applications. These applications include, but are not limited to: 1) composite overwrap pipeline repair, 2) high-temperature pipe overwrap repair, 3) resin infusion repair of high-temperature composite materials. In this work, the thermal, mechanical, viscoelastic, and rheological properties of these composite materials are evaluated as they relate to their structure, chemistry, and processing characteristics. General conclusions are made concerning the suitability of the materials for the said applications.

1.2 Dissertation organization

This work is organized into main chapters, which are each manuscripts that have either been published in or prepared for submission to scholarly journals. First, however, Chapter 1: General Introduction outlines the background and motivation for the work done in each paper. Chapter 2 involves dynamic mechanical analysis of carbon/epoxy, which was evaluated as a material for structural pipeline repair. This covers discussion on the glass transition of these materials, as well as their viscoelastic response as it relates to predictions of long-term behavior. Chapter 3 involves the same material from Chapter 2, carbon/epoxy, but rather discusses creep testing, which was done to characterize and predict long-term response. Appendix A discusses the thermal expansion behavior of these composites.

Chapters 4 through 7 involve composites based on cyanate ester resins, which were identified as a candidate for the matrix material in composites for high-temperature repair applications because of their unique properties. Chapter 4 outlines the thermal and mechanical properties of carbon fiber/cyanate ester composites, which are the structural material for high-temperature pipe repair using an overwrap repair method in which the wrap is applied at ambient temperatures. The thermal expansion and processing of the cyanate ester matrix materials used in this evaluation is discussed in Appendix B.

For Chapters 5 through 7, a bisphenol E cyanate ester (BECy) is combined with fumed silica nanoparticles of two sizes to enhance the rheological, thermal, and mechanical properties of the polymer. The proposed applications for this include: 1) primer and filler adhesive for initial bond coat in high-temperature pipe repair, 2) adhesive for resin-infusion repair of high-temperature aerospace composites, and 3) starting material for development of three-phase composites including additional reinforcements, such as short fibers of various types and micron-sized particulates. Specifically, Chapter 5 deals with dynamic mechanical analysis (DMA) to determine mechanical properties and glass transition temperatures; Chapter 6 covers the thermal expansion behavior of the nanocomposites; and Chapter 7 deals with the rheology and curing kinetics of the nanocomposites.

Chapter 8 includes a general discussion of conclusions drawn through this work, as well as recommendations for future research. As mentioned above, Appendix A and Appendix B both deal with additional information on woven carbon fiber composites based on epoxy and cyanate ester. Appendix C gives a summary of transmission electron microscopy (TEM) images for the fumed silica/cyanate ester nanocomposites. Appendix D shows some initial results and explanations of recommendations for future research on three-phase composites that are based on fumed silica/cyanate ester nanocomposites. By altering rheology, the fumed silica can be used to reduce settling and phase separation in filled systems, which makes it possible to create

processable three-phase adhesives with potential for low thermal expansion and enhanced mechanical properties.

1.3 Literature review

A recent study by the U.S. Federal Highway Administration showed that corrosion costs the United States an astounding $276 billion dollars per year [1]. The corrosion problem affects much of the nation's aging infrastructure, mainly carbon steel found in bridges, pipelines and other pipe work, water and wastewater systems, and electric power generation facilities. In addition, deterioration of non-metallic structures through aging and other factors causes a major concern. In the last few years, considerable attention has been focused on innovative techniques to arrest corrosion and restore the structural integrity of these systems, especially pipelines and bridges [2-5]. Many of these repair technologies utilize fiber-reinforced polymeric composite materials and while effective, they are limited to low-temperature applications. While these temperature limitations are of no concern for most infrastructure systems, industries like oil and gas processing and nuclear, fossil fuel, and water electric power generation have metallic components (i.e. pipes, pressure vessels, etc.) operating at high temperatures that need repair.

A major barrier to the use of polymer composites in repair applications above 80 °C is the relatively low glass transition temperature, T_g, of most thermosetting polymer resins used in these applications. Near and above the T_g of the polymer matrix, the composite material's properties degrade significantly. There are some thermosetting polymers that have glass transition temperatures well above 80 °C and are the most obvious candidates for high-temperature structural repair. However, there are two main issues associated with the use of polymer composites with high T_g's for structural repair: 1) thermosetting polymers with high T_g's tend to have highly undesirable processing characteristics for these types of applications, and 2) the large thermal expansion mismatch between the polymer and metallic components causes significant

thermal stresses when temperature fluctuations are large. As an extension of previous work on structural pipeline repair with carbon fiber/epoxy matrix composites, a particular class of high-temperature thermosetting polymers—cyanate esters—has been identified as a candidate for the matrix material in composite materials for these types of repairs. The goal of the proposed research is to develop suitable composite materials, based on cyanate esters, which possess the appropriate processing, thermal, and mechanical properties for the repair of metallic process components at temperatures at or above 150 °C.

1.3.1 Current repair technologies

Corrosion of gas and liquid transmission pipelines accounts for nearly one-third of the total corrosion costs associated with the United States' infrastructure [6]. Traditional repair methods for corroded or damaged pipelines, such as welded sleeve repairs or the replacement of a section of pipe, can be costly and time-consuming. Often, the pipeline must be taken off-line to make the repair, resulting in a large amount of lost revenue, and in some cases, the repair process can pose safety problems. Alternative repair methods utilizing fiber-reinforced polymers (FRPs) have gained recent favor. There are numerous reports of composite repair systems used to repair externally corroded or damaged pipelines [7-10]. Kessler et al. used carbon fiber/epoxy matrix composites to repair externally corroded or damaged piping, while Frassine reported on an aramid fiber/polyamide matrix gas pipeline repair system [8-9]. Patrick reported on a unidirectional glass fiber/polyester matrix composite pipeline repair system, and Alexander and Wilson used a woven glass fabric/epoxy matrix composite repair system [7,10]. Composite repairs using FRPs have become widely accepted because they can be made in a short amount of time and can often be done without disrupting the flow of fluid through the pipe. An industry analysis showed that, on average, composite repair systems are 24% cheaper than welded sleeve repairs and 73%

cheaper than replacing the damaged section of pipe [11]. In addition, since FRPs do not oxidize, further external corrosion of the pipe is arrested, even for through wall defects [12].

Composite pipeline repair technologies have been extended for use in repairing other types of piping, such as those used in the process industry. Repairs of process piping with carbon/epoxy composites have been documented by Smith for use in the chemical and pharmaceutical industries, as well as on offshore oil and gas platforms [13-14]. Some of these repairs have shown savings in the millions of dollars because they prevented a forced shutdown of production by repairing the pipe while it was online [14]. The repair can even be designed to be permanent. Furthermore, in these types of plant settings, making a composite repair can eliminate the cost and problems associated with the use of heavy equipment for traditional repairs. Composite repairs can be very effective for situations involving tight spaces or pipe work that is hundreds of feet above ground [14]. As an added benefit, a composite repair of a pressure vessel can eliminate the need for the revalidation of a sensitive process that would be altered if a new vessel were installed [14].

1.3.2 Need for high temperature repairs

Due to the unique nature of polymers and polymeric composites, their glass transition temperature, T_g, a temperature above which polymer material properties degrade significantly, limits their use for structural repairs. Most of the thermosetting polymers currently used for these repairs (epoxies and polyesters) typically have glass transition temperatures that limit their use to temperatures below 80°C [7,9-10]. However, some exceptions exist: currently, the highest reported temperature limit for a pipe repair system stands at 200°C, which was documented in 2004 [14]. The same author reported an upper temperature limit of 150°C in 2002 [13]. While low-T_g epoxies and polyesters can be used for the majority of infrastructure components needing repair, some industries need repair of components that operate at temperatures above 150°C.

These components would mainly be found in processes that utilize pressurized steam and other process piping, pressure vessels and storage tanks, heat exchangers, burners, furnaces, and industrial exhaust. These high-temperature components may be found in aging facilities for oil and gas processing, chemical processing, and nuclear, fossil fuel, and water electric power generation.

1.3.3 High-temperature thermosetting polymers for structural repair

The use of composite repair technologies on high-temperature components would require the use of composite materials with polymer matrices that would be considered "high-temperature." High-temperature polymers are loosely classified as polymers that maintain their useful properties after thousands of hours in air at 200°C [15]. Currently, no repair systems for metallic structural components using high-temperature polymers have been documented. However, the repair of polymer composites for the aerospace industry using high-temperature polymer matrix composites has been documented [16-17].

There are several factors that limit the ability to successfully repair metallic components with high-temperature polymer matrix composites. The high-temperature polymer matrix material would need to have good mechanical, adhesive, and moisture absorption properties, and the processing of the polymer matrix material must be suitable for hand lay-up or resin transfer molding (RTM), which are the preferred methods for repair using FRPs [9-10,16-17]. The cure characteristics of the polymer are also critical. Often, polymerization is induced with an electric heating element or steam tracing line. However, in some cases, the situation may only allow curing of the polymer through the inherent heat of the repaired substrate. For this reason, it may be necessary that the T_g of the polymer exceed the final cure temperature. Finally, the thermal expansion behavior of the repair materials is critical because mismatches in coefficients of thermal expansion (CTEs) will cause thermal stresses when temperatures fluctuate. Even in

situations where the temperature of the substrate that is being repaired is essentially constant, a scheduled shutdown of the system may damage the repaired section when the temperature drops to ambient levels.

High-temperature thermosetting polymer matrices include cyanate esters (polycyanurates), polyimides, and bismaleimides (BMIs). Of these, polyimides have the highest T_g's [18], and the T_g's of polycyanurates are usually lower than BMI's [15]. The suitability of a high-temperature polymer as the matrix material in a woven fiber composite for a field repair is significantly dependent on the state of the monomer at room temperature. In order for hand lay-up or ambient RTM to be possible, the pre-polymer (monomer) should be a liquid at room temperature with a relatively low viscosity that allows wetting of the fiber reinforcement. The low-temperature epoxies and polyesters currently used for pipeline repairs meet this requirement, but most high-temperature pre-polymers are either solids or highly viscous liquids at room temperature. In general, polymers with higher T_g's in the cured state tend to have higher viscosities at room temperature. Figure 1-1 shows the correlation between the cured state T_g and the temperature at which the uncured thermoset monomer has a viscosity of 0.15 Pa·s (150 cP) [19]. Polyimides are not shown in Figure 1-1 because their lowest melt viscosities are higher than 0.15 Pa·s (150 cP) [20].

From Figure 1-1, the one exception to the trend that a higher T_g corresponds to a higher viscosity is a unique type of cyanate ester monomer called the bis(4-cyanatophenyl)-1,1-ethane monomer (or bisphenol E cyanate ester) [19-21]. A standard bisphenol A cyanate ester has a melting point of 82°C, but the bisphenol E dicyanate has excellent processing capabilities even at low temperatures with an extremely low viscosity of 0.09 to 0.12 Pa·s (90 to 120 cP) at room temperature [19-21].

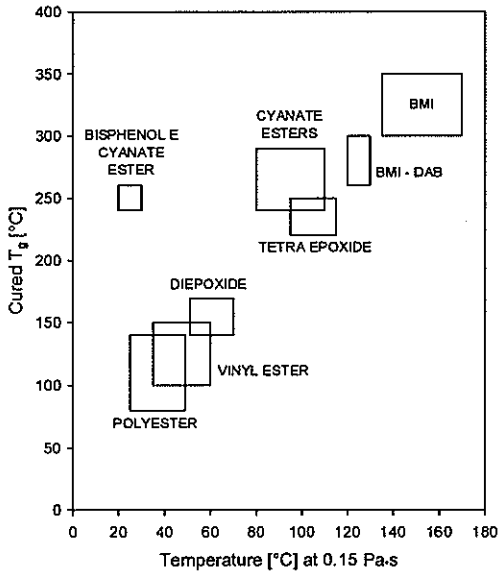

Figure 1-1. Cured T_g vs. 0.15 Pa·s (150 cP) temperature for thermosetting polymers [19].

These processing characteristics make the bisphenol E cyanate ester (BECY) an excellent candidate for the high-temperature polymer matrix for composites in high-temperature structural repairs. The unique properties of the bisphenol E cyanate ester monomer also allow for its use as a diluent for other cyanate esters and thermosetting resins, allowing enhanced low-temperature processability. Blends of the bisphenol E cyanate ester monomer with other cyanate esters have been shown to facilitate filament winding processing by lowering the monomer viscosity without sacrificing thermal stability [22]. The low room-temperature viscosity of the monomer blend enables the resin to be applied to the filament without heating, simplifying the manufacturing process. Other applications for the bisphenol E cyanate ester that may require low-temperature processability include resin transfer molding (RTM) and wet lay-up. Bisphenol E cyanate esters reinforced with woven carbon fiber fabric have been used for wet lay-up patch repair of aerospace composite structures because of their low viscosity, excellent fiber wetting, and thermal stability [17].

1.3.4 Cyanate esters

Cyanate esters are a relatively new class of thermosetting polymers that have become a popular replacement for other thermosets in the aerospace and microelectronics sectors because they possess a good combination of high temperature stability and excellent mechanical properties [23]. In addition, cyanate esters have excellent adhesive properties, are more resistant to moisture absorption than other thermosets (such as bismaleimides (BMIs) and epoxies), and have very low dielectric constants [23]. These desirable properties have justified their use in a variety of applications, despite their relatively high cost. In addition to their desirable properties in the cured state, cyanate ester resins have low oral and dermal toxicity [15] and can be processed using a variety of methods, including resin transfer molding (RTM), filament winding, hand lay-up, and composite prepregs [24]. The largest difference in processing between epoxies and cyanate esters is the latter's need for relatively high curing temperatures. Curing of cyanate esters is catalyzed by heat or a combination of heat and a catalyst, which is most commonly a carboxylate or chelate salt of a transition metal dissolved in an active hydrogen co-catalyst such as nonylphenol [15]. In general, cyanate esters, correctly named as polycyanurates in the polymer form, are characterized by monomers containing reactive ring-forming cyanate (-O-C≡N) functional groups [24,25]. While catalysts are often used, cyanate esters with two or more cyanate functional groups will homopolymerize under heat through cyclotrimerization to from a 3-dimensional network, as shown in Figure 1-2 [15,26].

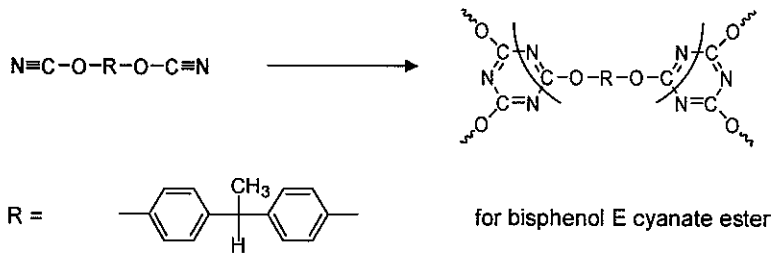

Figure 1-2. Cyclotrimerization of a bifunctional cyanate ester monomer, along with the structure for the bisphenol E cyanate ester monomer [15,26].

In theory, a catalyst of some type is needed to start the reaction, but the presence of trace amounts of impurities (which are a result of synthesis and impossible to remove) will provide this catalyst and allow homopolymerization [27]. However, uncatalyzed systems require extremely high curing temperatures to reach high levels of conversion [15,27]. Because the polymerization of cyanate esters is an addition reaction, no by-products or Volatile Organic Compounds (VOCs) are generated [27,28]. This may not be true, however, if there are impurities present in the prepolymer or catalyst.

1.4 Research objectives

1.4.1 Characterization of the thermal and viscoelastic properties of carbon/epoxy composites for pipeline repair

In this work, characterization of a carbon fiber/epoxy matrix pipe overwrap repair system developed by Kessler et al. [9] involved determination of the use temperature limits, thermal expansion, and long-term behavior of the carbon/epoxy material [29]. Previous work at The University of Tulsa by Duell included evaluation of mechanical properties, adhesion, and Finite Element Analysis (FEA) [30]. Wilson characterized the composites (cure kinetic properties, workability, galvanic corrosion, and, combustion, and fatigue behavior) and developed a model to predict failure of leaking pipes repaired with the carbon/epoxy composite [31]. The research also included full-scale testing of repaired pipes with external defects under static [32] and fatigue [33] loading.

1.4.2 Design and characterization of cyanate ester resin composites for high-temperature pipe repair

The objective of this stage of the research is to design and characterize cyanate ester matrix composites for use in high-temperature structural repair applications. This is an extension

of the process used to repair pipelines with the carbon/epoxy overwrap repair system. The design addresses two fundamental issues associated with high-temperature repair of metallic process components with polymer composites: 1) the lack of processability of high-temperature polymers at low temperatures and 2) thermal expansion mismatch between the steel substrate and the initial polymer adhesive layer.

For pipe overwrap repair applications, there are two main composite materials that must be designed with the appropriate properties to facilitate an effective repair. These include a 1) continuous fiber composite material and a 2) primer and filler adhesive. Two possible geometries for a repair are shown below in Figure 1-3.

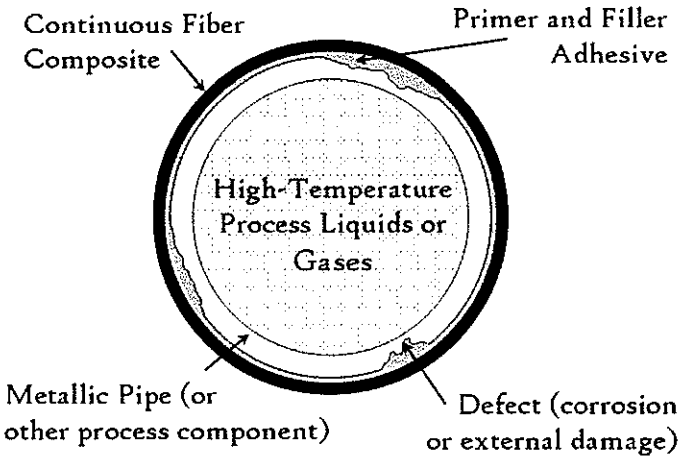

Figure 1-3. High-temperature pipe repair geometry showing the cross-section of a corroded pipe with a composite overwrap repair applied (constituent materials are identified by text and arrows).

The continuous fiber composite material provides the main structural function for the repair. The fibers used are typically high modulus fibers, such as carbon, glass, or aramid. The fiber arrangement in the composite can either be unidirectional or woven. The primer and filler adhesive is a high viscosity, thixotropic material, which provides an initial coating of the substrate for good bonding and a way to fill external defects.

A procedure for the repair of pipelines using carbon/epoxy composites described by Goertzen and Kessler [34] is shown in Figure 1-4.

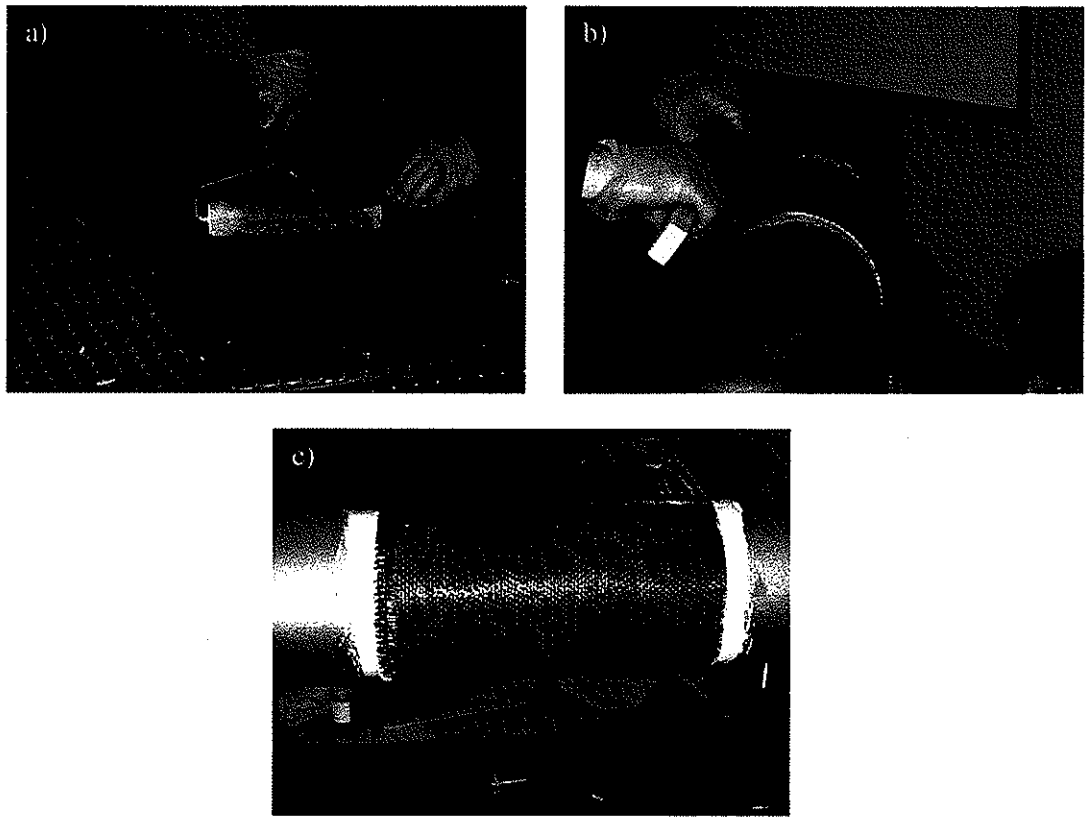

Figure 1-4. Procedure for the repair of piping using a carbon/epoxy composite pipe overwrap repair system.

After applying an epoxy based primer (light color in figure) to prevent galvanic corrosion and increase adhesion, the woven carbon fiber fabric is wetted with the mixed two-part epoxy resin (a), and the wetted fabric is wrapped by hand around the pipe (b). The final product is shown in (c).

The design of the cyanate ester composite to be used as a primer and filler adhesive should lead to a thixotropic paste adhesive that has a reduced CTE, when compared to the neat cyanate ester resin. The CTE of neat cyanate esters is generally around 60-64 ppm/°C, while the CTE of metallic components, such as steel or aluminum, ranges between 10 and 30 ppm/°C (Steel

is about 15 ppm/°C and Aluminum is about 24 ppm/°C). A decrease in the CTE, α, of the repair adhesive to approximately 41 ppm/°C would reduce thermal expansion mismatch ($\alpha_{composite} - \alpha_{steel}$) by a factor of two (on average), and a reduction to 24 ppm/°C would reduce CTE mismatch by factor of 10 (on average). The thixotropic behavior of the paste adhesive will allow the uncured material to be applied to the repair substrate under high shear, but will prevent the material from flowing during cure when under low shear. The primer and filler composite adhesive should also have excellent mechanical properties, allowing for effective load transfer between the repair substrate and the continuous fiber composite material. The design of the paste and filler adhesive will be accomplished through the addition of fumed silica or fumed silica and one or more discontinuous low-CTE fillers to a cyanate ester resin. The BECy monomer will be used because of its desirable processing characteristics mentioned above. The BECy monomer's asymmetric structure gives it a low viscosity liquid state at room temperature and resistance to crystallization during storage, resulting in excellent shelf life. These characteristics will facilitate the storage and application of the primer and filler adhesive and modified matrix material at room temperature. The continuous fiber composite material will employ a woven fiber fabric and a cyanate ester resin matrix, which will be based upon preliminary work on woven carbon fiber/cyanate ester resin composites by Goertzen and Kessler [35].

1.4.3 Development and characterization of processable adhesives for resin infusion repair of high-temperature aerospace composite materials

Standard methods used to repair damage in aerospace structural composites, such as scarf repair and resin infusion repair, generate a large amount of hazardous waste and VOCs because of the heavy use of solvents. Solvents are needed to prepare areas where material has been removed for scarf repair, and the low viscosity needed for resin infusion repair requires the use of solvents with resins like epoxies, which have high viscosities. The use of the BECy monomer is under

investigation in our research group as a replacement for other methods of repair because of its low viscosity at room temperature, excellent storage characteristics, and high glass transition temperature. Additionally, it may be necessary to incorporate nanoparticles into the resin in order to further enhance properties. It is desired that the prepolymer suspension would have a shear thinning and thixotropic nature in order for the resin to be infused into the damaged area under high shear (see Figure 1-5 for example of repair geometry) but remain in the damaged area when under low shear.

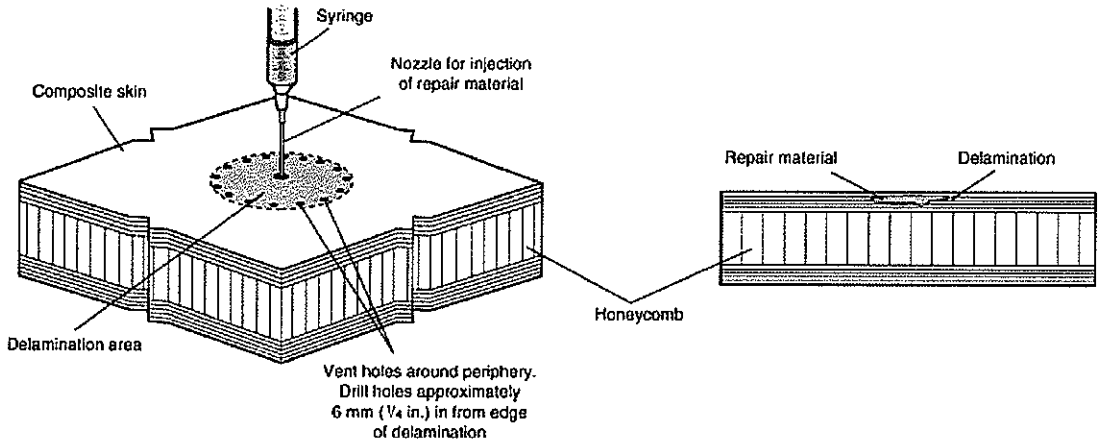

Figure 1-5. Resin infusion repair technique for laminated aerospace composite with delamination.

Additionally, it is desired that the nanocomposite would have enhanced modulus, strength, fracture toughness, and impact resistance. It may also be beneficial for the nanocomposite to have decreased thermal expansion so that mismatch between the fiber-reinforced composite and repair material is minimized. Thermal properties should be maintained or improved, and the curing temperature needed to achieve the desired properties should be as low as possible. Finally, the addition of the nanoparticles should not increase the evolution of VOCs during cure. Cyanate esters do not generate VOCs during cure where no impurities are present in the catalyzed prepolymer [27,28], but the addition of nanoparticles may have an effect if there are any side reactions.

1.5 References

[1] Jacobson, G. A. "Corrosion – A Natural But Controllable Process," *The AMPTIAC Quarterly*, v 7, n4, 2003.

[2] Mableson, R., Patrick, C., Dodds, N., and Gibson, G., Refurbishment of Steel Tubulars Using Composite Materials, *Plastics, Rubbers, and Composites*, v 29, n 10, 2000.

[3] Greenwood, C. (ed.), Composite Pipe Repair Method Shows Versatility, Long-Lasting, *Pipeline and Gas Journal*, February 2001.

[4] Meier, U., Composite Materials in Bridge Repair, *Applied Composite Materials*, v 7, n 2, 2000, p 75-94.

[5] Radford, D.W., et al., Composite Repair of Timber Structures, *Construction and Building Materials*, v 16, n7, 2002, p 417-425.

[6] Jacobson, G. A., Cost of Corrosion Study Unveiled, *Materials Performance*, July 2002.

[7] Patrick, A. J., High pressure composite repair applications, *Pipeline World*, v 6, 2004, p 37-38.

[8] Frassine, R., Long-term performance of a polymer composite repair system for gas pipelines, *Advances in Polymer Technology*, v 16, n 1, 1997, p 33-43.

[9] Kessler, M. R., et al., Evaluation of carbon/epoxy composites for structural pipeline repair, *Proceedings of the Biennial International Pipeline Conference*, IPC,v 2, 2004, p 1427-1432.

[10] Alexander, C. R. and Wilson, F. D., Development and testing of the Armor Plate pipeline repair system, *Proceedings of the 1999 ASME Energy Sources Technology*, 1999.

[11] Koch, G. H., Brongers, M. P., Tompson, N. G., Virmani, Y. P., and Payer, J. H., "Corrosion Cost and Preventative Strategies in the United States," *Federal Highway Administration, Office of Infrastructure Research and Development*, 2001, p 260-311.

[12] Cuthill, J., "Advances in Materials, Methods, Help Gain New Users," *Pipeline and Gas Journal*, v 229, n 11, 2002, p 64-66.

[13] Smith, P. and Cuthill, J., Patching up pipework with carbon-fibre composites, *Materials World*, v 10, n 5, 2002, p 28.

[14] Smith, P., Composite Solution, *Process Engineering (London)*, v 85, n 5, 2004, p 15-17.

[15] Hamerton, I., *Chemistry and Technology of Cyanate Ester Resins*, London: Chapman and Hall, 1994.

[16] Mehrkam, P. A., and Cochran, R., Evaluation of Materials for Composite Repair Applications, *Journal of Thermoplastic Composite Materials*, v 10, n 1, 1997, p 51-60.

[17] Mehrkam, P. A. and Cochran, R., Liquid Dicyanate Ester Monomer Resin for Elevated Temperature Composite Repair Applications, *Proceedings of the American Society for Composites*, 1992, p 12-21.

[18] *ASM Handbook*, ASM International, v 21 (Composites), on-line edition.

[19] Shimp, D. A., and Craig, Jr., W. M., New Liquid Dicyanate Monomer for Rapid Impregnation of Reinforcing Fibers, *Proceedings of the 34th Annual International SAMPE Symposium*, May 1989, p 1336-1346.

[20] Meador, M. A., Recent Advances in the Development of High-Temperature Polymers, *Annual Review of Materials Science*, v 28, 1998, p 599-630.

[21] Snow, A. W., The Synthesis, Manufacture, and Characterization of Cyanate Ester Monomers, in *Chemistry and Technology of Cyanate Ester Resins* (Hamerton, I.), Blackie Academic and Professional, 1994.

[22] Esslinger, Jr., J. R. and Fruchtnicht O. C., Cyanate Ester Matrix Technology for Improved Thermal Performance of Filament Wound Missile Structures. *SAMPE Journal*, v 40, n 6, 2004, p 9-15.

[23] Hillermeirer, R. and Seferis, J., Environmental Effects on Thermoplastic and Elastomer Toughened Cyanate Ester Composite Systems. *Journal of Applied Polymer Science*, v 77, n 3, 1997, p 556-567.

[24] Hamerton, I. and Hay, J., Recent Technological Developments in Cyanate Ester Resins. *High Performance Polymers*, v 10, n 2, 1998, p 163-174.

[25] Shimp, D. A., Christenson, J.R., and Ising, S.J., Cyanate Esters – An Emerging Family of Versatile Composite Resins. In: *Proceedings of the 34th Annual International SAMPE Symposium*, May 1989. p.222-233.

[26] Georgjon, O. and Galy, J., Effects of Crosslink Density on Mechanical Properties of High Glass Transition Temperature Polycyanurate Networks. *Journal of Applied Polymer Science*, v 65, n 12, 1997, p 2471-2479.

[27] Simon, S. L. and Gillham, J. K., Cure kinetics of a thermosetting liquid dicyanate ester monomer/high-T_g polycyanurate material, *Journal of Applied Polymer Science*, v 47, n 3, Jan 15, 1993, p 461-485.

[28] Ramirez, M. L., Walters, R., Lyon, R. E., Savitski, E. P., Thermal decomposition of cyanate ester resins, *Polymer Degradation and Stability*, v 78, 2002, p 73-82.

[29] Goertzen, W. K., M.S. Thesis, *The Effects of Time and Temperature on Carbon/Epoxy Composite Pipe Overwrap Repair Systems*, The University of Tulsa Graduate School, 2005.

[30] Duell, J. M., M.S. Thesis, *Characterization and FEA of a Carbon Composite Overwrap Repair System*, The University of Tulsa Graduate School, 2004.

[31] Wilson, J. M., Ph.D. Dissertation, *Characterization of a Carbon Fiber Reinforced Polymer Repair System for Structurally Deficient Steel Piping*, The University of Tulsa Graduate School, 2006.

[32] Wilson J. M., Kessler M. R., Duell J. M., Rupture testing of A-106, Grade B steel pipes repaired with carbon/epoxy composites. In: *Proceedings of the 2004 ASME Pressure Vessels and Piping Conference*, July 25-29, 2004. San Diego, CA, published in PVP Vol. 483, *Transportation, Storage, and Disposal of Radioactive Materials*.

[33] Wilson J., Kessler M., Walker R., Duell J., Kadakia D., Sousa N., Fatigue testing of steel pipes repaired with carbon/epoxy composites. In: *Proceedings of the 2005 Rio Pipeline Conference and Exposition*, Rio de Janeiro, Brazil, Oct. 2005. Paper IBP1089_05.

[34] Goertzen, W. K. and Kessler, M. R., Dynamic mechanical analysis of carbon/epoxy composites for structural pipeline repair, *Composites Part B: Engineering*, v 38, n 1, 2007, p 1-9.

[35] Goertzen, W. K. and Kessler, M. R., Thermal and mechanical evaluation of cyanate ester composites with low-temperature processability, *Composites Part A: Applied Science and Manufacturing*, v 38, n 3, 2007, p 779-784.

CHAPTER 2: DYNAMIC MECHANICAL ANALYSIS OF CARBON/EPOXY COMPOSITES FOR STRUCTURAL PIPELINE REPAIR

A paper published in *Composites Part B: Engineering*[1]

William K. Goertzen[2,3] and M.R. Kessler[2,4]

2.1 Abstract

The viscoelastic behavior of a carbon fiber/epoxy matrix composite material system used for pipeline repair has been evaluated through dynamic mechanical analysis. The effects of the heating rate, frequency, and measurement method on the glass transition temperature (T_g) were studied. The increase in T_g with frequency was related to the activation energy of the glass transition relaxation. The activation energy can be used for prediction of long term performance. The measured tan delta peak T_g's of room temperature cured and post cured composite specimens ranged from 60 to 129°C. Analysis of T_g data at various cure states was used to determine use temperature limits for the composite repair system.

Keywords: A. Polymer-matrix composites (PMCs); A. Carbon fibers; B. Thermal properties; Dynamic mechanical analysis

---

[1] Reprinted with permission of *Composites Part B: Engineering*, v 38, n 1, January 2007, p 1-9.

[2] Graduate student and Assistant Professor, respectively, Department of Materials Science and Engineering, Iowa State University

[3] Primary researcher and author

[4] Author for correspondence

2.2 Introduction

Fiber-reinforced polymeric composites (also called fiber-reinforced plastics (FRPs)) have gained acceptance for use in many industries including aerospace, automotive, infrastructure, and recently oil and gas. FRPs possess superior strength to weight ratios over traditional materials and their processing is well-suited to many applications. A recent application of fiber-reinforced polymeric composites for the oil and gas industry involves the repair of pipelines. Due to the age of the majority of piping systems in the United States, billions of dollars are lost each year due to the repair of corroded or damaged piping [1]. Much of this lost revenue is associated with traditional repair methods which require that the damaged section of pipe be removed and replaced with a new section of pipe. This requires taking the system offline, which results in a large amount of lost revenue. In the last five years, there have been numerous reports on the use of fiber reinforced polymer matrix composite wraps for the repair of pipe work; see for example Refs. [2-6]. These composite overwrap repairs save time and money because they can be done while the pipe is online and are typically less labor-intensive than traditional repairs.

In recent research, Kessler et al. [7-9] have developed and characterized woven carbon fiber reinforced epoxy matrix composite overwrap repair systems and investigated the expansion of their use for applications involving high pressures, greater than 1.0 MPa (150 psig), and temperatures above the current ASME B31.3 process piping code limit of 60°C (140°F) [10]. This work has included extensive laboratory testing to characterize the mechanical and thermal properties of the material, as well as full scale pressure testing of piping repaired with the system. The procedure used to repair a pipe using the carbon/epoxy system is shown in Figure 2-1. After applying an epoxy-based primer to prevent galvanic corrosion and increase adhesion, the woven carbon fiber fabric is wetted with the mixed two-part epoxy resin (a), and the wetted fabric is wrapped by hand around the pipe (b). The final product is shown in Figure 2-1 (c).

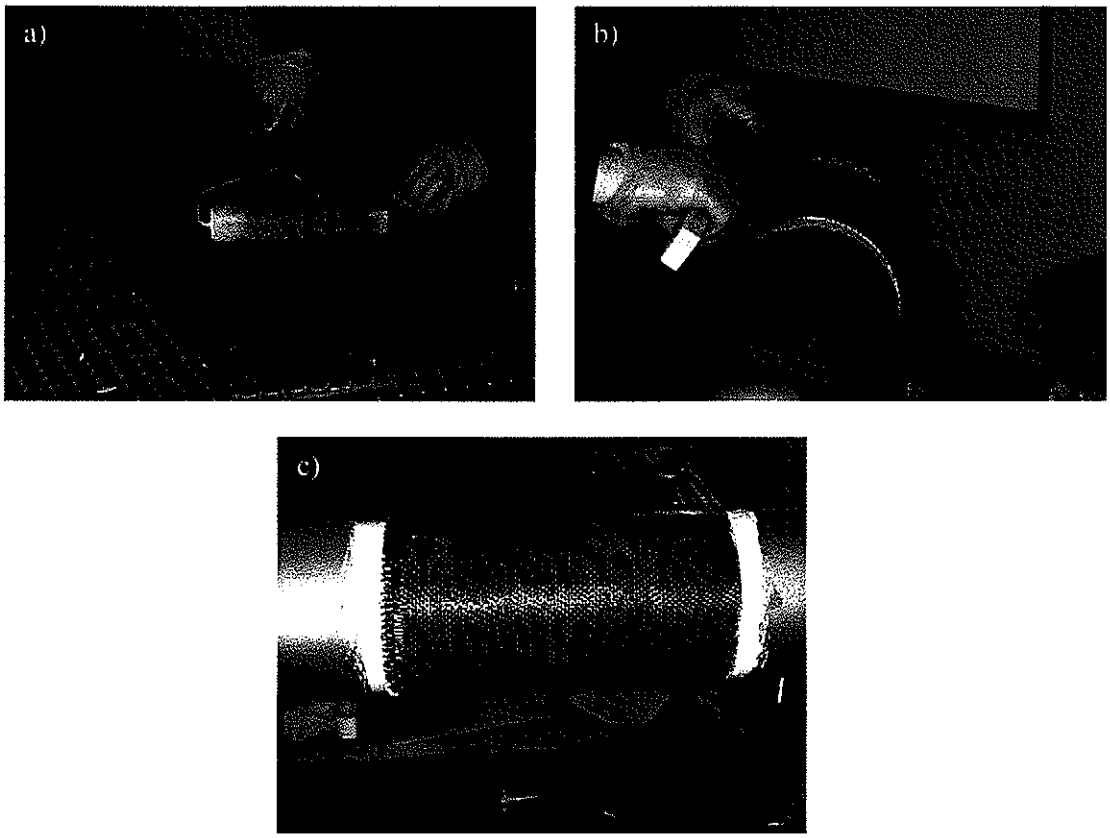

Figure 2-1. Procedure for the repair of piping using a carbon/epoxy composite pipe overwrap repair system.

Because of the nature of pipe repair applications, both the short-term and long-term durability of the repair materials is of importance. It is critical to know whether a composite material used in a structural application will continue to perform satisfactorily over the lifetime of the part or structure. This includes the material's ability to both sustain a load and resist further deformation. Additionally, if the material is subjected to harsh environmental conditions, such as elevated temperatures, chemicals, or moisture, the characterization of the material's performance is even more critical because of the viscoelastic nature of polymeric composites. The polymeric matrices of fiber reinforced composites exhibit a glass transition, T_g, a temperature above which the properties of the material degrade significantly. It is necessary that the application

temperature for a polymeric composite is below the glass transition in order to assure that the mechanical stiffness and creep resistance of the material is satisfactory.

Both thermosets and amorphous thermoplastics exhibit changes in material properties such as volume, enthalpy, heat capacity, thermal expansion, and elastic modulus as the material is heated through the T_g and goes from the glassy to the rubbery state [11]. The glass transition temperature, or typically a temperature well below the T_g, is often used as an upper limit for the use of polymeric composites in structural applications [11]. In setting levels for use temperatures the "moist" or "saturated" T_g is often used to yield a more conservative limit. The T_g of a material is usually measured by such thermal analysis techniques as differential scanning calorimetry (DSC), dynamic mechanical analysis (DMA), which is sometimes referred to as dynamic mechanical thermal analysis (DMTA), or thermo mechanical analysis (TMA). Of these methods, DMA is typically the most sensitive way to measure subtle transitions in polymers [12]. The T_g's of highly cross-linked thermosetting resins are often only measurable by DMA because methods like DSC and TMA may not be sensitive enough [11]. Additionally, the measurement of the T_g of a composite with a thermoset matrix and a high fiber volume fraction is often only possible through DMA.

This article examines, by DMA, the thermal and mechanical properties of the carbon fiber/epoxy matrix material used in the pipe repair technology under investigation. During the glass transition, a change in matrix stiffness of several orders of magnitude can occur. For composite pipe repairs, the T_g of the material may limit the maximum service temperature of the repair because the ability of the matrix to adequately transfer load to the fibers is compromised above the T_g, making the repair less effective. Not only is the repair rendered less effective due to a decrease in the composite's initial modulus, but near and above the T_g, the level of creep for polymer matrix composites is greatly increased. As a result, the long-term viability of a composite repair also becomes an issue. There is a great need for pipe repairs at temperatures

above room temperature due to the nature of much of the piping used in process industries around the world. Process plants like refineries, power plants, and various manufacturers have miles of pipe work that channels fluids at many temperature ranges, and in many cases the age of this piping may be near or beyond the original design life. As a result, current systems need to be evaluated to determine their temperature limits, and future systems with greater temperature limits need to be developed.

DMA is simply a dynamic method of characterizing the viscoelasticity of a material. This is done by applying a sinusoidal force (or displacement) and measuring the response to that input. If the material is not purely elastic, the response will be out of phase with the input. From the out of phase response, measures of viscoelasticity can be made. The cyclic nature of the test is essentially equivalent to a creep test for a time inversely proportional to the frequency induced [13].

The stress applied as a function of time at a given frequency, ω, is given as

$$\sigma(t) = \sigma_0 \sin(\omega t + \delta) \tag{1}$$

where σ_0 is the maximum stress applied and δ is the phase angle [14]. The strain, which lags by the phase angle, δ, is given by

$$\varepsilon(t) = \varepsilon_0 \sin(\omega t) \tag{2}$$

where ε_0 is the maximum strain amplitude [15]. Through Hooke's Law, the input and the response are related by the dynamic modulus, $E^*(\omega)$,

$$\sigma(t) = E^*(\omega)\varepsilon(t). \tag{3}$$

The dynamic (or complex) modulus has in phase and out of phase components, and is given by

$$E^*(\omega) = E'(\omega) + iE''(\omega) \tag{4}$$

where the in phase, or real, portion is $E' = (\sigma_0/\varepsilon_0)\cos\delta$, and the out of phase, or imaginary, portion is $E'' = (\sigma_0/\varepsilon_0)\sin\delta$. The storage modulus, E', is proportional to the energy stored per cycle [16].

The loss modulus, E'', is proportional to the lost or dissipated energy per cycle. The storage modulus characterizes the elastic behavior of the material, and the loss modulus characterizes the viscous behavior of the material [14]. Viscoelastic materials exhibit a combination of both elastic and viscous behavior. The ratio of energy dissipated to energy stored is the tangent of the phase angle, δ, called tan delta, which is given by

$$\tan\delta = \frac{E''(\omega)}{E'(\omega)}. \tag{5}$$

To determine T_g using DMA, measurements of the complex modulus are typically made as temperature is increased at a constant heating rate. Time scans and frequency scans at constant temperatures may also be employed for other purposes. The specimen can be tested in many different configurations, including dual cantilever, single cantilever, three-point bending, torsion, shear, tension, and compression. The choice of the fixture depends on the material used and the desired result. Thin films are often measured in tension because of the low stiffness of the material. A common configuration for composites is the three-point bending configuration, because it eliminates the combined loading induced by a single or double cantilever mode and it produces measurable strains in relatively stiff materials [16].

In order to analyze the DMA data, the storage modulus and loss modulus or tan delta are plotted against temperature. A typical set of curves are shown in Figure 2-2. From a DMA curve, the T_g is found from either the onset of the drop in storage modulus (T_{gA}), the peak of the loss modulus curve (T_{gB}), or the peak of the tan delta curve (T_{gC}). The T_g is different for each method, especially for highly cross-linked thermosets, which have a broad transition range [16]. Due to differences in methodology, the glass transition temperature reported for a material using DMA may vary by up to 25°C [15]. ASTM D 4065 suggests that T_g should be taken as the peak of the loss modulus [17]. The most conservative method is to take the T_g as the first inflection point, or the onset of the drop in modulus, while the least conservative method is the tan delta

peak [16]. Furthermore, the T_g taken from a DMA curve is most often slightly larger than a T_g measured using DSC. Because of these discrepancies, the maximum use temperature for a polymeric material used in a structural application is often set a certain number of degrees below the T_g.

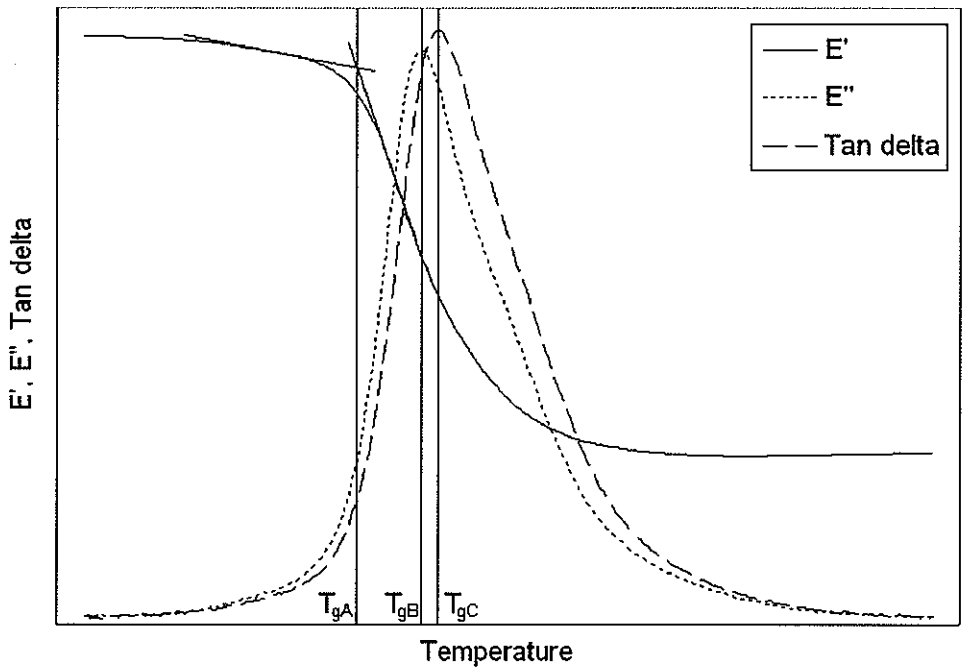

Figure 2-2. Typical DMA Plot.

Additionally, test parameters, such as heating rate and frequency, will change the T_g measurement [11,14-18]. If a large heating rate is used, the entire specimen may not reach thermal equilibrium, and data will be altered. Also, thermosets that continue to polymerize with added heat may undergo changes during a test with a very small heating rate. While the effect of heating rate on T_g has been studied, it is very complex and often specific to the instrument or material [12].

The effect of frequency on the dynamic mechanical response of polymers is well documented [11,14-18]. An increase in test frequency will shift the peak of the tan delta curve to

a higher temperature [11,14-18]. This phenomenon is based on the fundamental relationships between temperature and the frequency of molecular conformational changes in polymers [11,18]. The effect of temperature on the frequency of conformational changes, such as the glass transition relaxation, is explained by a form of the Arrhenius equation. The effect that the temperature, T, has on the frequency, ω, is given by [11,18]

$$\omega = \omega_0 \exp\left(-\frac{\Delta H}{RT}\right) \tag{6}$$

where ω_0 is a pre-exponential factor, R is the universal gas constant and ΔH is the activation energy [11,18] .

The activation energy of the glass transition relaxation represents the energy barrier that must be overcome for the occurrence of molecular motions causing the transition [19] and can be estimated using DMA testing of a polymer at different test frequencies [14-20]. While Equation 6 shows the temperature dependence of frequency, the same equation can be used to quantify the DMA test frequency dependence of the T_g measured by the tan delta or loss modulus peak [11,18]. From Equation 6, the ratio of one test frequency, ω_1, to another, ω_2, is related to the corresponding change in absolute T_g from T_{g1} to T_{g2} by [16,18]

$$\frac{\omega_1}{\omega_2} = \frac{\exp\left(-\frac{\Delta H}{RT_{g1}}\right)}{\exp\left(-\frac{\Delta H}{RT_{g2}}\right)} \tag{7}$$

where ΔH is the activation energy of the glass transition relaxation. Equation 7 can be expressed in terms of the temperature shift factor, a_T, by [16]

$$\log a_T = \log\left(\frac{\omega_1}{\omega_2}\right) = \frac{\Delta H}{R}\left(\frac{1}{T_{g2}} - \frac{1}{T_{g1}}\right)\log e \,. \tag{8}$$

Therefore, the activation energy of the glass transition, ΔH, can be calculated from the slope of a plot of $\ln(\omega)$ vs. $1/T_g$ or $\ln(f)$ vs. $1/T_g$ ($f = \omega/(2\pi)$) using [16]

$$\Delta H = R\frac{(\ln(\omega_1) - \ln(\omega_2))}{\left(\frac{1}{T_{g2}} - \frac{1}{T_{g1}}\right)} = -R\frac{d(\ln(\omega))}{d\left(\frac{1}{T_g}\right)} = -R\frac{d(\ln(f))}{d\left(\frac{1}{T_g}\right)} . \quad (9)$$

2.3 Experimental

2.3.1 Materials

The composite specimens for DMA testing were constructed using bi-directional woven carbon fiber reinforcement (supplied by Citadel Technologies™, Tulsa, OK) This reinforcement was plain weave fabric consisting of 12K tow in the warp direction and 3K tow in the fill direction. The 12K indicates that there are approximately 12,000 carbon filaments (fibers) in each bundle (tow), while 3K indicates approximately 3,000 filaments per tow. The fabric is fairly coarse, with 4 tows/inch in the warp direction and 8 tows/inch in the fill direction.

The matrix material was a two part epoxy system developed by Citadel Technologies™ (Tulsa, OK) called the Standard Wet-Out system. The particular epoxy used is a diglycidyl ether of bisphenol-A (DGEBA) type epoxy cured with an aliphatic amine hardener. The exact chemical structure and nature of the DGEBA epoxy and aliphatic amine hardener used in the Standard Wet-Out system is proprietary. When stoichiometricly mixed, the epoxy and curing agent produce a hard, highly cross-linked thermoset with high solvent resistance and relatively high impact strength.

2.3.2 Specimen manufacturing

The epoxy matrix was formulated by mixing the two part Standard Wet-Out system using a resin-to-hardener ratio of 2.65:1. The plain weave carbon fabric was manually impregnated

with the epoxy prepolymer. Composite panels 300 mm x 250 mm were fabricated by hand layup with 2 plies. The layup was done in a Teflon release spray coated pan and a Plexiglas caul plate (sprayed with a Teflon release spray) was placed on the top of panel with less than 3.45 kPa (0.5 psi) of pressure. The Plexiglas was laid down in such a way as to remove the air bubbles from the epoxy and create a uniform surface on the top of the specimen sheet. The panels were cured at room temperature for at least 24 hours. The thickness per ply of the composite panels is similar to the thickness per ply of the composite overwrap system used to repair damaged pipelines and pipework. The fiber volume fraction of the composite was measured to be between 35% and 40%, using both the TGA burnoff and matrix digestion methods in accordance with ASTM D 3171 [21]. Once the panels were cured, they were machined into specimens with widths of 8-11 mm and lengths of approximately 45 mm. The thickness of each specimen varied, but was usually between 0.9 and 1.3 mm.

2.3.3 Experimental procedure

The Dynamic Mechanical Analyzer used for the characterization of the composite was a Tritec 2000 DMA manufactured by Triton Technology, Ltd (Keyworth, Notts, UK). Because of the high resolution of the drive and the measurement system, a dynamic stiffness range of more than 5 orders of magnitude can be measured. For the first set of tests, specimens from a two-layer panel were tested with constant test parameters of 2°C/min heating rate, 0.05 mm maximum displacement, and frequency of 1 Hz. Some of the specimens were subjected to varying levels of post cure beyond the initial room temperature cure, for 24 hours at temperatures between 35 and 170 °C. The glass transition temperature was determined from the peak of the tan delta curve.

For the second set of tests, specimens from the same panel were tested using a constant 0.05 mm maximum displacement, a heating rate of 0.5, 1, 2, or 3°C/min, and a multi-frequency input of 0.316, 1, 3.16, 10, and 31.6 Hz. The multi-frequency tests were done on room

temperature cured specimens only. The results from these tests were analyzed to find the activation energy of the glass transition relaxation and to characterize the effects of heating rate and test frequency on the T_g measurement. All testing was conducted using a three-point bending fixture with a free length of 20 mm. Figure 2-3 shows a specimen in the three-point bending DMA fixture.

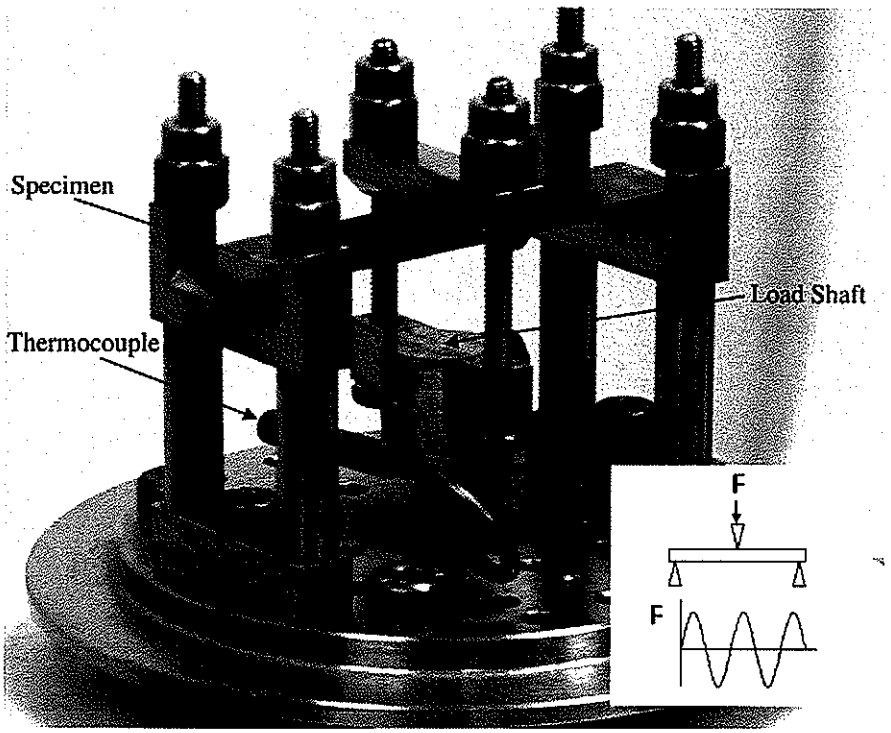

Figure 2-3. Specimen mounted in the DMA three-point bending fixture.

2.4 Results and discussion

2.4.1 T_g vs. post cure relationship

Figure 2-4 shows the dynamic properties vs. temperature for a specimen from the first set of tests that was not post cured. Figure 2-5 shows the dynamic properties vs. temperature for a specimen from the first set of tests that was post cured at 95 °C for 24 hours.

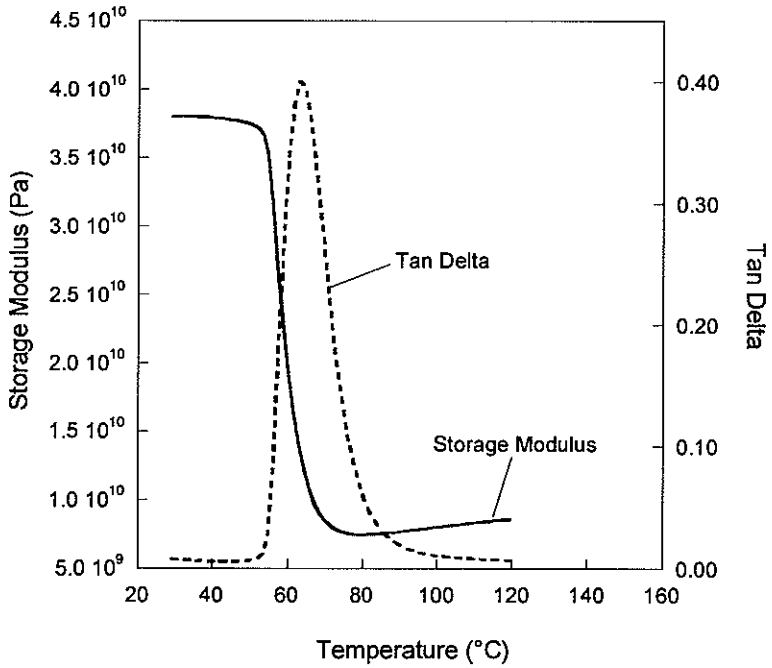

Figure 2-4. DMA data for room temperature cured specimen.

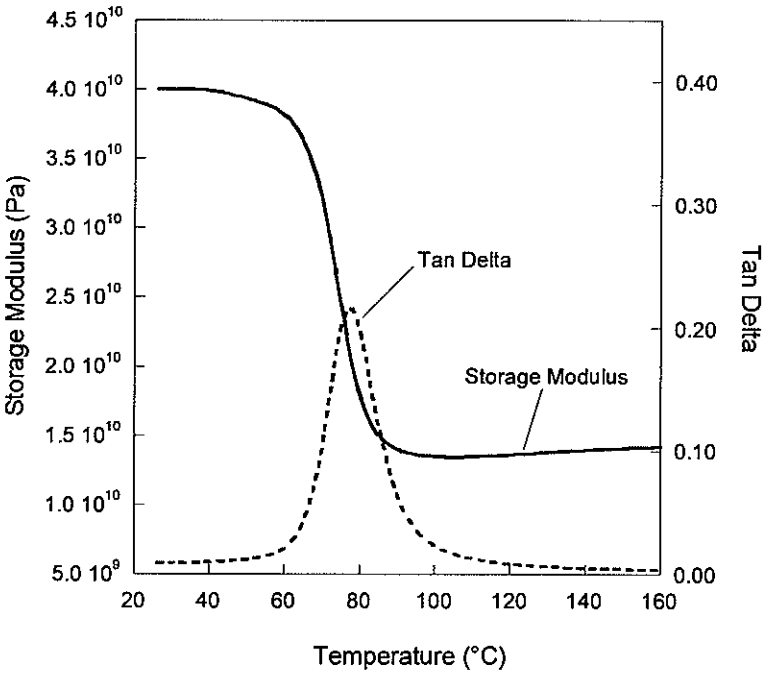

Figure 2-5. DMA data for a specimen with a post cure at 95°C for 24 hours.

When compared to the room temperature cured specimen, the magnitude of the tan delta peak for the post cured specimen is lower and the T_g (tan delta peak) is larger (an increase of 18 °C). This behavior is shown over a wider range of post cure temperatures in Figure 2-6.

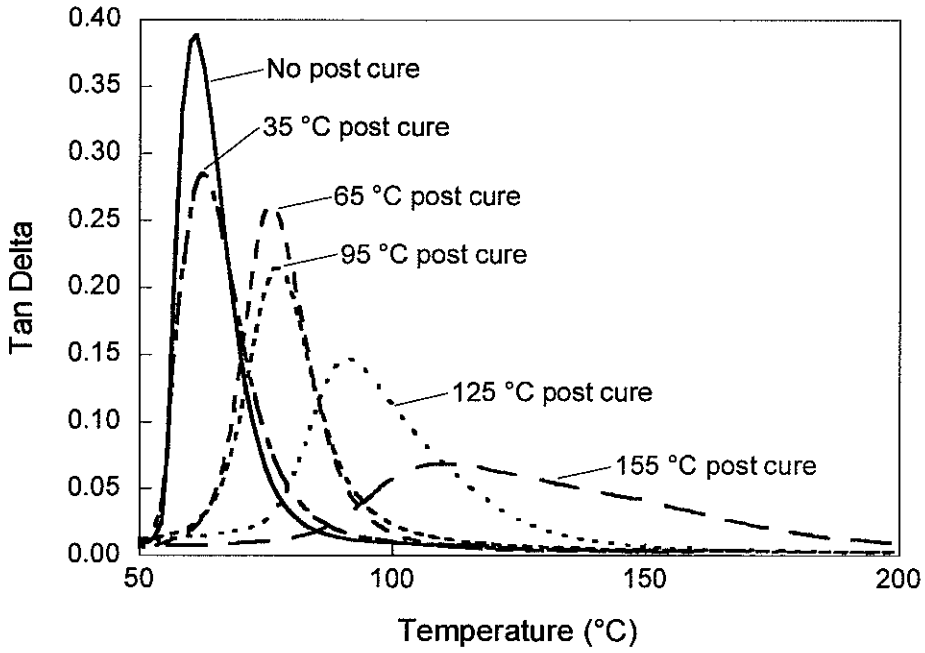

Figure 2-6. Tan delta curves for various 24 hour post cure temperatures.

As post cure temperature increases, the tan delta curve peaks are shifted to the right, increasing T_g. The increase in T_g, however, is not linear with post cure temperature. Furthermore, as post cure temperature increases, the magnitudes of the tan delta curve peaks decrease and the transitions are broader. This broadening suggests thermal degradation of the material, which may account for the high apparent T_g. It is evident that the soaking of the material above its T_g allows for additional cross-linking due to thermally activated diffusional mechanisms. The result is an increase in stiffness and a decrease in viscous losses due to decreased chain mobility caused by additional cross-linking in the post cured samples.

Figure 2-7 shows the relationship between the tan delta T_g and the 24 hour post cure temperature, $T_{PC,24}$. There is a general increasing trend in the relationship between T_g and post

cure temperature. As previously shown in Figure 2-7, this trend is not linear. The T_g vs. post cure temperature curve tends to plateau in the 60 to 100 °C range and rise more rapidly above 100 °C. The increase in T_g for post cure temperatures above 100 °C is believed to be due to thermal degradation effects which is known to increase the apparent glass transition at the expense of toughness and elongation at break. It should be noted that the T_g of the post cured specimens exceeds the post cure temperature for lower temperatures and is lower than the post cure temperature for higher temperatures. It is in this range that T_g transitions from being higher than the post cure temperature to being lower than the post cure temperature. The line $T_g = T_{PC,24}$ is shown on the figure, showing the crossover point, which is about 77 °C.

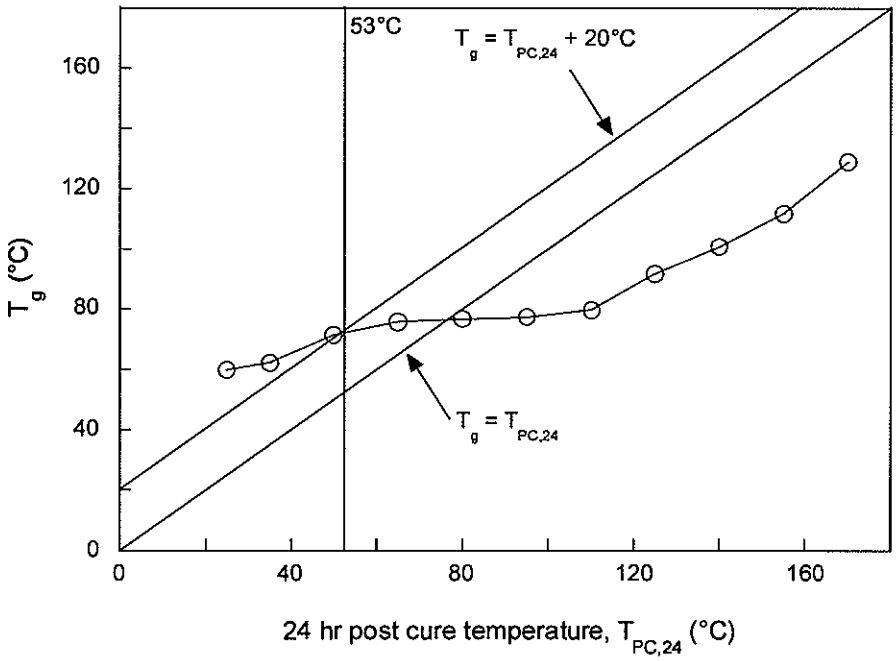

Figure 2-7. T_g vs. post cure temperature.

The newly approved ASME Post Construction Repair Standard, which governs the use of composite overwrap repairs on pipelines, requires that the T_g of the pipe repair material be at least 20 °C (36 °F) above the temperature of the repair [22]. If it is assumed that the 24 hour post cure represents the cure state of the composite applied to a pipe operating at that particular temperature

(or cycling up to that temperature), the point at which the T_g is 20 °C above the post cure temperature would give the maximum application temperature for the carbon/epoxy repair system. The point of intersection between the line, $T_g = T_{PC,24} + 20$ °C, and the curve in Figure 2-7 shows the maximum application temperature calculated by this method. In this case the maximum application temperature is 53 °C (127 °F), which would yield a T_g of approximately 73 °C (163 °F). While in some cases the material may be cured at the post cure temperature initially, and for more than 24 hours, these factors would only increase the T_g, which would make the maximum application temperature of 53 °C (127 °F) slightly conservative. For a situation where it is possible to post cure the pipe at a temperature above the normal operating temperature, the maximum service temperature of 53 °C could be exceeded. For instance, if a post-cure at 125 °C (257 °F) for 24 hours was introduced, the T_g would rise to 92 °C (198 °F), giving a maximum operating temperature of 72 °C (162 °F); however, thermal degradation effects should be considered.

2.4.2 Heating rate and frequency dependence of T_g

The second set of testing at multiple heating rates and frequencies was conducted on the same panel of two-layer specimens that was used for the second set of simple T_g measurements. Figure 2-8 shows the storage modulus, tan delta, and loss modulus curves for a room temperature cured specimen for each of the five different frequencies at a heating rate of 2 °C/min. As expected, an increase in test frequency results in an increase in T_g.

The increasing slope of the modulus in the rubbery region seen in Figure 2-8 (a) was seen in all tests of room temperature cured specimens, and is attributed to further polymerization of the resin at elevated temperatures. It should also be noted that all of the peaks of the loss modulus curves in Figure 2-8 are at lower temperatures than the peaks of the tan delta curves in Figure 2-8 (b).

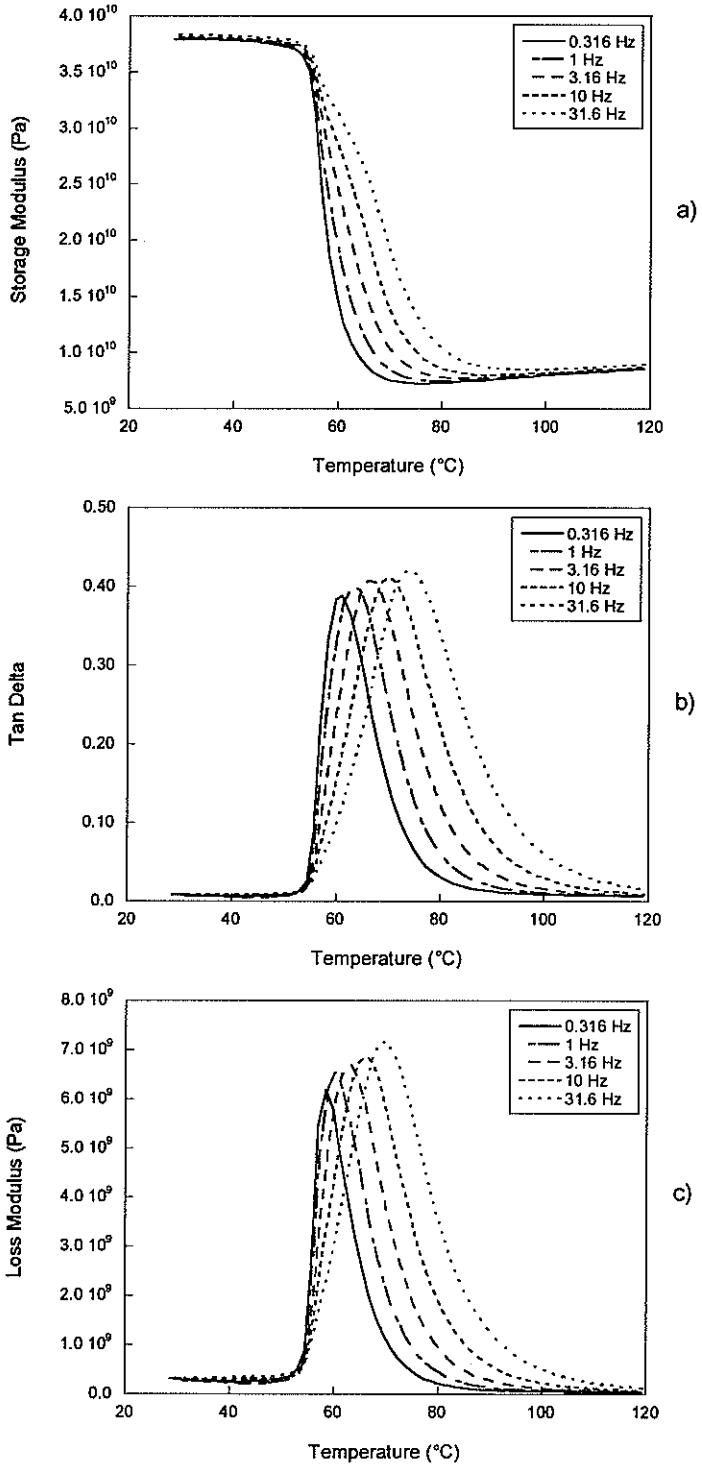

Figure 2-8. Dynamic data for different frequencies at 2 °C/min (room temperature cure): (a) storage modulus vs. temperature; (b) tan delta vs. temperature; (c) loss modulus vs. temperature.

Similar curves were plotted for the same multi-frequency test at heating rates of 0.5, 1, and 3 °C/min. The resulting T_g's, determined by both the loss modulus and tan delta peak methods, as a function of frequency and heating rate, are tabulated in Table 2-1.

Table 2-1. T_g vs. frequency and heating rate.

T_g (°C)	Heating Rate (°C/min)							
	0.5		1		2		3	
Freq (Hz)	tanδ	E"	tanδ	E"	tanδ	E"	tanδ	E"
0.316	62.0	58.2	60.3	57.1	60.6	58.4	61.5	59.2
1.000	65.2	61.0	63.2	59.9	63.3	60.1	63.3	60.2
3.160	68.9	64.5	66.5	62.8	66.5	62.9	66.3	62.5
10.00	73.0	68.0	70.5	66.0	70.0	66.0	69.5	64.5
31.60	77.7	72.3	74.4	69.9	74.0	69.6	73.5	69.0

The greatest difference in the measured T_g's (using both the tan delta and loss modulus peak methods) is 20.6 °C (57.1 to 77.7 °C). For the tan delta peak method, the greatest difference in measured T_g's is 17.4 °C (60.3 to 77.7 °C). The largest variation in measured T_g due to frequency changes alone was 15.7 °C, while the largest variation in measured T_g due to heating rate alone was 4.2 °C. In general T_g variations due to changes in frequency were more pronounced at lower heating rates, and T_g variations due to changes in heating rate were larger at higher frequencies.

2.4.3 Activation energy estimation

As shown in Equation 9, the activation energy of the glass transition relaxation is proportional to the slope of a plot of the natural log of frequency vs. the reciprocal of absolute T_g (K). Figure 2-9 shows a plot of $\ln(\omega)$ vs. $1/T_g$ for a heating rate of 2 °C/min, where T_g is taken as the tan delta peak. From the slope of the least squares regression line (Equation 9), the activation energy is

$$\Delta H = -R\frac{d(\ln(f))}{d(1/T_g)} = -(8.314\cdot 10^{-3})(-39.76\cdot 10^{3}) = 330.6 \text{ kJ/mol.}$$

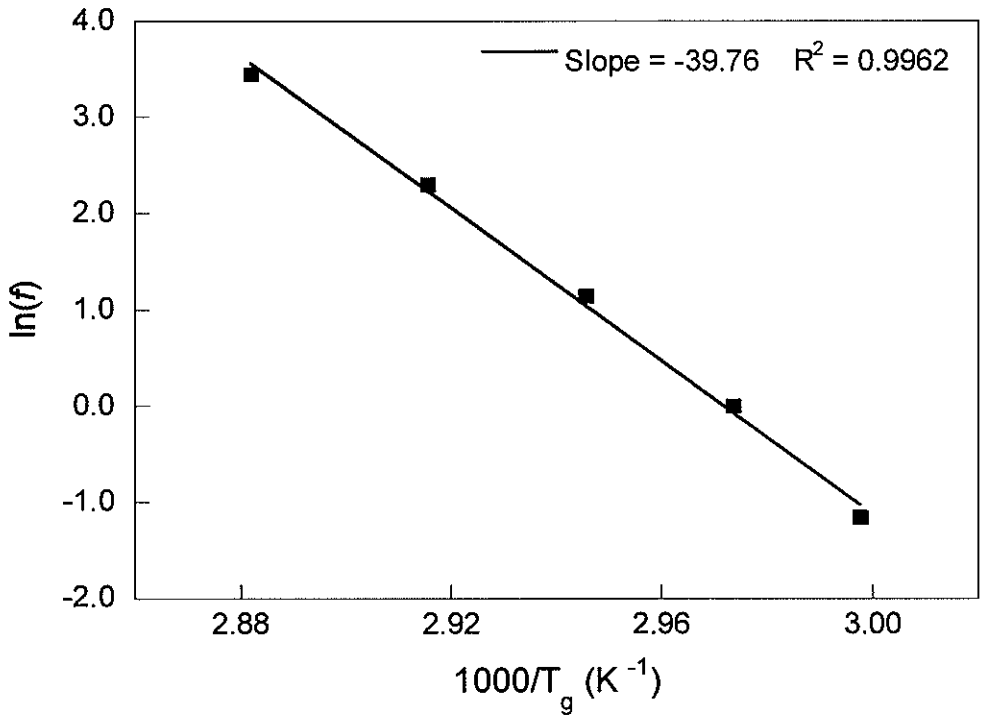

Figure 2-9. Variation of T_g as measured by the tan delta peak with the DMA test frequency (2 °C/min). Test frequency, *f*, in Hz ($\omega=2\pi f$). The slope of the curve is directly proportional to the activation energy of the glass transition.

Table 2-2 shows the calculated activation energies for each heating rate and method of T_g calculation, along with the R^2 values for each curve fit.

Table 2-2. Activation energies with R^2 values.

Heating Rate	Activation Energies			
(°C/min)	$\Delta H_{tan\delta}$ (kJ/mol)	R^2	ΔH_{E^*} (kJ/mol)	R^2
0.5	287	0.996	311	0.996
1	312	0.997	342	0.997
2	331	0.996	384	0.987
3	366	0.985	454	0.944
Avg.	324	0.994	373	0.981
St. Dev.	33.3	5.8E-03	61.9	2.5E-02

The estimation of the activation energy is the most consistent when T_g is taken as the tan delta peak, which is a trend that is consistent with the small amount of literature available on this subject [16,23,24]. Additionally, the R^2 of the regressions for the data using the tan delta peaks has a larger mean and a smaller standard deviation than that of the data using the loss modulus peaks. The activation energy increases with heating rate for both cases. Additionally, the difference between the activation energies estimated from the tan delta and loss modulus peaks increases as heating rate increases.

The estimation of the activation energy of the glass transition relaxation is quite useful because it can be used to estimate the temperature shift factors for time-temperature superposition without the construction of complete master curves [13,25-27]. Furthermore, using this estimation, the modulus or compliance of a polymer at the end of its service life (i.e. 50 years) can be predicted by a single test at an elevated temperature rather than plotting a complete set of master curves [13,25]. This, however, assumes linear viscoelastic behavior at constant stress or strain, which may not correspond to the actual condition of a composite pipe repair. In addition, Karbhari and Wang [24] suggest that monitoring the activation energy of the glass transition can be a valuable technique for assessing changes due to environmental exposure and/or ageing of the material.

2.5 Conclusions

As expected, results indicate that T_g increases and the magnitude of the tan delta peak decreases with increasing levels of cure. The measured tan delta peak T_g's of room temperature cured and post cured specimens ranged from 60 to 129 °C. The largest overall variation in T_g for room temperature cured specimens due to combined changes in heating rate, frequency, and measurement method (tan delta or loss modulus peak) was 20.6 °C. The activation energy and correlation coefficient with frequency was calculated using both the tan delta peak T_g and the loss

modulus peak T_g. It was found that the T_g measured by the tan delta peak was most consistent, resulting in a higher average correlation coefficient and a lower standard deviation with heating rate. In ongoing work, the activation energies calculated will be used to estimate design life creep levels through the approximation of shift factors for use in time-temperature superposition and compared to experimental creep data.

The glass transition temperature data measured through dynamic mechanical analysis allows intelligent decisions to be made concerning the maximum use temperatures for composite repairs with varying levels of cure. From an analysis of T_g vs. post cure temperature data, a conservative estimate of the maximum pipe application temperature for the repair material was made, based on the assumption that the T_g of the repair material must be 20 °C (36 °F) above the pipe temperature. However, this maximum application temperature could be exceeded by applying a one-time post cure to the pipe repair, which would raise the T_g. This could be done by cycling the pipe to a higher temperature after installation (if the process would allow) or by applying an electrical heating blanket around the pipe for a period of time. The T_g vs. post cure data presented in this paper allows an engineer to estimate the proper post cure temperature and time in order to achieve a repair material T_g that is satisfactory.

2.6 Acknowledgements

The authors would like to acknowledge and thank Scott Heaton for his help in manufacturing and testing DMA specimens. The technical advice and helpful discussions with Jeffrey Wilson, Joshua Duell, and Roger Walker of Citadel Technologies are also gratefully acknowledged. This material is based upon work supported under a National Science Foundation Graduate Research Fellowship. Additional funding has been provided by a grant from the Oklahoma Center for the Advancement of Science and Technology (OARS AR03(1)-050).

2.7 References

1. Jacobson G. Corrosion - a natural but controllable process. The AMPTIAC Quarterly 2003;7(4).

2. Mableson R, Patrick C, Dodds N, Gibson G. Refurbishment of steel tubulars using composite materials. Plast Rubber Compos 2000;29(10):558-65.

3. Greenwood C. Composite pipe repair method shows versatility, long-lasting, Pipeline Gas J 2001: February.

4. Alexander C, Wilson F. Development and testing of the Armor Plate pipeline repair system. In: Proceedings of the 1999 ASME Energy Sources Technology Conference, Houston, Texas, USA: American Society of Mechanical Engineers, Petroleum Division, 1999.

5. True W. Composite wrap approved for U.S. gas-pipeline repairs, Oil Gas J 1995;93(41).

6. Smith P, Cuthill J. Patching up pipework with carbon-fiber composites, Mater World 2002;10(5):28.

7 Kessler M, Walker R, Kaakia D. Wilson J, Duell J, Goertzen W, Evaluation of carbon/epoxy composites for structural pipeline repair. In: Proceedings of the Biennial International Pipeline Conference, vol 2. IPC: 2004, p. 1427-1432.

8. Wilson J, Kessler M, Duell J. Rupture testing of A-106, Grade B steel pipes repaired with carbon/epoxy composites. In: Proceedings of the 2004 ASME Pressure Vessels and Piping Conference, July 25-29, 2004. San Diego, CA, published in PVP Vol. 483, Transportation, Storage, and Disposal of Radioactive Materials.

9. Wilson J, Kessler M, Walker R, Duell J, Kadakia D, Sousa N. Fatigue testing of steel pipes repaired with carbon/epoxy composites. In: Proceedings of the 2005 Rio Pipeline Conference and Exposition, Rio de Janeiro, Brazil, Oct. 2005. Paper IBP1089_05.

10. ASME B31.3, Process Piping, American Society of Mechanical Engineers and the American National Standards Institute, April 2002

11. Pascault J-P, Sautereau H, Verdu J, Williams R. Thermosetting polymers. New York: Marcel Dekker, Inc., 2002.

12. Wolfrum J, Ehrenstein G, Avondet M. Dynamic mechanical thermoanalysis of high performance reinforced materials, J Therm Anal Calorim 1999;56(3):1147-1154.

13. Rudin A. Polymer science and engineering. 2nd ed. New York: Academic Press, 1999.

14. Hatakeyama T, Quinn F. Thermal analysis: fundamentals and applications to polymer science. 2nd ed. Chichester, UK: John Wiley & Sons, 1999.

15. Menard K. Dynamic mechanical analysis: a practical introduction. Boca Raton, FL, USA: CRC Press, 1999.

16. Li G, Lee-Sullivan P, Thring R. Determination of activation energy for glass transition of an epoxy adhesive using dynamic mechanical analysis, J Therm Anal Calorim 2000;60(2):377-390.

17. ASTM Standard D 4065-01, Standard Practice for Plastics: Dynamic mechanical properties: determination and report of procedures. West Conshohocken, PA, USA: American Society for Testing and Materials, 2004.

18. Ward I, Hadley D. An introduction to the mechanical properties of solid polymers. Chichester, UK: John Wiley & Sons, 1993.

19. LaPlante G, Lee-Sullivan P. Moisture effects on FM300 structural film adhesive: stress relaxation, fracture toughness, and dynamic mechanical analysis, J Appl Polym Sci 2005; 95(5):1285-1294.

20. White S, Mather P, Smith M. Characterization of the cure-state of DGEBA-DDS epoxy using ultrasonic, dynamic mechanical, and thermal probes, Polym Eng Sci 2002;42(1):51-67.

21. ASTM Standard D 3171-99, Standard test methods for constituent content of composite materials. West Conshohocken, PA, USA: American Society for Testing and Materials, 2004.

22. ASME PCC-2, Repair and Testing Standard, Section 4, Non Metallic Repairs, Article 4.1, Non-Metallic Composite Repair Systems for Pipelines and Pipework: High Risk Applications, 2005.

23. Barral L, Cano J, Lopez A, Nogueira P, Ramirez C. Determination of the Activation Energies for α and β transitions of a system containing DGEBA and 1,3-BAC. J Therm Anal 1994;41(6):1463-1467.

24. Karbhari V, Wang Q. Multi-frequency dynamic mechanical thermal analysis of moisture uptake in E-glass/vinylester composites, Compos Part B-Eng 2004;35(4):299-304.

25. Kumar A, Gupta R. Fundamentals of polymer engineering. 2nd ed. New York: Marcel Dekker, 2003.

26. Miyano Y, Nakada M. Accelerated testing for long-term durability of FRP laminates for marine use, J Compos Mater 2005;39(1):5-20.

27. Goertzen WK, Kessler, MR. Creep behavior of carbon fiber/epoxy matrix composites, Mat Sci Eng A-Struct 2006;421(1-2):217-225.

CHAPTER 3: CREEP BEHAVIOR OF CARBON FIBER/EPOXY MATRIX COMPOSITES

A paper published in *Materials Science and Engineering: A, Structural Materials: Properties, Microstructure and Processing*[1]

William K. Goertzen[2,3] and M.R. Kessler[2,4]

3.1 Abstract

The creep behavior of a carbon fiber/epoxy matrix composite was studied through tensile and flexural creep testing. No creep rupture failures were observed in short-term (less than 1600 hours) room temperature tensile creep tests at loads up to 77% Ultimate Tensile Strength (UTS). For elevated temperature flexural creep compliance data taken at isotherms between 30 and 75 °C, the principle of time-temperature superposition held. Master curves were generated by shifting the data by hand and also using the constant activation energy of the glass transition relaxation to estimate the shift factors. It was shown that the constant activation energy assumption worked fairly well, but only for temperatures below the onset T_g of the material. Predictions were made concerning the creep levels at the end of a proposed 50 year design life.

Keywords: Polymer-matrix composites (PMCs); Carbon fibers; Epoxy; Creep; Thermal properties

---

[1] Reprinted with permission of *Materials Science and Engineering: A, Structural Materials: Properties, Microstructure and Processing*, v 421, n 1-2, 2006, p 217-225.

[2] Graduate student and Assistant Professor, respectively, Department of Materials Science and Engineering, Iowa State University

[3] Primary researcher and author

[4] Author for correspondence

3.2 Introduction

In many fiber-reinforced polymer (FRP) composite structures, both the short-term and long-term durability of the material is of importance. While the structure may not fail when subjected to stresses over a short period of time, it may be prone to failure or increased strain when subjected to stresses over an extended period of time. Even if failure does not occur, the slow deformation of the composite material may cause the structure to become less and less effective. The characterization of the long-term performance of FRP composites is especially important because of the viscoelastic behavior of the polymer matrix. FRP matrices exhibit a glass transition, T_g, a temperature above which the properties of the composite degrade significantly. Typically, it is necessary that the application temperature for the composite structure is below the glass transition in order to assure that the mechanical stiffness and creep resistance of the material is satisfactory. However, the glass transition relaxation occurs over a range of temperatures, so creep testing and predictions of long-term creep behavior at particular application temperatures are important so that the material's long-term mechanical performance can be evaluated.

3.2.1 Theory

Creep is the time-dependent deformation of a material under constant load. While all materials exhibit an initial elastic strain when loaded, this strain may increase over time if the material is susceptible to creep. If a material is perfectly elastic, either linear or non-linear, the strain, ε, will not increase over time and will be a function of the stress, σ, only (for the following set of equations, it is assumed that environmental conditions such as temperature, moisture, etc. are held constant) and is given by

$$\varepsilon = f(\sigma). \qquad (1)$$

Elastic solids store energy when they are loaded and use this energy to return to their original shape when unloaded [1]. Liquids, on the other hand, are viscous in that they flow when loaded externally, and the extent to which they deform is time-dependent. However, if a material exhibits behavior that is a combination of viscous and elastic responses to external forces, the material is considered viscoelastic, or time-dependent [1]. The strain of a viscoelastic material will be a function of both stress and time [2] and is expressed by

$$\varepsilon = f(\sigma,t). \qquad (2)$$

A viscoelastic material can be characterized as either linear or non-linear with respect to stress. In Equation 2, $f(\sigma,t)$ can be divided into two functions, one dependent on time, $h(t)$, and one dependent on stress, $g(\sigma)$. This implies that the stress and time dependencies of the strain are separable [2]. Equation 2 becomes

$$\varepsilon = g(\sigma)h(t). \qquad (3)$$

If it is assumed that the material is linear viscoelastic, the function $g(\sigma)$ would be linear with respect to stress [1]. Likewise, if the material is non-linear viscoelastic, then $g(\sigma)$ would not be linear. For a linear viscoelastic material, the constant associated with $g(\sigma)$ could be included with $h(t)$ in a newly defined function, $S(t)$, which is called creep compliance. Therefore, Equation 3 becomes

$$\varepsilon = S(t)\sigma. \qquad (4)$$

Rearranging Equation 4, the creep compliance is given by

$$S(t) = \varepsilon(t)/\sigma. \qquad (5)$$

If the material is linear viscoelastic, the creep compliance, $S(t)$ will be identical for any given constant stress, $\sigma = \sigma_o$ [2,3]. However, for a material that is assumed to be linear elastic (strain does not increase with time), the creep compliance is simply $\varepsilon/\sigma = 1/E$, where E is the elastic

modulus of the material. For a non-linear viscoelastic material, the compliance would be dependent on both time and stress and is given by

$$S(t,\sigma) = \varepsilon(t,\sigma)/\sigma . \qquad (6)$$

Creep compliance, *S(t),* is the desired result from a creep test that measures strain as a function of time for a given stress, regardless of whether the material is linear or non-linear viscoelastic. In contrast to strain data alone, creep compliance is normalized with respect to stress, allowing creep data from tests at differing stress levels to be compared.

Since the desired lifetime of these materials is often measured in tens of years, it is impractical in most cases to conduct long-term creep testing for the entire design lifetime of the material. Thus, much research has been conducted and published on accelerated characterization of creep in composite materials [3,4]. Accelerated models use short-term creep data and corresponding models to predict the long-term behavior of the material in question. Examples of these models include time-temperature superposition (TTSP), the Findley model, the Schapery model, and thermal activation energy theory. Alternatively, it has been shown that dynamic mechanical testing can be used to produce frequency dependent dynamic data that can be transformed into time-domain creep compliance data using an inverse Fourier transform [4].

3.2.2 Time-temperature superposition

The time-temperature superposition (TTSP) principle is widely used in creep testing of composites to determine the effect of temperature on the creep of FRPs. This theory was originally developed for use with solid polymers [1], but has been expanded for use with fiber-reinforced composites [4]. By the principle of TTSP, the effect of elevated temperature is assumed to be equivalent to stretching the real-time of the creep response by a certain shift factor. Through this assumption, creep compliance is assumed to be a function of time and temperature such that

$$S = S(t,T). \qquad (7)$$

Through this method, short-term creep tests at a range of temperatures can be used to generate a transient creep long-term compliance master curve [4]. The length of time of the master curve is in most cases significantly longer than the short-term curves. With this method, the short-term creep curves at each isotherm are plotted on a log scale. A reference temperature is chosen and the other curves are shifted on a log scale by a shift factor, $\log a_T$ [2]. The shift factor is determined graphically by manually lining up the curves or by using a computer program. Alternately, the shift factors can be estimated by determining the activation energy of the glass transition relaxation from the frequency dependence of T_g's measured through dynamic mechanical analysis [5,6,7].

In the present work, the creep behavior of carbon fiber/epoxy matrix composites used for wrapping and repairing damaged pipelines and pipe work [8-10] is evaluated using both room temperature tensile creep experiments and elevated temperature flexural creep experiments. The generation of creep compliance master curves is explored using both a manual shifting method and using shift factors calculated from the activation energy of the glass transition relaxation. The results are compared, and predictions are made concerning the creep levels that will occur during the design lifetime of the composite material.

3.3 Experimental

3.3.1 Materials

The composite specimens were constructed using bi-directional woven carbon fiber reinforcement (supplied by Citadel Technologies™, Tulsa, OK). This reinforcement was plain weave fabric consisting of 12K tow in the warp direction and 3K tow in the fill direction. The 12K indicates that there are approximately 12,000 carbon filaments (fibers) in each bundle (tow), while 3K indicates approximately 3,000 filaments per tow. The fabric is fairly coarse, with 4

tows/inch in the warp direction and 8 tows/inch in the fill direction. The matrix material was a two part epoxy system, SWR/SWH, developed by Citadel Technologies™ (Tulsa, OK). The particular epoxy used is a diglycidyl ether of bisphenol-A (DGEBA) type epoxy cured with an aliphatic amine hardener. The exact chemical structure and nature of the DGEBA epoxy and aliphatic amine hardener used in the SWR/SWH system is proprietary. When stoichiometricly mixed, the epoxy and curing agent produce a hard, highly crosslinked thermoset with high solvent resistance and relatively high impact strength.

3.3.2 Specimen manufacturing

The epoxy matrix was formulated by mixing the two-part epoxy/amine system using a resin-to-hardener ratio of 2.65:1. The plain weave carbon fabric was manually impregnated with the epoxy prepolymer. Composite panels 12 in x 10 in were fabricated by hand layup with 2 plies. The layup was done in a Teflon release spray coated pan and a Plexiglas caul plate (sprayed with a Teflon release spray) was placed on top of the panel with less than 3.45 kPa (0.5 psi) of pressure. The Plexiglas was laid down in such a way as to remove the air bubbles from the epoxy and create a uniform surface on the top of the specimen sheet. The panels were cured at room temperature for at least 24 hours. The thickness per ply of the composite panels is similar to the thickness per ply of the composite overwrap system used to repair damaged pipelines and pipe work. The fiber volume fraction of the composite was measured to be between 35% and 40%, using both the TGA burnoff and matrix digestion methods in accordance with ASTM D 3171 [11].

Once the panels were cured at room temperature, they were machined to produce dog-bone specimens for tensile creep testing and rectangular specimens for flexural creep testing. The dog-bone test specimen preparation and geometry are acceptable according to ASTM D638 [12]. Vishay MM CEA 06-500UW-120 strain gages were bonded to the gage section of the coupons

using M-Bond 200 adhesive. A picture of a typical creep rupture specimen with dimensions is shown in Figure 3-1. The thicknesses of the creep rupture specimens ranged from 1.1 to 1.2 mm.

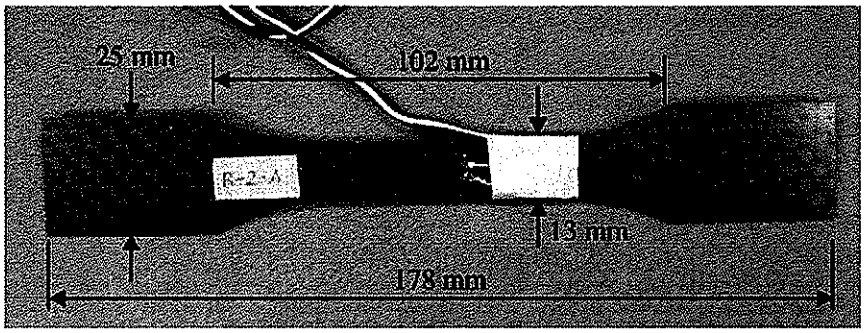

Figure 3-1. A gaged specimen used for tensile creep testing (with dimensions in mm).

3.3.3 Equipment

Tensile creep testing was conducted using an in-situ creep rupture fixture (see Figure 3-2) developed by Lombart and Henshaw at the University of Tulsa [13]. The Dynamic Mechanical Analyzer (DMA) used for the flexural creep testing of the composite was a Tritec 2000 DMA manufactured by Triton Technology, Ltd (Keyworth, Notts, UK). It has a load range of –10 to +10 N and a displacement range of –1 to 1 mm. A three-point bending mode with a free length of 20 mm was used. The three-point bending DMA fixture is shown in Figure 3-3.

3.3.4 Experimental procedure – tensile creep

The procedure used for the tensile creep testing was a revised version of the testing procedure developed by Lombart [13]. The fixture uses a load multiplier to achieve a 187:1 ratio of load of the specimen to weight hung from the machine. The first major load multiplication is done through a system of pulleys and the second load multiplication is done by a lever arm with an output to input load ratio of 6:1. The load is monitored by 4400 N load cell attached to the output cable that is attached to the lever arm (see Figure 3-2). Strain, load, temperature, and humidity are recorded by a data acquisition system with LabVIEW software.

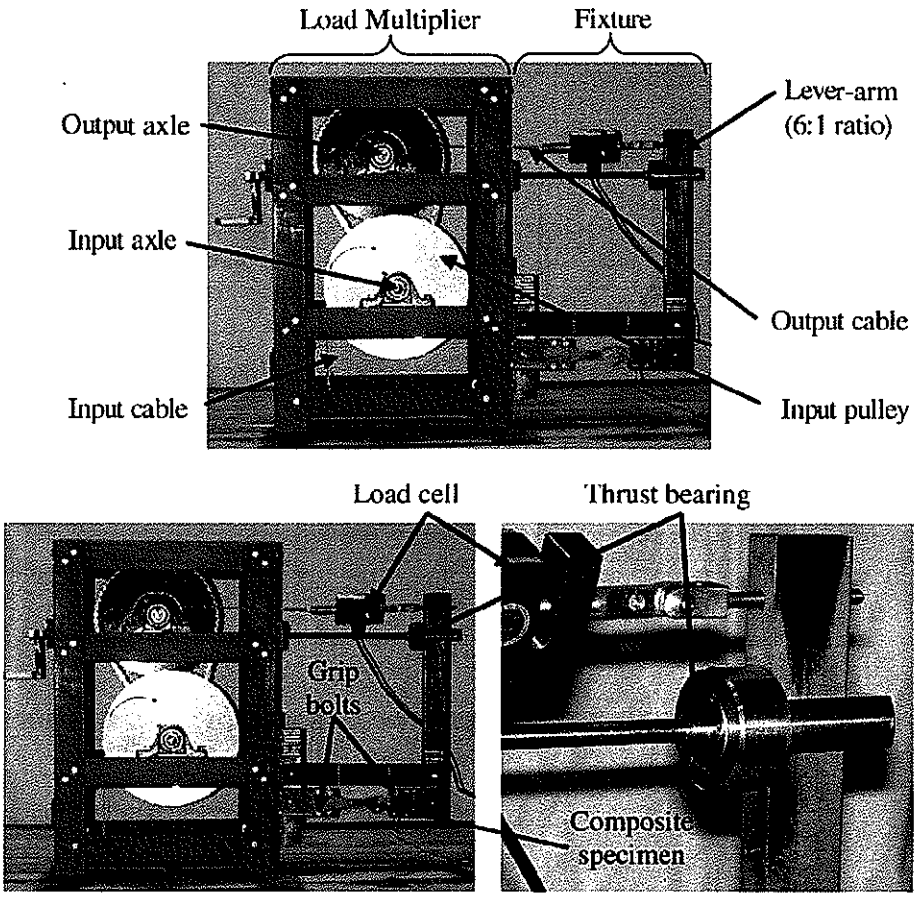

Figure 3-2. In-situ creep rupture fixture [13].

Before loading the specimen in the grips, the lever-arm is placed in a vertical position and the threaded rod is turned until it contacts the thrust bearing (see Figure 3-2). The specimen is then placed in the grips and the bolts are tightened to a specified torque. Then, the strain gage is calibrated using the LabVIEW software. Next, the weights are attached to the cable to achieve the desired output load. After starting the recording of data, the specimen is loaded by slowly turning the threaded rod until it does not touch the lever arm. As the lever arm deflects, however, the weights must be raised to prevent them from hitting the ground. This is done by engaging the clutch and rotating the input pulley.

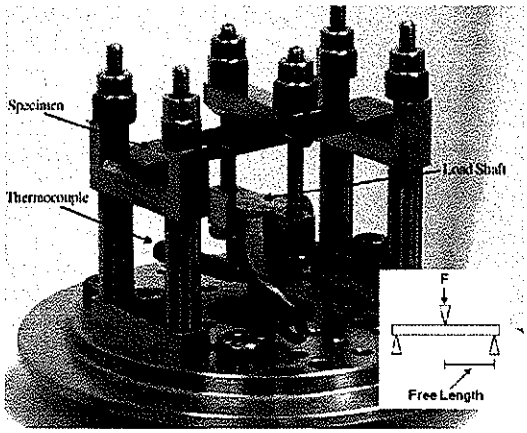

Figure 3-3. Three-point bending with constant force.

3.3.5 Experimental procedure – flexural creep

Creep and creep recovery cycles were conducted at isotherms between 30 and 75 °C in intervals of 5 °C. For each isotherm, a constant force of 4 N (corresponding to a stress of 32 MPa (4.7 ksi)) was applied for 3 hours, followed by a 3 hour recovery period. The load was applied at a rate of 24 N/min, and data points were taken every 30 seconds, with a measurement delay time of 30 seconds. Prior to testing, the specimen was post-cured twice at 60 °C (140 °F) for times of 24 hours and 72 hours. The T_g of the material at this cure state is 82 °C for the tan delta peak method and 63 °C for the onset method, measured by DMA at 1 Hz and 2°C/min.

3.4 Results and discussion

3.4.1 Tensile creep testing

In initial testing, 4-layer composite specimens were used and slippage in the grips was experienced, causing erroneous results. This was due to the large average loads placed on the specimens, which were around 13300 N (3000 lbf). To eliminate grip slippage, loads were reduced by using 2-layer specimens instead of 4-layer specimens, new fine tooth grips were used, and the bolt torque was optimized. As a result of many tests performed with different torques

applied, an optimum torque of 10.8 N-m (96 lb-in) was found. This torque was applied to each bolt in a star pattern prior to each test.

The Ultimate Tensile Strength (UTS) value for the 2-ply composite specimens was determined by tensile testing of specimens from the same batch using a model 810 MTS load frame in displacement control. The average UTS for the 12K direction was 645 MPa (93.6) ksi ± 45 MPa (6.5 ksi) (uncertainty is for 95% confidence). All of the creep specimens were tested in the 12K direction as well. Two successful 1000-plus hour room temperature creep tests were performed at stress levels of 65% UTS (1000 hours) and 77% UTS (1600 hours) using the new bolt torque. Due to a data acquisition error, data was not recorded for the last 260 hours of the 65% UTS test and the last 600 hours of the 77% UTS test. However, the specimens stayed loaded for the entire test period without failure before being unloaded and removed from the fixture.

Figure 3-4 shows the creep compliance, $S(t) = 1/E(t) = \varepsilon(t)/\sigma(t)$, for the tests conducted at 417 MPa (60.5 ksi) (65% UTS) and 496 MPa (72.0 ksi) (77% UTS).

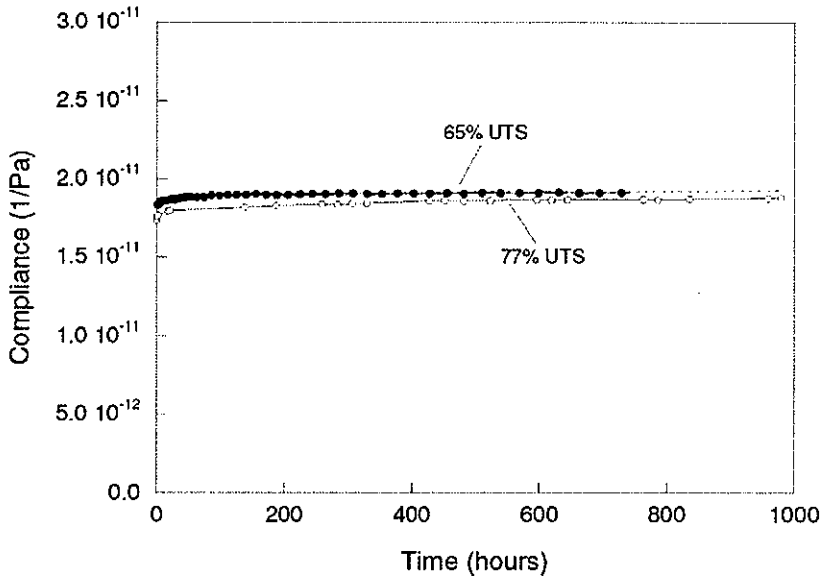

Figure 3-4. Tensile creep compliance vs. time, 65% and 77% UTS.

While the compliance values for the 65% UTS test are all larger than that of the 77% UTS test, this is due to fluctuations in the modulus of the composite material from specimen to specimen. The uncertainty in the modulus data for this material, as tested by Duell, is approximately 7% [14], but the compliance difference between the 65% and 77% UTS tests at a given time is never larger than 4.6%.

Figure 3-5 shows the data for the 77% UTS test and the curve fit for the 65% UTS test on a log time scale.

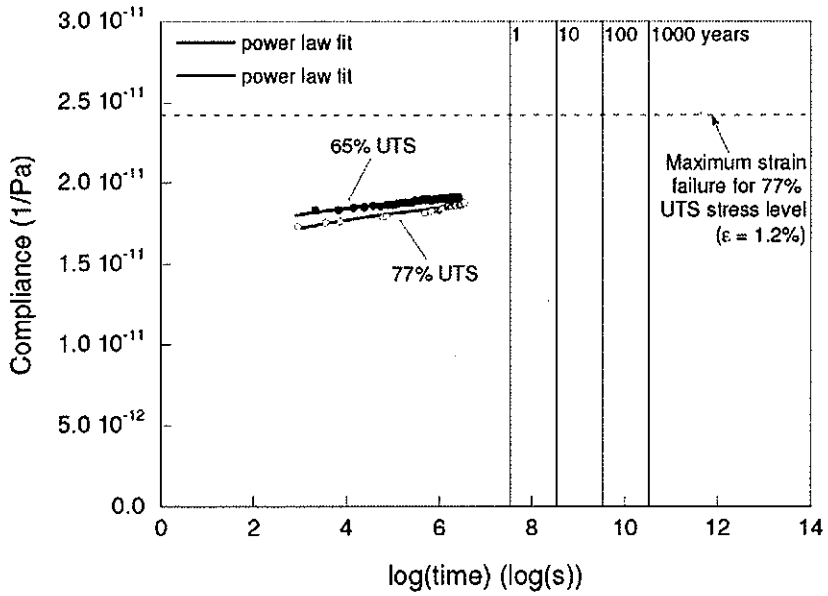

Figure 3-5. Tensile creep compliance vs. log time, 65% and 77% UTS.

There is little difference between the creep compliance curves for the two stress levels. This would support the notion that the material's behavior was nearly linear viscoelastic in this stress range. It should be noted that the load of 77% UTS nears the limit of the load range for creep rupture testing of this material because of the 14.6% uncertainty in ultimate strength observed during tensile testing by Duell [14]. The curve fits shown are power law relations, used for the characterization of creep of viscoelastic materials under constant stress. According to this model,

the compliance is given by $S(t) = kt^n$. The data for both tests follows the power law trend well, with regression coefficients (R^2) of 0.948 and 0.935 for the 65% and 77% UTS tests, respectively. If the creep behavior of the material followed this trend for its entire life, extrapolation of these curve fits would allow predictions to be made concerning the compliance values at the end of a design life, e.g. 50 years. For the 65% UTS test, extrapolation to 438,000 hrs (50 years) would result in a compliance of $2.00 \cdot 10^{-11}$ 1/Pa ($1.38 \cdot 10^{-7}$ 1/psi), which corresponds to a strain of 0.84%. According to a maximum strain failure criterion, the composite would not reach the ultimate strain of 1.2% during this 50 year period at this 65% UTS. Although the creep failure mechanism for this composite may be quite complex due to the elastic nature of the carbon fibers and the viscoelastic nature of the epoxy matrix, a maximum strain failure criterion is used because of its simplicity and because of a lack of creep rupture data for this particular composite. Using the maximum strain failure criterion in this situation allows for simple comparisons to be made concerning the levels of creep for the material under constant load. For the 77% UTS test, extrapolation of its curve fit to 438,000 hrs (50 years) hours would result in a compliance of $1.97 \cdot 10^{-11}$ 1/Pa ($1.36 \cdot 10^{-7}$ 1/psi), which corresponds to a strain of 0.97%. According to a maximum strain failure criterion, the composite would not reach the ultimate strain of 1.2% during this 50 year period at this 77% UTS. However, because of the relatively short test period involved, it would be dangerous to extrapolate these curves and assume that the creep behavior of the composite would continue to behave identically throughout the entire 50 year period. More reliable predictions for such lengths of time can only be made using proven predictive models, such as time-temperature superposition.

3.4.2 Flexural creep at elevated temperatures

Since it is impractical to conduct creep tests for the entire lifetime of a material, predictions must instead be made concerning the creep levels or time-to-failure at a given load.

Since no creep rupture failures were observed in the room temperature tensile creep tests outlined in the previous section, predicting time-to-failure using an extensive creep rupture test program would be impossible without multiple creep fixtures and elevated temperature capabilities. This section will outline the use of time-temperature superposition to predict the lifetime creep behavior of the composite from flexural creep tests at a range of elevated temperatures. The DMA is an ideal apparatus for this type of testing because it is capable of testing at a wide range of temperatures. Although the DMA creep tests will be conducted at low stress levels and in a bending mode, some qualitative creep level predictions can still be made through this method.

Figure 3-6 shows the creep compliance vs. actual test time for the entire test (the breaks in the data correspond to the recovery periods, in which data was not recorded).

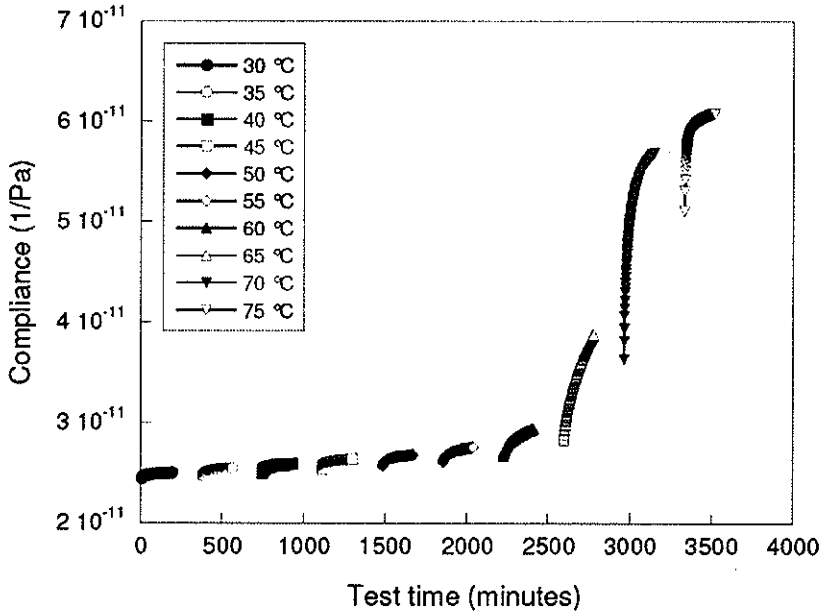

Figure 3-6. Compliance vs. actual test time [Data taken every 30 seconds. Symbols are used to differentiate the curves].

Figure 3-7 shows the unshifted data on a log time scale, along with the corresponding master curve.

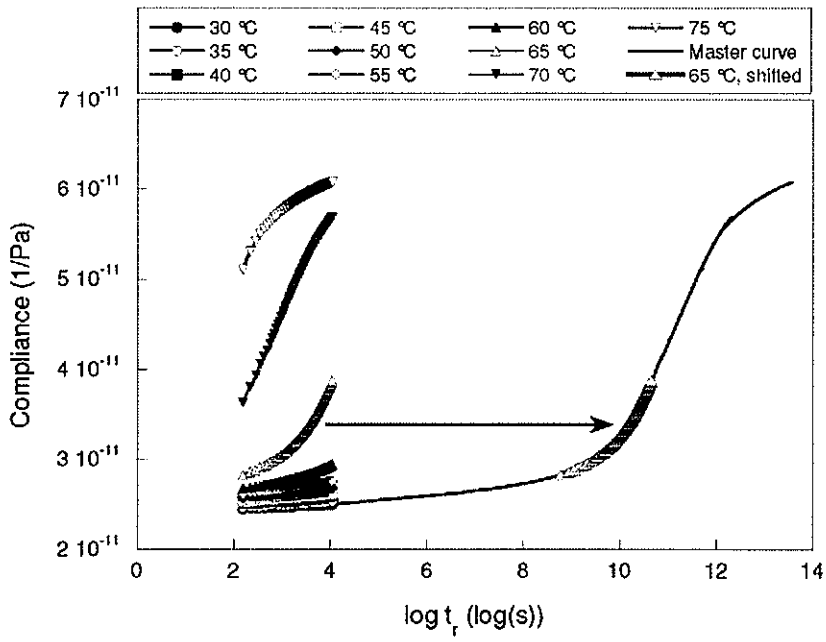

Figure 3-7. Unshifted creep compliance data and corresponding master curve for T_{ref} = 30 °C, manual shift [Data taken every 30 seconds. Symbols are used to differentiate the curves].

According to the principle of time-temperature superposition, each curve was shifted by an appropriate temperature shift factor, $\log a_T$, which is given by

$$\log a_T = \log \frac{t}{t_r} \qquad (8)$$

where t is the actual test time and t_r is the reduced time. The reduced time, t_r, is the expanded time scale for the creep master curve at an isothermal reference temperature. The reduced time (on a log scale) is given by

$$\log t_r = \log t - \log a_T . \qquad (9)$$

The creep compliance curve for the reference temperature, T_{ref}, is left unshifted ($\log a_T$ is zero), while the creep compliance curves for the other temperatures are shifted on the log scale by the shift factor. For temperatures greater than T_{ref}, the curve is shifted to the right ($\log a_T$ is

negative), and for temperatures less than T_{ref}, the curve is shifted to the left ($\log a_T$ is positive). The shift factors are chosen by hand so that the isothermal curves overlap.

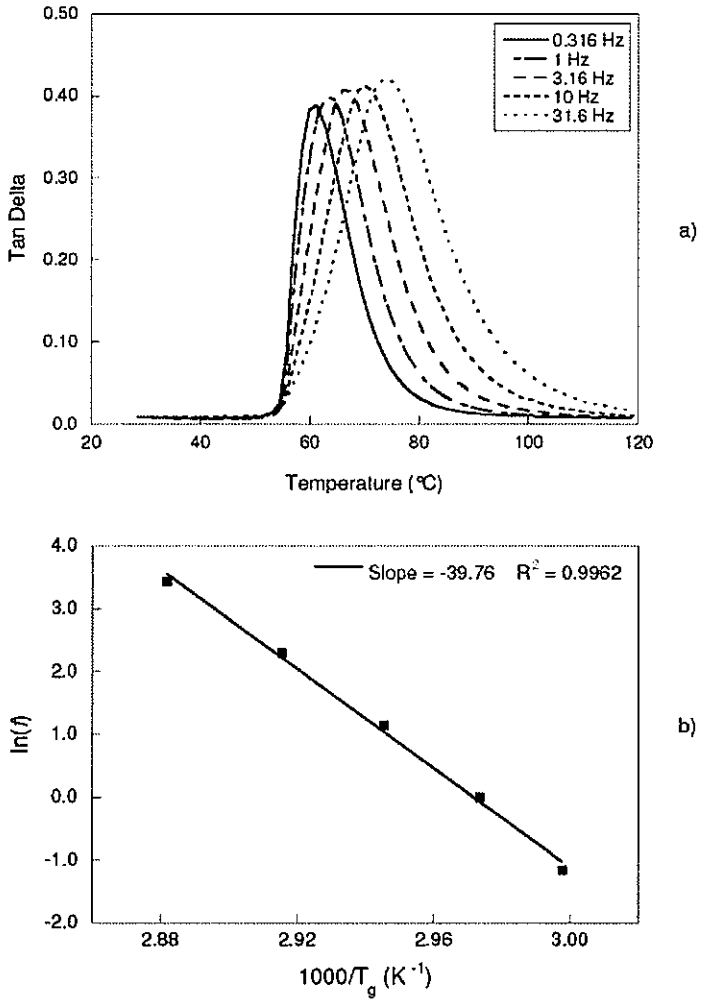

Figure 3-8. Calculation of the activation energy of glass transition from the frequency dependence of tan delta curve peak T_g's: (a) tan delta curves for different frequencies at 2 °C/min (b) Variation of T_g as measured by the tan delta peak with the DMA test frequency (2 °C/min). Test frequency, *f*, in Hz ($\omega=2\pi f$). The slope of the curve is directly proportional to the activation energy of the glass transition.

Alternatively, shift factors can be estimated from the activation energy of the glass transition relaxation. The activation energy of the glass transition relaxation represents the

energy barrier that must be overcome for the occurrence of molecular motions causing the transition [15], and was estimated from the frequency dependence of T_g's measured through dynamic mechanical analysis. Figure 3-8 (a) shows tan delta curves for a range of test frequencies at a heating rate of 2°C/min. The activation energy is calculated from the slope of a plot of $\ln(f)$ vs. $1/T_g$, which is shown in Figure 3-8 (b), by [16]

$$\Delta H = -R\frac{d(\ln(f))}{d(1/T_g)} = -(8.314\cdot 10^{-3})(-39.76\cdot 10^{3}) = 330.6 \text{ kJ/mol.}$$

Table 3-1 shows the calculated activation energies for T_g's taken from tan delta and loss modulus peaks for different heating rates (the test specifics and influence of heating rate and T_g measurement method are discussed in our previous work [17]).

Table 3-1. Activation energies with R^2 values.

Heating Rate	Activation Energies			
(°C/min)	$\Delta H_{tan\delta}$ (kJ/mol)	R^2	$\Delta H_{E''}$ (kJ/mol)	R^2
0.5	287	0.996	311	0.996
1	312	0.997	342	0.997
2	331	0.996	384	0.987
3	366	0.985	454	0.944
Avg.	324	0.994	373	0.981
St. Dev.	33.3	5.8E-03	61.9	2.5E-02

The estimation of the activation energy of the glass transition relaxation is quite useful because it can be used to estimate the temperature shift factors for time-temperature superposition without the construction of complete master curves [5,6,7]. Furthermore, using this estimation, the modulus or compliance of a polymer at the end of its service life (i.e. 50 years) can be predicted by a single test at an elevated temperature rather than plotting a complete set of master curves [5,7]. In addition, Karbari and Wang [18] suggest that monitoring the activation energy of the glass transition can be a valuable technique for assessing changes due to environmental

exposure and/or aging of the material. Using a constant activation energy assumption, the shift factors are given by [6,7,19]

$$\log a_T = \frac{\Delta H}{R}\left(\frac{1}{T} - \frac{1}{T_{ref}}\right)\log e, \qquad (10)$$

which is derived from the Arrhenius relationship. Equation 10 holds for temperatures below the T_g of the polymer, where the Williams-Landel-Ferry (WLF) equation is not applicable [6,7]. For this example, the activation energy used to estimate shift factors was the average obtained through the tan delta method, ΔH = 324 kJ/mol (see Table 3-1). For a reference temperature of 30 °C, the creep compliance master curve generated using shift factors estimated from a constant activation energy assumption is shown in Figure 3-9.

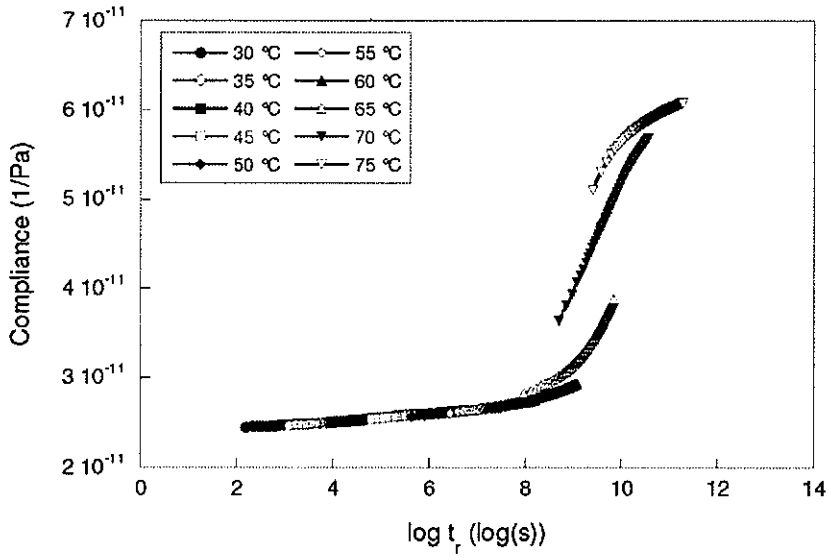

Figure 3-9. Creep compliance master curves for T_{ref} = 30 °C, constant activation energy [Data taken every 30 seconds. Symbols are used to differentiate the curves].

Figure 3-10 shows the shift factors versus the reciprocal of absolute temperature, along with the shift factors obtained using an assumption of constant activation energy. The assumption of constant activation energy gives a linear relationship for $\log a_T$ vs. 1/T [1]. The

manual shift factors follow the linear activation energy shift factor curve well until 1000/T = 3.0 or T = 60 °C, after which the magnitude of the shift factors for the manually shifted data is larger.

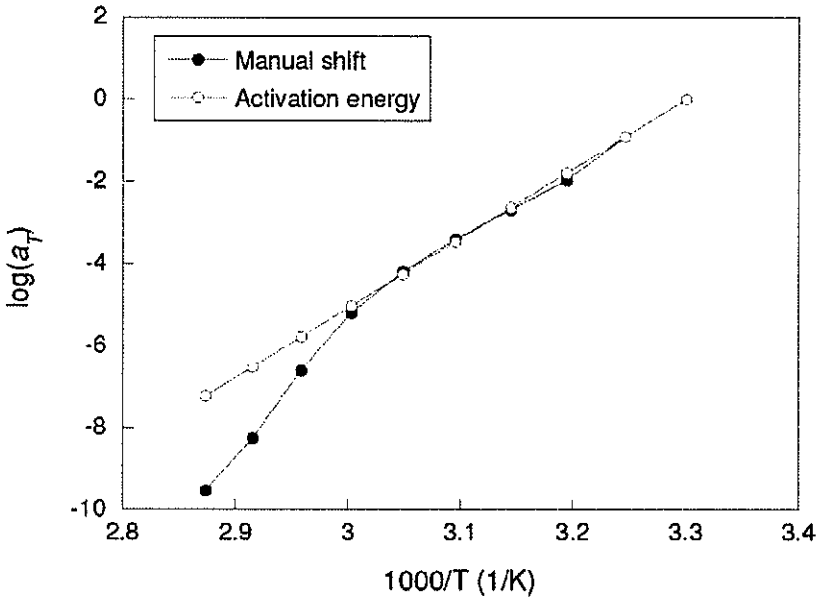

Figure 3-10. Shift Factors vs. 1/T for manual shift and constant activation energy estimation.

The fact that the constant activation energy assumption is only valid below T_g, is illustrated in Figure 3-9 by the fact that the data for the constant activation energy master curve line up well only through the 60 °C curve. To further illustrate the difference between the shifted data using the manual shift and constant activation energy, Figure 3-11 shows an exploded view of the shifted curves for the 30 to 60 °C isotherms using each method. This data further illustrates the point that the prediction of shift factors using the constant activation energy assumption is only valid for temperatures below the T_g of the material. For this particular case, the cutoff corresponds to the onset T_g, which is approximately 63 °C (measured by dynamic mechanical analysis).

In order to show the lifetime creep behavior of the material, Figure 3-12 shows master curves for reference temperatures of 30, 40, and 50 °C with lines showing times of 1, 10, 100, and 1000 years.

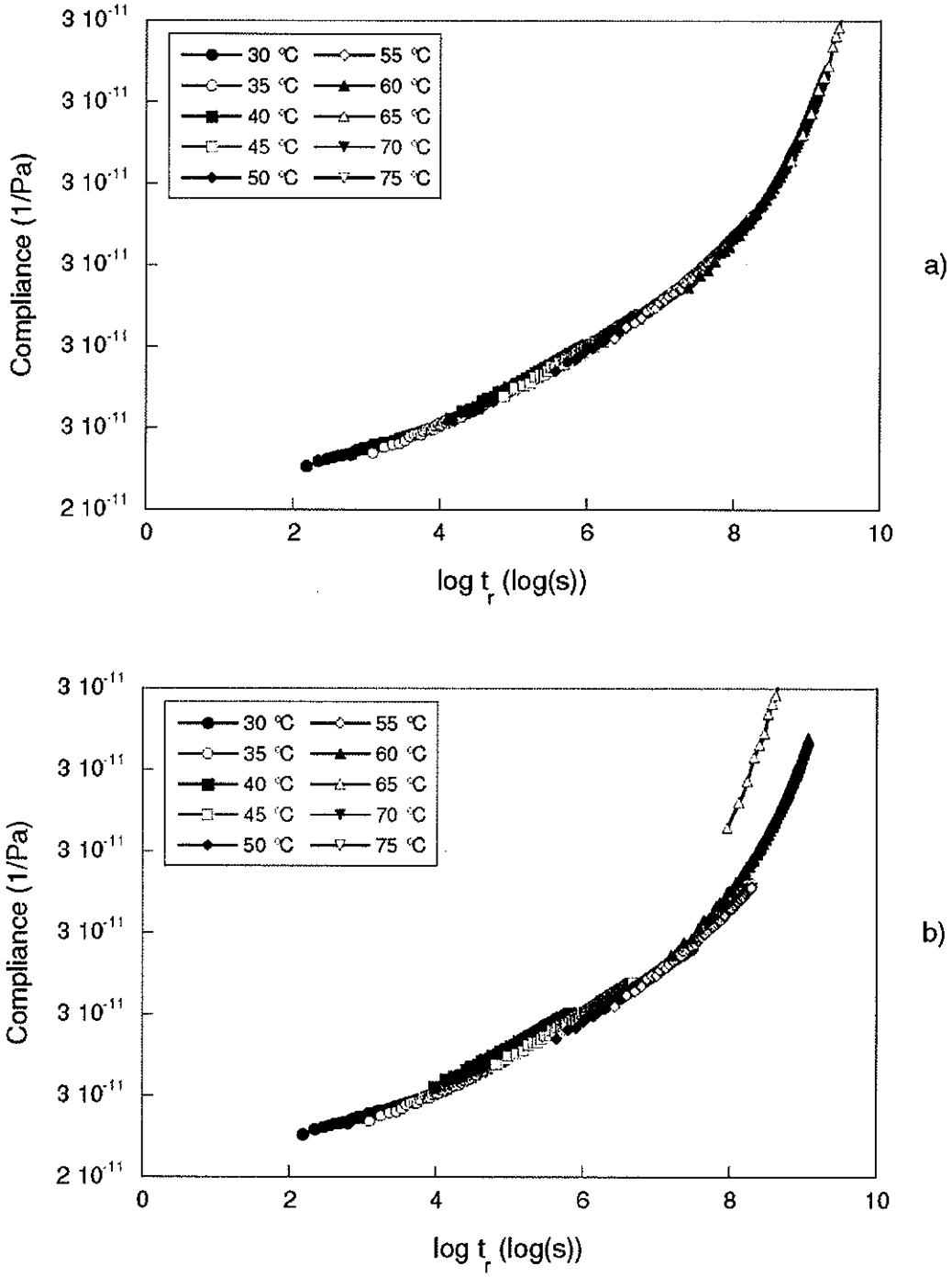

Figure 3-11. Master curve exploded view, T_{ref} = 30 °C, a) manual shift; b) constant activation Energy [Data taken every 30 seconds. Symbols are used to differentiate the curves].

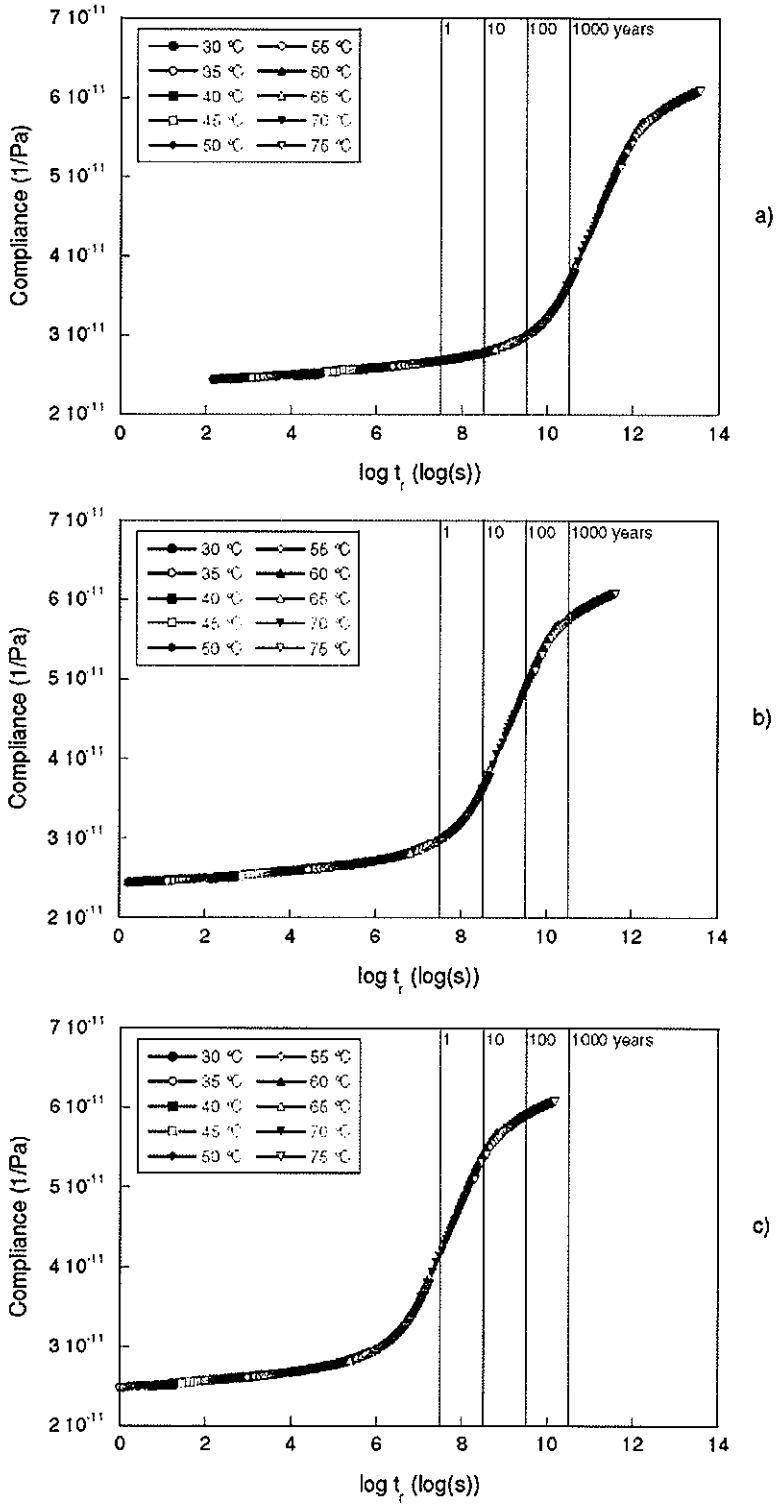

Figure 3-12. Master curves with time references in years for a) T_{ref} = 30 °C; b) T_{ref} = 40 °C; c) T_{ref} = 50 °C [Data taken every 30 seconds. Symbols are used to differentiate the curves].

Using the master curves at reference temperatures, T_{ref}, of 30, 40, and 50 °C, initial predictions of compliance levels for a composite structure operating under constant load at the reference temperature of interest are possible. For these predictions, several assumptions must be made. First, the composite material is assumed to be linear viscoelastic, such that creep compliance levels are the same at any stress level. Second, a maximum strain failure criterion is used to determine failure, and a constant load is assumed. While loads for the application may vary with time, this example is used to make comparisons of creep levels for the simplest case. Finally, since the flexural compliance (and modulus) of the material tested in bending is different from the material's compliance (and modulus) in tension, the ratio of the flexural compliance (and modulus) to the tensile compliance (and modulus) is assumed constant.

From each of the master curves at the three different reference temperatures, the flexural creep compliance value was found at a time of 50 years (S(50 yrs)), a typical maximum design life for a composites pipeline repair system for which the carbon/epoxy composite is intended. By comparing these compliance values to the original compliance values, S_o, the stress level to cause failure at 50 years was calculated. The results are tabulated in Table 3-2, showing the % UTS level to cause failure at 50 years for each reference temperature.

Table 3-2. 50-year design life creep predictions.

Tref	50 yr. Compliance Prediction, S(50 yrs.)[a]		50 year	50 year
	Flexural	Tensile	Failure Stress	Reduction in
(°C)	(1/Pa)	(1/Pa)	(% UTS)	Modulus (%)
30	2.92E-11	2.22E-11	83.9%	16.1%
40	4.48E-11	3.39E-11	54.8%	45.2%
50	5.79E-11	4.39E-11	42.4%	57.6%

[a]Original Flexural Compliance, S_o: 2.45 E-11 1/Pa

[a]Original Tensile Compliance, S_o: 1.86 E-11 1/Pa

Thus, the stress level required to cause failure at the 50 year point for a constant temperature of 30 °C (86 °F) would be approximately 84% UTS. This data point supports the initial prediction

made from the results of the tensile creep testing described earlier, which stated that at a 77% UTS stress level, the composite material would not fail in 50 years. However, the original creep compliance level prediction of $1.97 \cdot 10^{-11}$ 1/Pa ($1.36 \cdot 10^{-7}$ 1/psi) for room temperature in the previous section was slightly lower than the 30 °C creep compliance prediction from the time-temperature superposition data, which is $2.22 \cdot 10^{-11}$ 1/Pa ($1.53 \cdot 10^{-7}$ 1/psi). Percent reductions in modulus levels at 50 years are also tabulated in Table 3-2, such that at 30 °C, the modulus of the material would reduce by approximately 16 %, according to the predictions. At 50 °C, the modulus would reduce by 58% over the 50 year period.

While the initial predictions explained above are useful, a safety factor should be built in to all design calculations in order to account for measurement uncertainties and the complexity of the relationship between the material's cure state, T_g, and creep behavior. It would be very useful to conduct further creep testing to validate these predictions. For instance, the most practical check of these predictions would be to test the material at an elevated temperature, such as 50 or 60 °C, for a relatively short test period (i.e. 1000 hours) and compare the compliance levels to the master curve for that particular reference temperature. Test temperatures of this magnitude would be required because the creep levels at room temperature would not be significant enough to make comparisons for any reasonable test period.

3.5 Conclusions

Creep testing is an important part of the characterization of composite materials. It is crucial to determine long-term deflection levels and time-to-failure for these advanced materials. The tensile creep testing of the composite specimens showed that the carbon fiber composites are resistant to creep rupture under ambient conditions. The creep curves for the two tests were very similar, and no failures were observed at loads of up to 77% of the ultimate tensile strength at times of up to 1600 hours. Additionally, the level of creep in the tests was small, such that

extrapolation of the creep data would indicate that the material would not fail at the 65% UTS load or the 77% UTS load during a reasonable lifetime.

Further creep testing was performed using a DMA at a range of elevated temperatures in order to make more reliable predictions of long-term behavior using the proven principle of time-temperature superposition. Although tests must be made in bending mode at low stress levels, the DMA provides an efficient method for obtaining creep data at a wide range of temperatures. The principle of time-temperature superposition held for the material tested at isotherms between 30 and 75 °C. Master curves were generated by shifting the data by hand and also using a constant activation energy to estimate the shift factors. It was shown that the constant activation energy assumption held fairly well, but only for temperatures below the onset T_g of the material. A total of three master curves were generated at temperatures of 30, 40, and 50 °C, and using the compliance data, predictions were made concerning the creep levels at the end of a proposed 50 year design life. The stress levels to induce failure at 50 years ranged from 84 % at 30 °C to 42 % at 50 °C. The corresponding reductions in modulus over the 50 year period ranged from a 16 % reduction over 50 years at 30 °C to a 58% reduction for 50 years at 50 °C.

3.6 Acknowledgements

The authors would like to acknowledge and thank Scott Heaton for his help in manufacturing specimens. The technical advice and helpful discussions with Jeffrey Wilson, Joshua Duell, and Roger Walker of Citadel Technologies are also gratefully acknowledged. The authors would also like to thank John Henshaw of the University of Tulsa for the use of his creep rupture fixture and technical advice. This material is based upon work supported under a National Science Foundation Graduate Research Fellowship. Additional funding has been provided by a grant from the Oklahoma Center for the Advancement of Science and Technology (OARS AR03(1)-050).

3.7 References

1. I.M. Ward, D.W. Hadley, An Introduction to the Mechanical Properties of Solid Polymers, John Wiley & Sons, 1993.

2. J. Nairn, Polymer Characterization, MSE 5473 Class Notes, University of Utah, 2005.

3. B. Abdel-Magid, R. Lopez-Anido, G. Smith, S. Trofka, Compos. Struct., 62 (2003) 247-253.

4. D.W. Scott, J. S. Lai, A-H. Zureick, J. Reinf. Plast. Comp. 14 (1995) 588-617.

5. A. Kumar, R. Gupta, Fundamentals of Polymer Engineering, 2nd ed., Marcel Dekker, New York, 2003.

6. R. Li, Mat. Sci. Eng. A-Struct. 278 (2000) 36-45.

7. A. Rudin, Polymer Science and Engineering, 2nd ed., Academic Press, New York, 1999.

8 M. Kessler, R. Walker, D. Kadakia, J. Wilson, J. Duell, W. Goertzen, Proceedings of the Biennial International Pipeline Conference, vol 2. IPC: 2004, p. 1427-1432.

9. J. Wilson, M. Kessler, J. Duell, Proceedings of the 2004 ASME Pressure Vessels and Piping Conference, PVP vol. 483, 2004.

10. J. Wilson, M. Kessler, R. Walker, J. Duell, D. Kadakia, N. Sousa, Proceedings of the 2005 Rio Pipeline Conference and Exposition, Rio de Janeiro, Brazil, Oct. 2005. Paper IBP1089_05.

11. ASTM Standard D 3171-99, Standard test methods for constituent content of composite materials. West Conshohocken, PA, USA: American Society for Testing and Materials, 2004.

12. ASTM D638, Standard Test Method for Tensile Properties of Plastics, 2001.

13. V. Lombart, M.S. Thesis, The University of Tulsa Graduate School, 2002.

14. J. Duell, M.S. Thesis, The University of Tulsa Graduate School, 2004.

15. G. LaPlante, P. Lee-Sullivan, J. Appl. Polym. Sci. 95 (2005) 1285-1294.

16. G. Li, P. Lee-Sullivan, R. Thring, J. Therm. Anal. Calorim. 60 (2000) 377-390.

17. W. Goertzen, M. Kessler, Compos. Part B-Eng. submitted.

18. V. Karbhari, Q. Wang, Compos. Part B-Eng. 35 (2004) 299-304.

19. M. Tajvidi, R. Falk, J. Hemanson, J. Appl. Polym. Sci. 97 (2005) 1995-2004.

CHAPTER 4: THERMAL AND MECHANICAL EVALUATION OF CYANATE ESTER COMPOSITES WITH LOW-TEMPERATURE PROCESSABILITY

A paper published in *Composites Part A: Applied Science and Manufacturing*[1]

William K. Goertzen[2,3] and M.R. Kessler[2,4]

4.1 Abstract

A low viscosity bisphenol E cyanate ester monomer was used as a reactive diluent in a bisphenol A/novolac cyanate ester to achieve a low viscosity prepolymer with a viscosity suitable for processing at room temperature. Dynamic mechanical analysis was conducted on carbon fiber composite specimens manufactured from two cyanate ester blends with varying catalyst compositions. It was shown that post curing was needed to produce a polymer matrix with a single glass transition relaxation, but increases in post cure temperature above 204°C resulted in slight reductions in T_g and modulus. Also, increasing catalyst composition was shown to have a negative effect on T_g.

Keywords: A. Polymer-matrix composites (PMCs); A. Thermosetting resin; B. Thermal Properties; E. Lay-up (manual/automated)

---

[1] Reprinted with permission of *Composites Part A: Applied Science and Manufacturing*, v 38, n 3, March 2007, p 779-784.

[2] Graduate student and Assistant Professor, respectively, Department of Materials Science and Engineering, Iowa State University

[3] Primary researcher and author

[4] Author for correspondence

4.2 Introduction

Cyanate esters, correctly named polycyanurates in the polymer form, are characterized by monomers containing reactive ring-forming cyanate (-O-C≡N) functional groups [1,2]. Cyanate esters with two or more cyanate functional groups will homopolymerize with the addition of heat through cyclotrimerization to from a 3-dimensional network, as shown in Figure 4-1 [1,3].

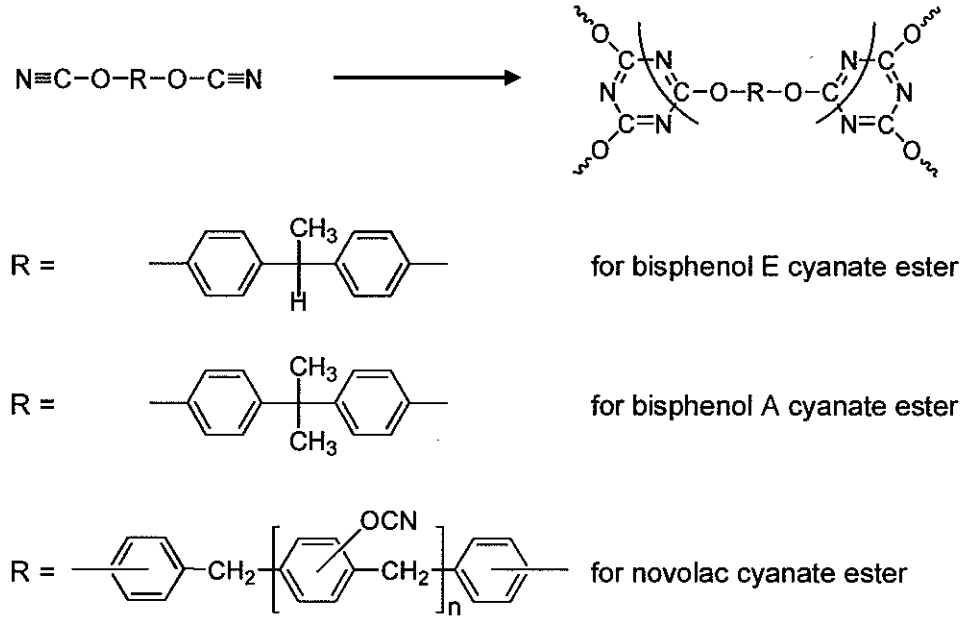

Figure 4-1. Cyclotrimerization of a multifunctional cyanate ester monomer [1,26]. The structures of the three cyanate esters that make up the commercial cyanate ester resins used in this study are shown.

Cyanate esters are a relatively new class of thermosetting polymers that have become a popular replacement for other thermosets in the aerospace and microelectronics sectors because they possess a good combination of high temperature stability and excellent mechanical properties [4]. In addition, cyanate esters have excellent adhesive properties, are more resistant to moisture absorption than other thermosets (such as bismaleimides (BMIs) and epoxies), and have very low dielectric constants [23]. These desirable properties have justified their use in a variety

of applications, despite their relatively high cost. In addition to their desirable properties in the cured state, cyanate ester resins have low oral and dermal toxicity [1] and can be processed using a variety of methods, including resin transfer molding (RTM), filament winding, hand lay-up, and composite prepregs [5]. The largest difference in processing between epoxies and cyanate esters is the latter's need for relatively high curing temperatures. Curing of cyanate esters is catalyzed by heat or a combination of heat and a catalyst, which is most commonly a carboxylate or chelate salt of a transition metal dissolved in an active hydrogen co-catalyst such as nonylphenol [1].

Cyanate esters are part of a group of polymers used in structural composites called high-temperature thermosetting matrices, a group loosely classified as crosslinked polymers that maintain their useful properties after thousands of hours in air at 200°C [1]. Most high-temperature thermosets are solids or high viscosity melts at room temperature, but an exception to this trend is a unique type of cyanate ester monomer called the bis(4-cyanatophenyl)-1,1-ethane monomer (or bisphenol E cyanate ester) [6,7]. Figure 4-2 shows the correlation between the cured state glass transition temperature (T_g) and the temperature at which an uncured thermoset monomer has a viscosity of 0.15 Pa·s (150 cP) [6]. A common cyanate ester, bisphenol A dicyanate, has a melting point of 82°C, but the bisphenol E dicyanate has excellent processing capabilities even at low temperatures with an extremely low viscosity of 0.09 to 0.12 Pa·s (90 to 120 cP) at room temperature [6,7]. Of the high-temperature thermosets shown in Figure 4-2, the BMI's (bismaleimides) and BMI-DAB's (diallyl bisphenol A bismaleimides) have the highest T_g's but have high melt viscosities. Polyimides, another class of high-temperature thermosetting polymers with high T_g's, are not shown in Figure 4-2 because their lowest melt viscosities are higher than 0.15 Pa·s (150 cP) [8].

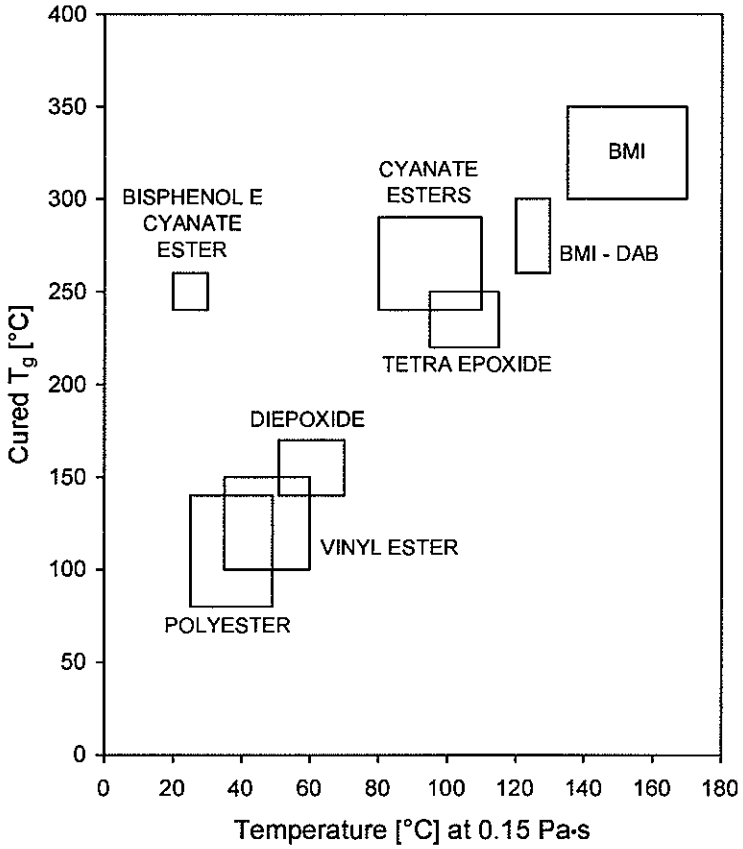

Figure 4-2. Cured T_g vs. 0.15 Pa·s (150 cP) temperature [6].

The unique properties of the bisphenol E cyanate ester monomer allow for its use as a diluent for other cyanate esters and thermosetting resins, allowing enhanced low-temperature processability. Blends of the bisphenol E cyanate ester monomer with other cyanate esters has been shown to facilitate filament winding processing by lowering the monomer viscosity [9] without sacrificing thermal stability. The low room-temperature viscosity of the monomer blend enables the resin to be applied to the filament without heating, simplifying the manufacturing process. Other applications for the bisphenol E cyanate ester that may require low-temperature processability include resin transfer molding (RTM) and wet lay-up. Bisphenol E cyanate esters reinforced with woven carbon fiber fabric have been used for wet lay-up patch repair of

composite structures because of their low viscosity, excellent fiber wetting, and thermal stability [10]. Fiber-reinforced low viscosity cyanate esters may also be good candidates for hand lay-up field repairs of metallic process components operating at high temperatures, such as pipes, pressure vessels, or exhaust structures. Current composite process repair technologies, which mainly utilize fiber-reinforced epoxies, are limited to temperatures well below 200°C [11]. A resin system with a high cured T_g that could be applied to the fiber reinforcement and the repair substrate at ambient temperatures without prior heating would expand the range of high service temperature repairs that are possible with polymer composites.

Above the T_g of fiber-reinforced polymer matrices the properties of the composite degrade significantly. Both thermoplastics and thermosetting matrix composites exhibit changes in material properties such as volume, enthalpy, heat capacity, thermal expansion, and elastic modulus through the T_g as the material goes from the glassy to the rubbery state [12]. Typically, it is necessary for the application temperature of the composite structure to be below the glass transition in order to assure that the mechanical stiffness and creep resistance of the material is satisfactory. The T_g's of highly crosslinked thermosetting resins and their composites are often measured by dynamic mechanical analysis (DMA) because of the technique's sensitivity in measuring even subtle transitions [11].

In this work, the effects that blend ratio, catalyst composition, and thermal conditioning have on the thermal and mechanical properties of carbon fiber/cyanate ester composites will be studied. Blends of two commercially available cyanate ester resins will be investigated, which have viscosities appropriate for wet lay-up. DMA will be used to determine glass transition temperatures and make comparisons for different systems.

4.3 Experimental

4.3.1 Materials

Two prepolymer blends of Bryte Technologies' (Morgan Hill, CA) EX-1510 and EX-1551-1 resins were used as the matrix in composite specimens for DMA. EX-1510 has intermediate thermal stability (post cured T_g of up to 260°C [13]), and is a low viscosity liquid at room temperature. From NMR analysis, it was determined that the EX-1510 consists mainly of bisphenol E cyanate ester monomer (see Figure 4-1 for chemical structure). EX-1551-1 is a higher viscosity resin that produces a polymer with excellent thermal stability (post cured T_g of up to 318°C [13]). From NMR analysis, it was determined that the EX-1551-1 is primarily a bisphenol A cyanate ester monomer with a small novolac cyanate ester prepolymer component. The additional cyanate groups present in the novolac cyanate ester provide additional sites for crosslinking, so the scheme for the cyclotrimerization would be slightly different. A liquid phase organometallic-based polymerization catalyst (Bryte Technologies, EX-1551-1B) was also used as a component in the prepolymer blend, in varying ratios. The composite specimens were constructed using plane weave bi-directional woven carbon fiber reinforcement with 12K tow in the warp direction and 3K tow in the fill direction (4 tows/inch in the warp direction and 8 tows/inch in the fill direction). The 12K indicates that there are approximately 12,000 carbon filaments (fibers) in each bundle (tow), while 3K indicates approximately 3,000 filaments per tow.

4.3.2 Specimen manufacturing

Two prepolymer blends were used in the test specimens: (1) 75% by weight of EX-1551 and 25% by weight of EX-1510 (denoted as "75/25") and (2) 55% weight of EX-1551 and 45% by weight of EX-1510 (denoted as "55/45"). The catalyst was mixed with the prepolymer blends in catalyst/resin weight ratios of 0.0%, 1.5%, and 3.0% (each prepolymer/catalyst system will be

denoted by the prepolymer blend ratio followed by the catalyst ratio, i.e. 75/25-1.5%). To make the composite panels, two pieces of 12K by 3K woven carbon fiber fabric, each 20 cm by 20 cm, were thoroughly wetted with the prepolymer/catalyst mixture, and placed between two sheets of Teflon® (ranging in thickness between 0.5 and 1.0 mm) on a steel pan. A 25 cm x 30 cm glass caul plate was placed on top of the top sheet of Teflon®, followed by a third sheet of Teflon® and steel bars for added weight. The weight of the steel bars was controlled such that the pressure on the glass caul plate was approximately 690 Pa (0.1 psi).

The entire setup was placed in a laboratory oven and cured for a two stage cycle, with the final cure stage conducted at 177 °C (350 °F) for 3 hours. The first stage was conducted at a lower temperature, 82 °C (180 °F), for 24 hours in order to achieve a better surface finish on the panel through a slight B-stage, which initiates partial polymerization and lowers resin flow during the 177 °C (350 °F) cure cycle. Some specimens were subjected to 2 hour post-cures at various temperatures. Specimens for DMA testing were manufactured by cutting the cured panels into specimens 10 mm wide and 45 mm long. An oil cooled diamond blade saw was used to make each cut. The average thickness of the panels and specimens was approximately 1 mm.

4.3.3 Experimental procedure

Viscosity measurements were made on the 75/25 and 55/45 prepolymer mixtures, as well as on the two constituent systems, EX-1551-1 (100/0) and EX-1510 (0/100), using a cone and plate Brookfield viscometer model CAP 2000+. The diameter of the temperature controlled plate is 5.00 cm, while the diameter and angle of the cone can be selected based on the viscosity range to be measured. For the two mixtures, a spindle rate of 900 rpm was combined with a cone angle of 1.8 degrees and a diameter of 2.4 cm corresponding to a constant shear rate of 3000 sec^{-1}. For the high viscosity EX-1551-1 system, the same spindle was rotated at 400 rpm for a constant shear rate of 1333 sec^{-1}. A constant shear rate of 12000 sec^{-1} was obtained for the low viscosity

EX-1510 (0/100) system by rotating a spindle with a cone angle of 0.45 degrees (diameter of 3.022 cm) at 900 rpm. Measurements were made from 25°C to 75°C in 5°C increments, and the average viscosity was taken from data recorded over a five minute period at each temperature. Measurements of the 100/0 system were not made below 35 °C because the torque on the viscometer exceeded the allowable level at the rotational speed used.

DMA was performed using a Tritec 2000 DMA manufactured by Triton Technology, Ltd (Keyworth, Notts, UK). The DMA was used in displacement control mode with a three-point bending fixture. Composite specimens manufactured using the six prepolymer/catalyst mixtures (75/25-0.0%, 75/25-1.5%, 75/25-3.0%, 55/45-0.0%, 55/45-1.5%, and 55/45-3.0%) were evaluated. For each set of tests, specimens were tested in the 12K fiber direction in the DMA using a constant set of test parameters: 3°C/min heating rate, 0.05 mm maximum displacement, free length of 20 mm, and frequency of 1 Hz. In addition to a DMA evaluation of the product from the initial cure (82°C for 24 hours, followed by 3 hours at 177°C), additional specimens were subjected to post cures for two hours at 204 °C (400 °F), 232C (450 °F), 260 °C (500 °F), and 288 °C (550 °F).

4.4 Results and discussion

Figure 4-3 shows plots of average viscosity vs. temperature for the four different systems. As expected, viscosity decreases with temperature, but the decrease is more pronounced for the systems with a higher content of EX-1551 (100/0 and 75/25). The system with the larger component of the low viscosity EX-1510 monomer (55/45) had a lower viscosity at all temperatures. At 75°C, the differences in viscosity between each system were small, with all viscosities being less than 0.15 Pa·s. From experience, it was noted that the room temperature (25 °C) viscosities of the 75/25 and 55/45 systems represented approximate upper and lower limits of the suitable viscosity range for wet-lay-up composite panel manufacturing or patch repair. This

gives an ideal viscosity range of between 0.5 and 1.5 Pa·s (5 and 15 Poise). In order to the use the 100/0 system for wet lay-up, the resin should be heated to at least 40 °C prior to manufacturing in order to achieve a desirable viscosity.

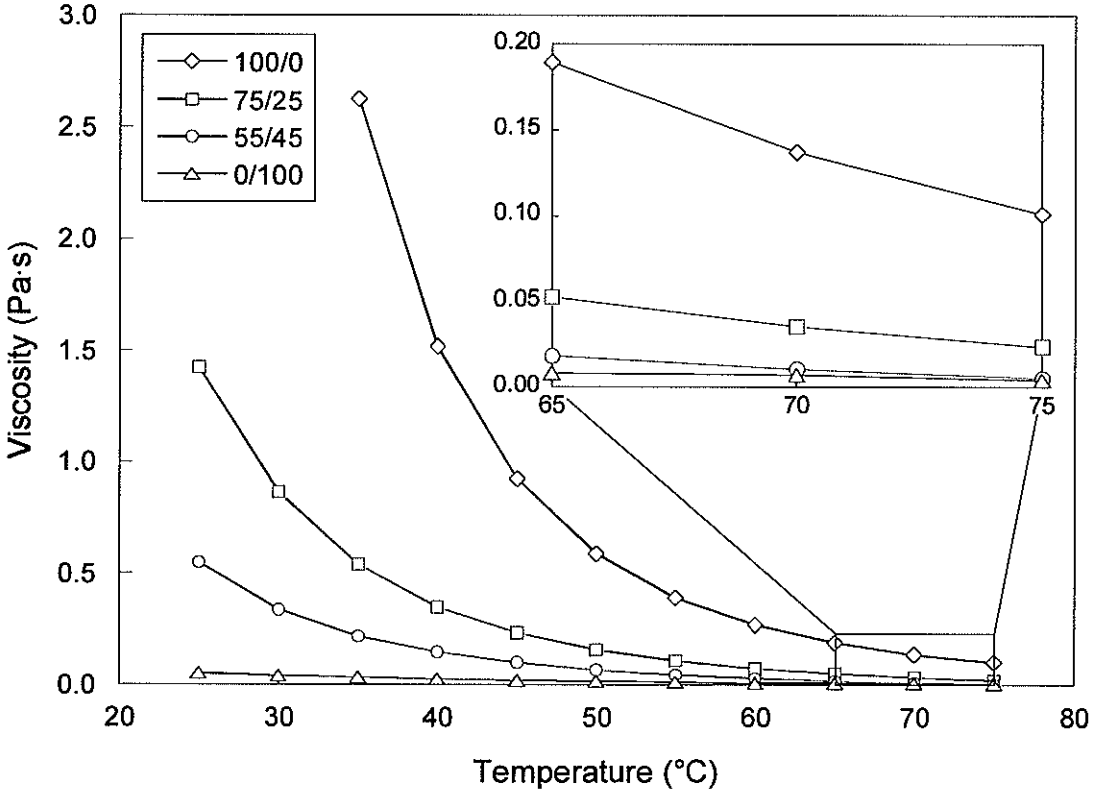

Figure 4-3. Viscosity vs. temperature for the four systems. The viscosity represents the average viscosity taken from data recorded over a five minute period at each temperature.

Figure 4-4 and Figure 4-5 show storage modulus and tan delta data for the 75/25 and 55/45 systems with 1.5% catalyst, illustrating the changes in the thermal and mechanical properties of the composite material that occur when subjected to varying cure temperatures. For the specimens with no post cure, two tan delta peaks were observed, which are denoted in the figures as T_{g1} and T_{g2}. For all catalyst ratios, the dual tan delta peak feature was most prominent for the 55/45 system (with the larger component of the EX-1510).

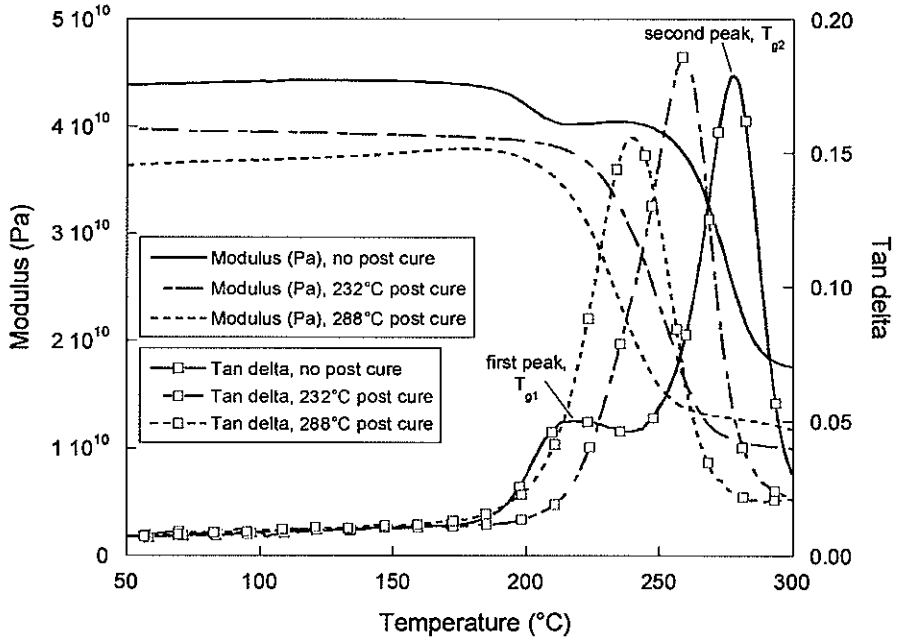

Figure 4-4. DMA data for the 75/25-1.5% system [Data taken every 15 s. Symbols are used to differentiate the curves].

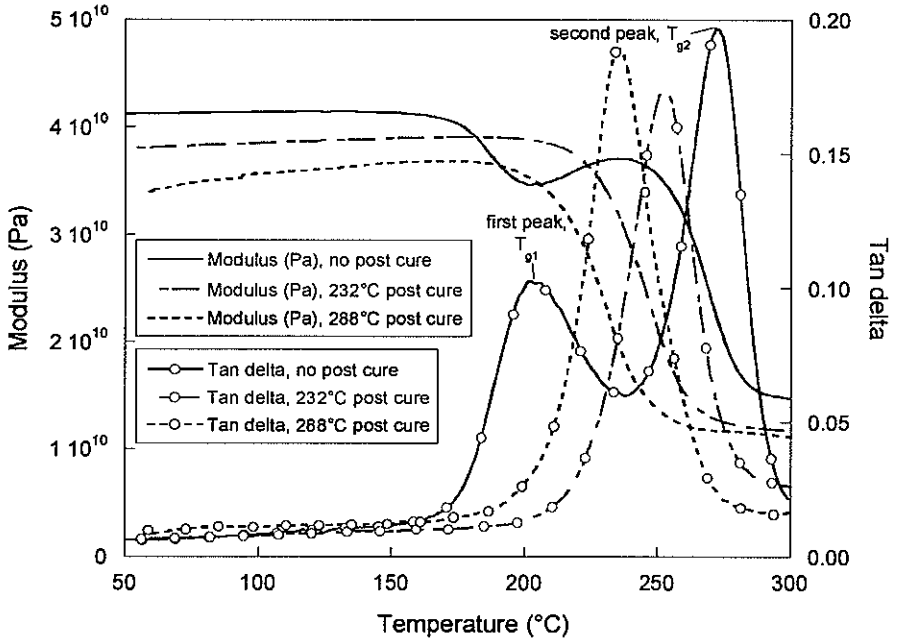

Figure 4-5. DMA data for the 55/45-1.5% system [Data taken every 15 s. Symbols are used to differentiate the curves].

This feature may be attributed to a low crosslink density and an incomplete formation of a fully integrated interpenetrating polymer network of the two polymer species. Esslinger, Jr. and Fruchtnicht observed the tan delta peak phenomenon in a similar system, and attributed it to separate polymer species that are not fully crosslinked [22]. Since the glass transitions of bisphenol E, bisphenol A, and novolac cyanate esters (the components in the systems) are each different when polymerized separately [24] and the reactivity of each cyanate ester is different, the dual tan delta peaks may represent glass transitions of the separate components of the polymer that are not fully crosslinked together. The slight increase in modulus after the first tan delta peak in Figure 4-4 and Figure 4-5 may not be significant, but could be attributed to further crosslinking of the polymer due the exposure of the material to temperatures in the post-cure range for significant amounts of time.

It is evident that post-curing at 232°C or 288°C results in a single glass transition relaxation, indicating that the crosslinked network is fully integrated at higher levels of cure. However, as the post-cure temperature is increased from 232°C to 288°C, the glass transition temperature decreases and the modulus decreases slightly for both systems. These two features indicate that thermal degradation of the matrix material is occurring, causing a reduction in crosslink density from the breaking of chain bonds [14].

Figure 4-6 shows the resulting tan delta glass transition temperature values obtained from DMA of specimens manufactured using the six cyanate ester/catalyst systems. For each catalyst amount, the 75/25 system exhibited a higher T_g than the 55/45 system. This is due to a higher content of the more thermally stable EX-1551-1. This was true for the tan delta peak T_g at every cure temperature, including each of the two tan delta peaks, T_{g1} and T_{g2}, observed for the samples without post cure. However, the difference in T_g between the 75/25 and 55/45 systems without post cure was larger for T_{g1} than T_{g2}, especially at low catalyst levels.

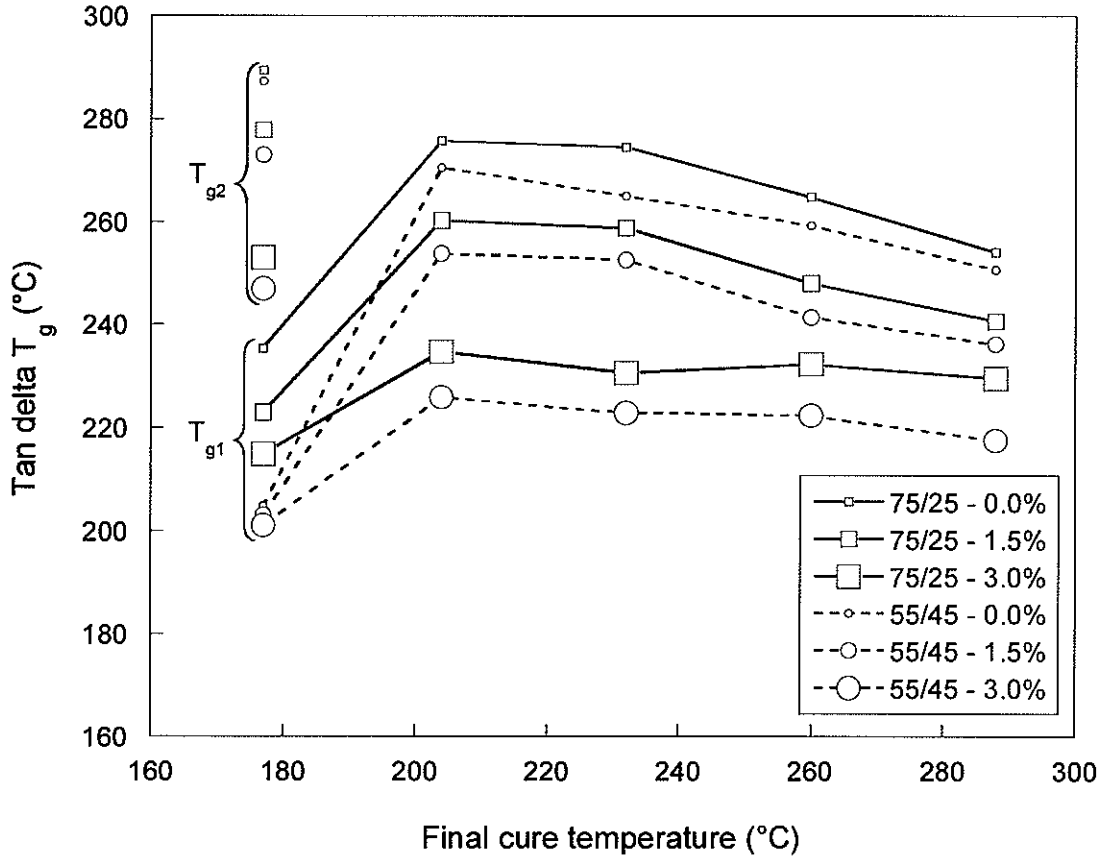

Figure 4-6. T_g vs. final cure temperature.

Post-curing at 204°C resulted in a single T_g between the two tan delta peak T_g's, T_{g1} and T_{g2}, observed for specimens without a post-cure. As the post cure temperature was increased beyond 204°C, almost every system showed a decrease in T_g with increasing post cure temperature, with the only exception being the 75/25-3.0% system, which showed similar T_g values at each final post-cure temperature.

The organometallic catalyst composition had a significant effect on the final thermal properties of the composites; for all systems, higher levels of catalyst corresponded to lower T_g values. This phenomenon seems counterintuitive, but may be attributed to the type of transition metal salt that is used in the catalyst or the amount of active hydrogen co-catalyst used (however, the composition of the catalyst used in this investigation is proprietary). It has been shown that

high zinc catalyst concentrations can cause an unusual behavior in post-cured samples, such that a 250°C post cure actually caused a decrease in the T_g of samples initially cured at 175°C [15]. This trend was not observed for other transition metal catalysts, such as manganese or cobalt. High concentrations of nonylphenol, a common active hydrogen co-catalyst used for cyanate ester resins, can also have a negative effect on T_g after post cure [15].

4.5 Conclusions

Two cyanate ester resin blends (Bryte Technologies' EX-1510 and EX-1551-1) were used to manufacture composites specimens for DMA. The two blends were chosen so that the viscosity of the liquid resin would be appropriate for the wet lay-up processing at room temperature. The EX-1510 (a bisphenol E cyanate ester monomer with extremely low viscosity at room temperature) was used as a reactive diluent in the EX-1551-1 (a bisphenol A/novolac cyanate ester with excellent thermal stability). Varying ratios of an organometallic catalyst supplied by Bryte Technologies were used, and the specimens were subjected to varying cure cycles to determine the effects that both of these parameters had on the final product.

The results of the DMA testing showed that the resin blends with a higher ratio of EX-1551-1 had better thermal properties, showing a higher glass transition temperature, T_g. Specimens that were not post cured showed a dual tan delta peak behavior, indicating that the crosslinked network of the constituent polymers had a low crosslink density and was not fully integrated. Although post curing resulted in a single glass transition and an intermediate T_g, in most cases it was found that increasing the post cure temperature lowered the T_g and modulus slightly. This decrease in T_g and modulus at high post cure temperatures was attributed to thermal degradation and reduction of crosslink density. It was also shown that increasing catalyst composition served to decrease thermal stability in the composites of each type. It is concluded that the benefit of enhanced low-temperature processability achieved with these cyanate ester

blends is only achieved at the expense of significant decreases in thermal properties. For applications of these blends that require low-temperature processability and excellent thermal stability, the lowest possible amount of EX-1510 that enables processability should be used.

4.6 Acknowledgements

The authors would like to acknowledge and thank Scott Heaton for his help in manufacturing specimens and performing tests. This material is based upon work supported under a National Science Foundation Graduate Research Fellowship. Additional funding has been provided by a NASA EPSCoR Research Initiation Grant (NCC5-586) and a grant from the Oklahoma Center for the Advancement of Science and Technology (OARS AR03(1)-050).

4.7 References

[1] Hamerton I. Chemistry and Technology of Cyanate Ester Resins. London: Chapman and Hall, 1994.

[2] Shimp DA, Christenson JR, Ising SJ. Cyanate Esters – An Emerging Family of Versatile Composite Resins. In: Proceedings of the 34th Annual International SAMPE Symposium, May 1989. p.222-233.

[3] Georgjon O, Galy J. Effects of Crosslink Density on Mechanical Properties of High Glass Transition Temperature Polycyanurate Networks. J Appl Polym Sci 1997;65(12):2471-2479.

[4] Hillermeirer R, Seferis J. Environmental Effects on Thermoplastic and Elastomer Toughened Cyanate Ester Composite Systems. J Appl Polym Sci 1997;77(3):556-567.

[5] Hamerton I, Hay J. Recent Technological Developments in Cyanate Ester Resins. High Perform Polym 1998;10(2):163-174.

[6] Shimp DA, Craig, Jr. WM. New Liquid Dicyanate Monomer for Rapid Impregnation of Reinforcing Fibers. In: Proceedings of the 34th Annual International SAMPE Symposium, May 1989. p.1336-1346.

[7] Snow AW. The Synthesis, Manufacture, and Characterization of Cyanate Ester Monomers. In: Chemistry and Technology of Cyanate Ester Resins (Hamerton, I.), London: Chapman and Hall, 1994.

[8] Meador MA. Recent Advances in the Development of High-Temperature Polymers. Annu Rev Mater Sci 1998;28:599-630.

[9] Esslinger, Jr. JR, Fruchtnicht OC. Cyanate Ester Matrix Technology for Improved Thermal Performance of Filament Wound Missile Structures. SAMPE J 2004;40(6):9-15.

[10] Mehrkam P, Cochran R. Liquid Dicyanate Ester Monomer for Elevated Temperature Composite Repair Applications. In: Proceedings of the American Society for Composites, 1992. p.12-21.

[11] Smith P. Composite Solution. Process Eng (London) 2004;85(5):15-17.

[12] Pascault J-P, Sautereau H, Verdu J, Williams R. Thermosetting polymers. New York: Marcel Dekker, Inc., 2002.

[13] Product Technical Data, Bryte Technologies, Inc., Morgan Hill, CA.

[14] Chung K, Seferis JC. Evaluation of Thermal Degradation of Carbon Fiber/Cyanate Ester Composite. Polym Degradation Stab 2001;71(3):425-434.

[15] Hay JN. Processing and Cure Schedules for Cyanate Ester Resins. In: Chemistry and Technology of Cyanate Ester Resins (Hamerton, I.), London: Chapman and Hall, 1994.

CHAPTER 5: DYNAMIC MECHANICAL ANALYSIS OF FUMED SILICA/CYANATE ESTER NANOCOMPOSITES

A paper to be submitted to *Composites Part A: Applied Science and Manufacturing*

William K. Goertzen[1,2] and M.R. Kessler[1,3]

5.1 Abstract

Fumed silica particles with average primary particle diameters of 12 and 40 nm were combined with a low viscosity bisphenol E cyanate ester resin to form composite materials with enhanced storage modulus and reduced damping behavior, as evidenced by dynamic mechanical analysis (DMA). The storage modulus increased with volume fraction of fumed silica in both the glassy and rubbery regions, but the increase was more pronounced in the rubbery region. The maximum increase in storage modulus in the glassy region was 75% for 20.7 vol% of 40 nm fumed silica, while the same composition showed a 231% increase in the rubbery storage modulus. Furthermore, decreases in damping showed that the polymer-particle interfacial adhesion was significant, and the effective interphase thickness was estimated to be as high as 13.2 nm for the 40 nm particles and 7.1 nm for the 12 nm fumed silica. The glass transition temperature, T_g, of the nanocomposites was not changed significantly with increasing volume fraction. However, it was shown that the addition of fumed silica of both sizes increased T_g at low cyanate ester conversions (low post cure temperatures), but decreased T_g at high conversions (high post cure temperatures).

---

[1] Graduate student and Assistant Professor, respectively, Department of Materials Science and Engineering, Iowa State University

[2] Primary researcher and author

[3] Author for correspondence

5.2 Introduction

Cyanate esters are an important class of high-temperature thermosetting polymers, which have excellent thermal and mechanical properties. A unique type of cyanate ester monomer called the bis(4-cyanatophenyl)-1,1-ethane monomer (or bisphenol E cyanate ester) is under investigation for use in resin-injection repair of high-temperature composites. The bisphenol E cyanate ester (BECy) is unlike other high temperature thermosets in that instead of existing as a solid at ambient conditions, it has an extremely low viscosity, 0.09 to 0.12 Pa·s (90 to 120 cP), at room temperature [1]. The low viscosity of this monomer at room temperature gives it excellent processability for many applications [2-4], and the cured polymer has a high glass transition temperature and excellent mechanical properties [5,6].

Fumed silica is well studied and has seen wide application as an agent to reinforce and modify the rheological properties of liquids, adhesives, and elastomers. Fumed silica has been used extensively with thermosetting polymers such as epoxies [7-11], polyurethanes [12,13], and polyesters [14] to modify processing and end-use mechanical properties. While the use of fumed silica with cyanate esters is discussed in the patent literature in various applications such as bleed-resistant cyanate ester adhesives [15,16], there has not been a study to date on the reinforcement of cyanate esters with fumed silica. In this work, the dynamic mechanical properties of fumed silica/cyanate ester nanocomposites are investigated using hydrophilic fumed silica with two primary particle diameters: 12 nm and 40 nm, with specific surface areas of 200 m^2/g and 50 m^2/g, respectively. In our parallel work, the effect that both particle size and volume fraction has on other properties, such as rheology, curing kinetics, and thermal expansion, was studied [17,18].

Here we report the effect of both particle size and volume fraction on storage modulus, damping behavior, and glass transition temperature. We compare the composites' storage modulus data to applicable theory for particulate-reinforced composite materials, comparing the

increase in storage modulus in both the glassy and rubbery regions. While the elastic modulus may not be significantly affected by interfacial adhesion, damping behavior is very sensitive to the polymer-particle interaction state [19-21]. We attempt to estimate the polymer-particle interaction by analysis of the decrease in damping realized through the addition of varying volume fractions of filler. It is suggested that the hydroxyl functionality of the fumed silica is responsible for a strong interaction with the polymer matrix through the formation of covalent bonds. Finally, factors that affect the glass transition temperature of the nanocomposites are discussed.

5.3 Experimental

5.3.1 Materials

The BECy monomer used is a commercially available resin and catalyst from Bryte Technologies (Morgan Hill, CA) called EX-1510. The liquid phase organometallic-based polymerization catalyst (Bryte Technologies, EX-1510-B) was supplied with the resin and was used at the manufacturer's suggested loading of 3 phr (parts per hundred resin). Hydrophilic fumed silica was supplied by Degussa (Frankfurt, Germany) under the trade names of AEROSIL® 200 and AEROSIL® OX 50 (CAS No.: 112945-52-5, synthetic amorphous, pyrogenic silica, purity $\geq$ 99.8%, true density = 2.2 g/cm^3). AEROSIL® 200 has an average primary particle diameter of 12 nm and a specific surface area of 200 m^2/g [22]. AEROSIL® OX 50 has an average primary particle diameter of 40 nm and a specific surface area of 50 m^2/g [22]. The flame hydrolysis process used to make fumed silica yields mostly aggregates (primary particles sintered together) that are about 0.2 to 0.3 μm in diameter [23].

5.3.2 Specimen manufacturing

BECy monomer/fumed silica suspensions were prepared by adding the fumed silica during mixing of the monomer with a 25 mm diameter high-shear blade at 1000 rpm. For the 12 nm particles, compositions of 0.5, 1, 2, 5, and 6.72 phr were made, with 6.72 phr (3.4 vol%) representing the maximum loading achieved with ease of processing. For the 40 nm particles, the compositions included 0.5, 1, 2, 5, 10, 20, 35, and 49.2 phr (max loading), representing volume fractions of up to 20.7 vol%. Prior to mixing, the fumed silica was dried under vacuum and the BECy monomer was preheated to 60 °C. The partially dispersed suspension was processed using a Fisher Model 100 Sonic Dismembrator with 3.2 mm diameter probe tip for 30 seconds at a frequency of 23 kHz. The power output ranged between 16 and 18 Watts during sonication. After sonication, the suspension was again mixed for 2 minutes at 2000 rpm, followed by an additional 30 seconds of sonication. The temperature of the suspension was maintained between 50 and 65 °C throughout the entire process. A predetermined amount of catalyst was added to the dispersed suspension, corresponding to 3 phr, and mixed at 2000 rpm for 2 minutes, followed by 15 seconds of sonication at the same power level. Finally, the suspensions were poured into high-temperature silicone rubber molds (27 × 48 × 8 mm^3) and degassed at 60 °C for 1 hour under vacuum at 23.4 mmHg, and then placed in a convection oven (preheated to 60 °C) for the final curing process (heat to 180 °C at 1 °C/min, hold for 2 hours, heat to 250 °C at 1 °C/min, hold for 2 hours and cool to ambient at 5 °C/min). Samples were machined from the solid block of material using a diamond blade saw (TechCut 5™ Precision Sectioning Machine with Diamond Wafering Blade, Low-Concentration Diamond Metal Bonded, 6" × .020" × ½", Allied High Tech Products, Inc.). Specimens for dynamic mechanical analysis (DMA) were machined to 23 × 6 × 1.6 mm^3, such that the thickness of each specimen varied by less than 15 μm over its length. Samples for a post-cure study were prepared at 1 phr in the same manner, except the final cure stage at 250 °C was eliminated, such that the initial cure cycle was: heat to 180 °C at 1 °C/min,

hold for 2 hours, and cool to ambient at 5 °C/min. After machining the specimens, free-standing post-cures were conducted at temperatures of 180, 210, 240, and 270 °C for 2 hours. Neat BECy control samples without fumed silica were prepared in the same manner as above. All samples were dried at 120 °C under vacuum for 6 hours and kept in a dry environment prior to testing.

5.3.3 Experimental procedure

Samples were tested using a TA Instruments (New Castle, Delaware, USA) DMA (Dynamic Mechanical Analyzer) Q800 with LN_2 GCA (Gas Cooling Accessory) from 30 °C to 330 °C at a heating rate of 3 °C/min. A constant amplitude of 30 μm at 1 Hz was applied throughout the test, with a static load tracking at 175% of the dynamic force. A low-friction three-point bending fixture with a length of 20 mm was utilized for each test. For each condition, multiple samples were tested (from 2 to 6) and the data was averaged. For measurements where the standard deviation was more than the size of the symbol used in plots, error bars representing one standard deviation were included.

5.4 Results and discussion

5.4.1 Storage modulus

Representative curves for storage modulus (E', the elastic component of the viscoelastic response) versus temperature for the 12 nm composites are shown in Figure 5-1. With an increase in volume fraction (ϕ_f), the magnitude of the storage modulus is increased in the glassy and rubbery regions, and all composites show the characteristic drop in modulus around the glass transition temperature, T_g, of the material. For the 40 nm fumed silica nanocomposites, representative storage modulus vs. temperature curves are shown in Figure 5-2.

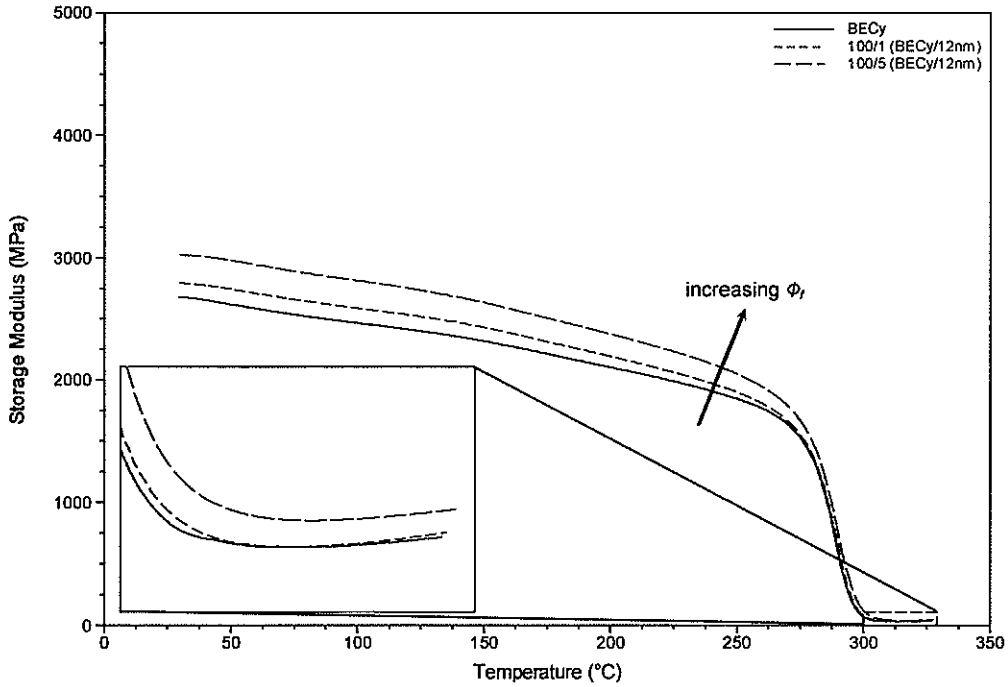

Figure 5-1. Storage modulus (E') versus temperature for 12 nm fumed silica nanocomposites.

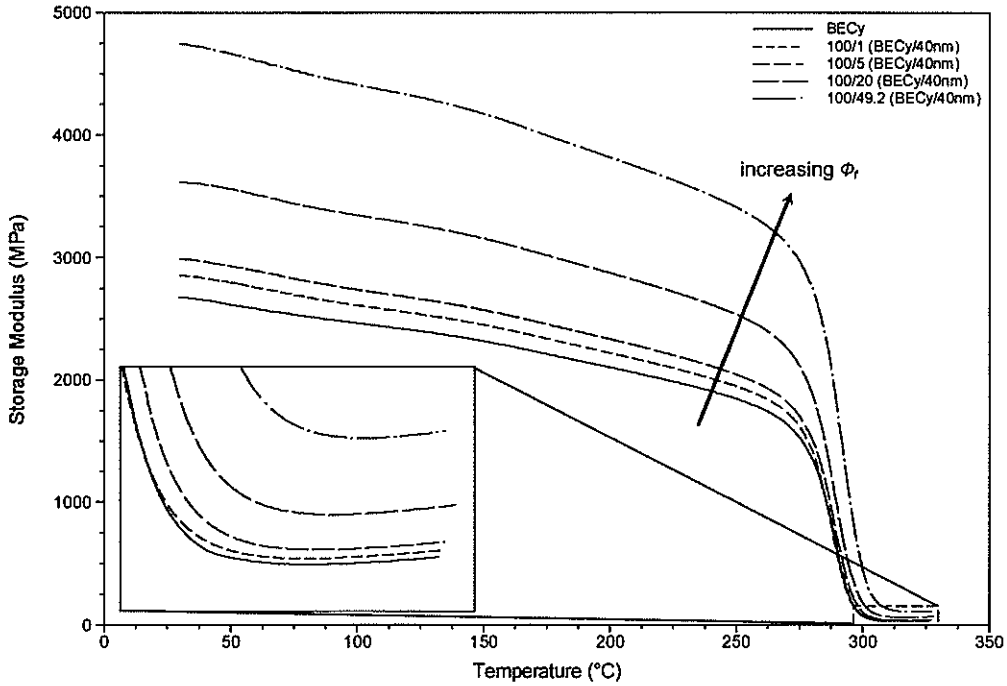

Figure 5-2. Storage modulus (E') versus temperature for 40 nm fumed silica nanocomposites.

For the 40 nm composites, there is also an increase in storage modulus with increased volume fraction of fumed silica. As expected, the largest increase in modulus for the 40 nm nanocomposites is for the sample at the highest loading (49.2 phr, 20.7 vol%), which represents an increase of approximately 75% over the unfilled system. The increase in storage modulus at 30 °C as a function of volume fraction for both sizes of fumed silica is shown in Figure 5-3, along with theoretical predictions. The isostress model (or Reuss average) assumes that the matrix and filler are stressed equally, giving the composite modulus, E_c, as

$$E_c = \left(\frac{\phi_f}{E_f} + \frac{\phi_m}{E_m} \right)^{-1} \qquad (1)$$

where E_f is the modulus of the filler, E_m is the modulus of the matrix, ϕ_f is the volume fraction of the filler, and ϕ_m is the volume fraction of the matrix [24]. This model gives a theoretical lower bound for the composite modulus. The absolute upper bound would be given by an isostrain model, such as the rule of mixtures, where a constant strain is assumed in each of the phases. This is more suitable, however, for composites with unidirectional reinforcement and is not shown here. The predictions by the well-known Halpin-Tsai equations [25], which are explained elsewhere, are shown for the sake of comparison, with the assumption of a circular geometry factor. Possibly the most applicable model for particulate-reinforced composites is the Kerner equation, which is analogous to an equivalent model by Hashin and Strikman [26]. Lewis and Nielsen gave the Kerner equation in a generalized form, where the ratio of the modulus of the composite to the modulus of the matrix is given by

$$\frac{E_c}{E_m} = \frac{1 + AB\phi_f}{1 - B\psi\phi_f} \qquad (2)$$

where A is a constant related to the filler geometry and the Poisson's ratio of the matrix [26].

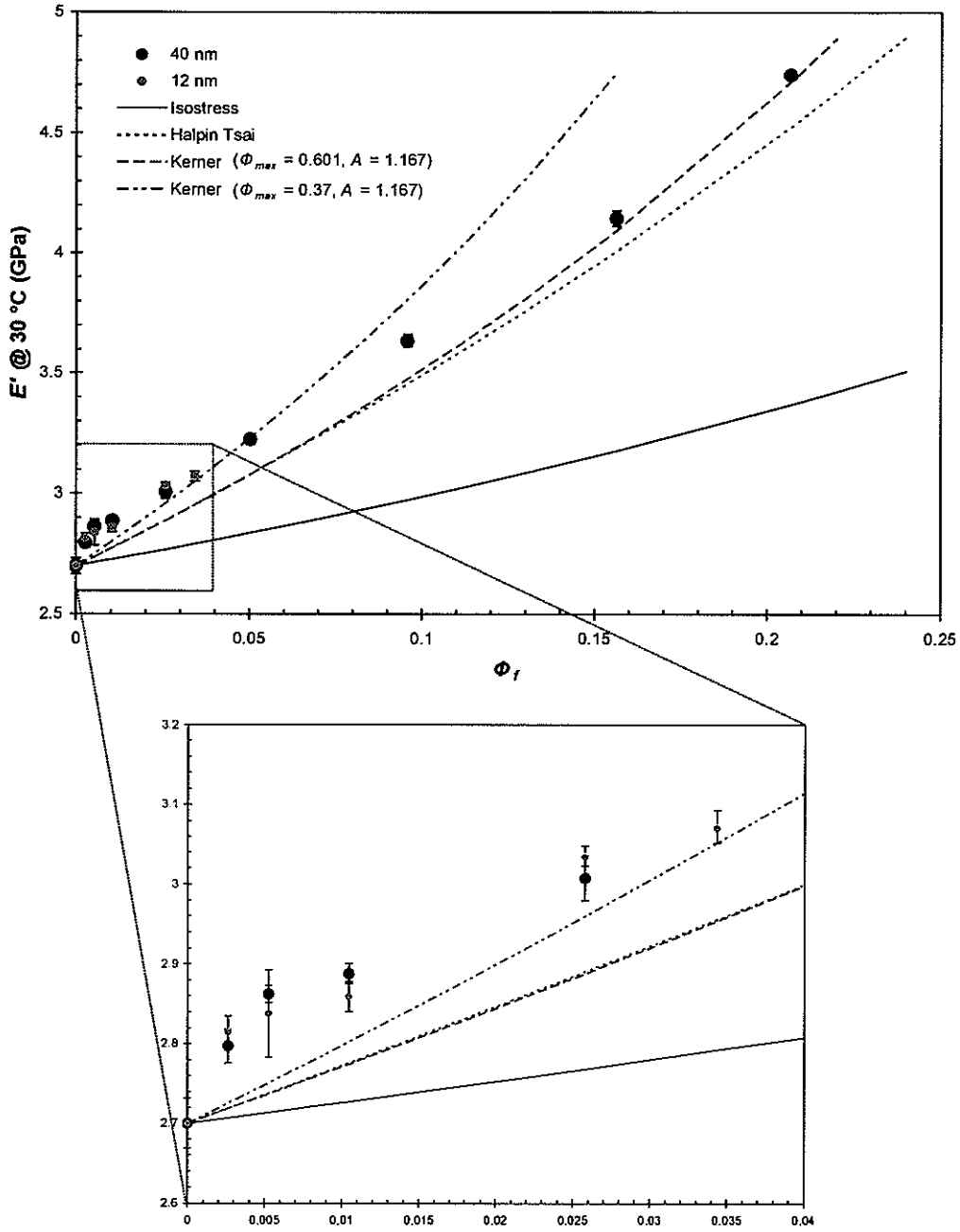

Figure 5-3. Storage modulus at 30 °C vs. volume fraction of fumed silica.

For the general case of spherical particles in a matrix, A is given by: $A = (7-5\nu)/(8-10\nu)$, where ν is the Poisson's ratio of the matrix. However, A can be larger for different filler geometries, such as reinforcements with aspect ratios [26]. The constant, B is given by

$$B = \frac{E_f / E_m - 1}{E_f / E_m + A}. \qquad (3)$$

The limit of B is 1, where the modulus of the filler is much greater than the modulus of the matrix. The ψ term is dependent on the maximum packing fraction of the particles, ϕ_{max}, and can be calculated using an equation by Lewis and Nielsen or McGee and McCullough with nearly identical results [21,26]. From McGee and McCullough, ψ is given as

$$\psi = 1 + \frac{\phi_m}{\phi_{\max}}\left[\phi_{\max}\phi_f + (1 - \phi_{\max})\phi_m\right]. \qquad (4)$$

The maximum packing fraction, ϕ_{max}, is the ratio of the true volume of the filler to the apparent volume occupied by the filler, and has a maximum of 0.74 for hexagonal close packing spheres but decreases for agglomerated spheres to as low as 0.37 [26].

For all volume fractions, the isostress and Halpin-Tsai equations underestimate the composites' modulus at 30 °C. The best fit to the data is shown by the Kerner equation, where A is 1.167 (for matrix Poisson's ratio of 0.35), and either a ϕ_{max} of 0.601 (for random loose packing, non-agglomerated [26]) or 0.37 (random close packing, agglomerated). While the maximum packing factor of 0.601 gives good approximation at high loadings, 0.37 gives better fit at intermediate loadings. However, neither model will fit the data at low fractions, starting with the anomalous increase of approximately 4% in modulus for only 0.25% by volume of fumed silica. Interestingly, this result was very similar for both sizes of fumed silica, with a slightly larger increase in modulus realized for the 12 nm particles. In general, however, the packing factor of 0.601 gives the best fit to that data because it does not grossly overestimate the modulus at high volume fractions.

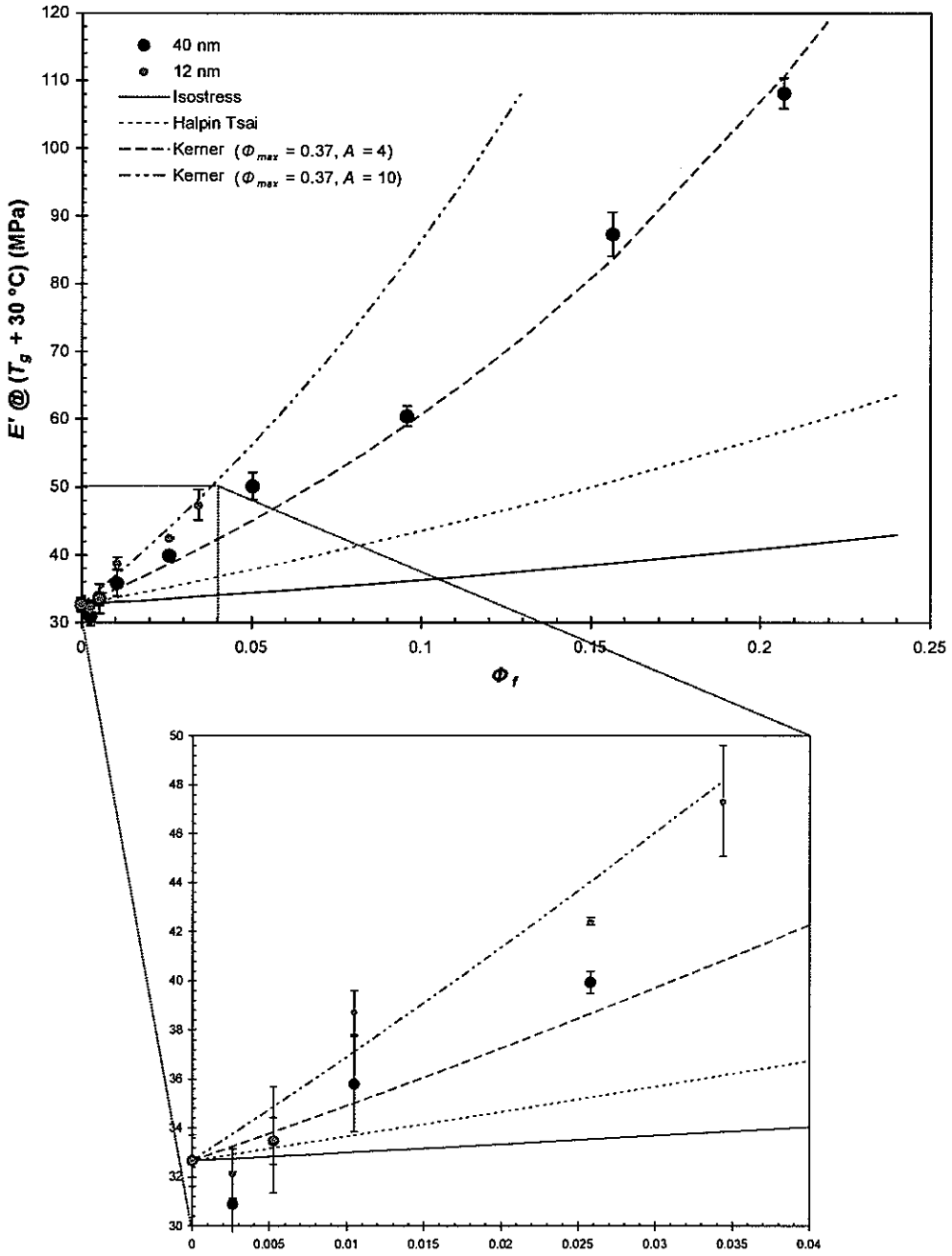

Figure 5-4. Rubbery storage modulus (@ T_g + 30 °C) vs. volume fraction.

For the rubbery region, the increase in modulus with volume fraction is more pronounced. Figure 5-4 shows this relationship for the storage modulus taken at T_g + 30 °C,

where the T_g is defined for this purpose as the peak in the loss modulus, E'' (the viscous component of the viscoelastic response). There is a general increasing trend in the composites' rubbery modulus for both sizes of fumed silica above $\phi_f = 0.005$, but anomalously there is a slight decrease in the rubbery storage modulus at the lowest volume fraction, $\phi_f = 0.0025$, where the marked increase was observed in the glassy region. This may not be significant, as the standard deviation for the rubbery modulus at these loadings actually includes the base value of the resin (See Figure 5-4). Also, due to the fact that these values are taken at 30 °C above T_g, there may be slight temperature effects due to the changes in T_g for each composition. Regardless, above 0.5 vol%, there is a marked improvement in rubbery modulus, such that the Halpin-Tsai equations greatly underestimate the increase in modulus. In order to provide a fit to the experimental data in the rubbery region, a ϕ_{max} of 0.37 (random close packing, agglomerated) must be adopted. All packing factors larger than this underestimate the increase in modulus. Furthermore, using A = 1.5 (for rubber Poisson's ratio of 0.5) underestimates the modulus, such that a value for A of 4 is needed for the 40 nm composites, while an A of 10 is needed for the 12 nm particles. In general, the value for A will increase if the aspect ratio of the filler increases, and the same result is given for agglomerated fillers [26].

The trend of a greater increase in modulus in the rubbery region than for the glassy region is not new; this has been observed by several researchers for both micron- and nano-sized filler composites [20,21]. Goyanes et al. [20] showed a similar result for quartz/epoxy composites, attributing this to the fact that, below T_g, the rigid polymer matrix can exert large forces on the agglomerates, causing some particle motion and slippage, and a decrease in modulus. For the rubbery state, however, the relaxation of the matrix allows the agglomerates to stay rigid and provide more reinforcement [20]. Vassileva and Friedrich [21] also showed this phenomenon for alumina nanoparticle/epoxy composites.

The storage modulus data suggests that there is a presence of agglomerates in the nanocomposites, which are more prevalent in the rubbery state, especially for the 12 nm particles. This is consistent with analysis of TEM micrographs for the composites, as shown in Figure 5-5 and Figure 5-6.

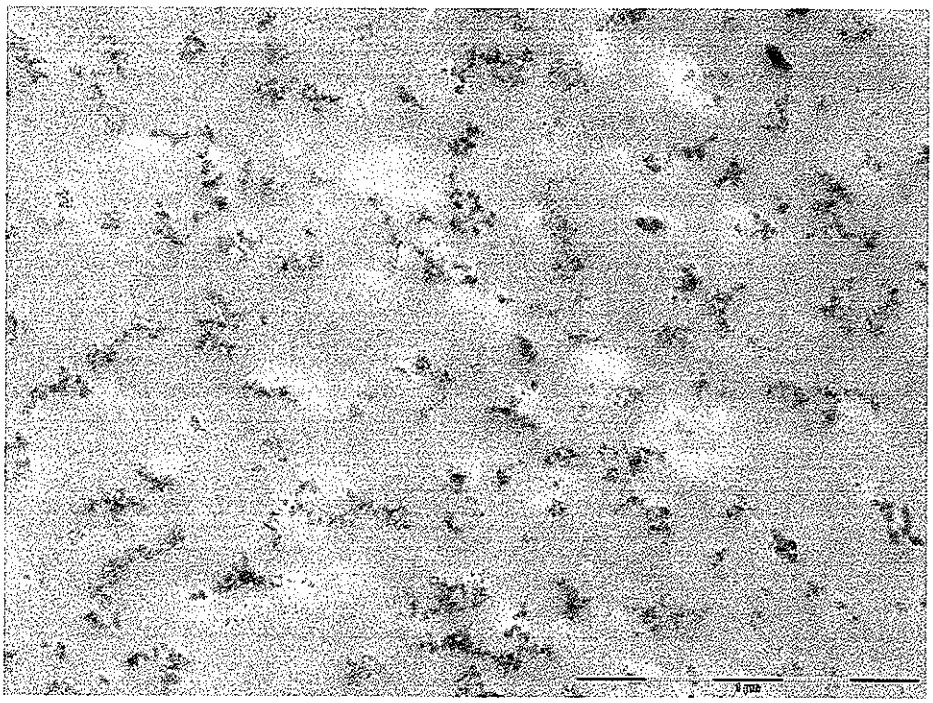

Figure 5-5. TEM micrograph of 12 nm composite at loading of 2.6 vol%, scale bar is 1 μm.

It is obvious that the smaller fumed silica particles (12 nm) form much more dominant agglomerates (aggregates entangled together) than the 40 nm particles. For the 40 nm composite, there are aggregates and agglomerates of a small number of particles and some particles that exist alone, while for the 12 nm particles, nearly all particles exist as agglomerates of many particles. Although the total aggregate and agglomerate size is larger, the larger 40 nm particles behave more like dispersed spheres than the highly aggregated and agglomerated 12 nm particles. This explains the need for a higher A for the 12 nm particles in the rubbery region, since these agglomerates have a much more dominant effect above T_g.

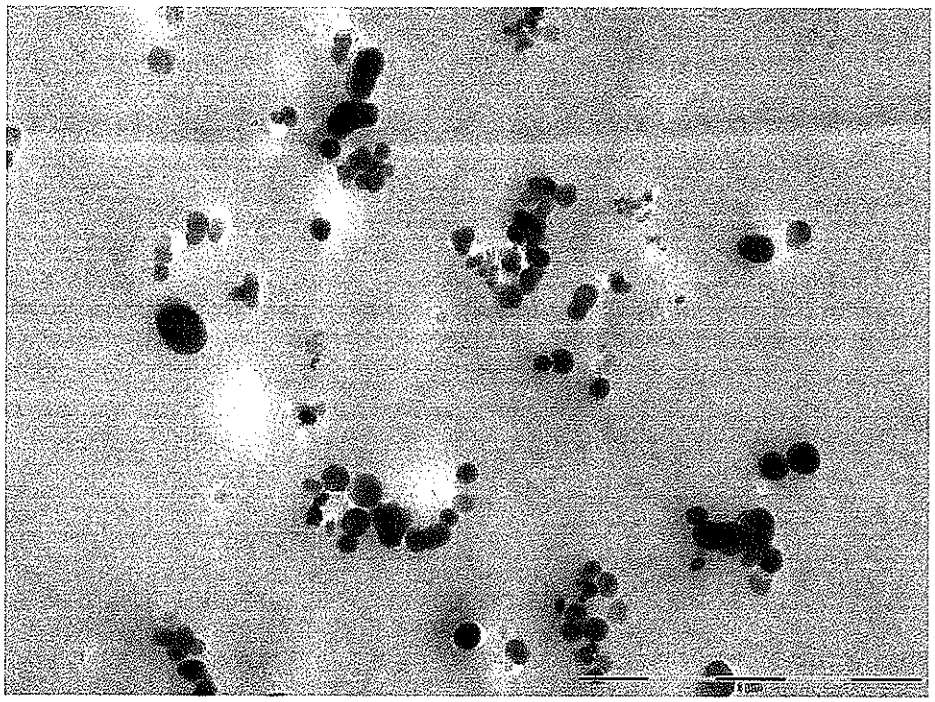

Figure 5-6. TEM micrograph of 40 nm composite at loading of 2.6 vol%, scale bar is 1 μm.

5.4.2 Tan delta

Figure 5-7 shows tan delta (E''/E', ratio of energy dissipated to energy stored per cycle) as a function of temperature for the 12 nm nanocomposites, and Figure 5-8 shows tan delta for the 40 nm nanocomposites.

While the peak position does not change drastically (indicating little change in T_g, which will be discussed later), the magnitude of the tan delta peak decreases with increasing filler content for both particle sizes. If the damping of the rigid filler is neglected, the decrease in damping as a result of replacing polymer with filler is given by

$$\tan\delta_c = \tan\delta_m\left(1-\phi_f\right) \qquad (5)$$

where $\tan\delta_c$ is the damping of the composite and $\tan\delta_m$ is the damping of the matrix [21,26]. However, the damping of the composite can decrease beyond the prediction of Equation 5 if there

is a significant interaction between the filler and matrix, such that a correction parameter, P, is introduced [20,21], giving

$$\tan\delta_c = \tan\delta_m\left(1 - P\phi_f\right). \qquad (6)$$

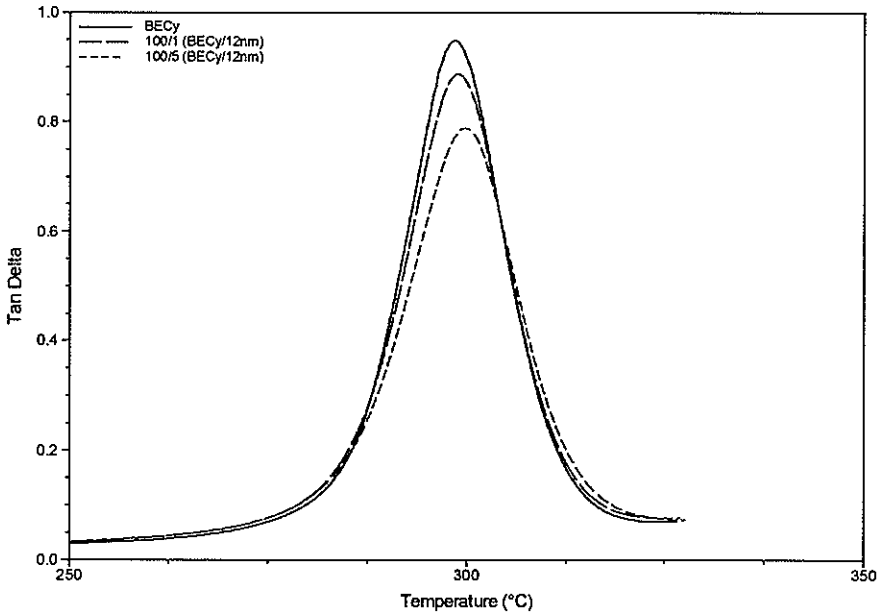

Figure 5-7. Tan delta (damping) as a function of temperature near the glass transition (12 nm).

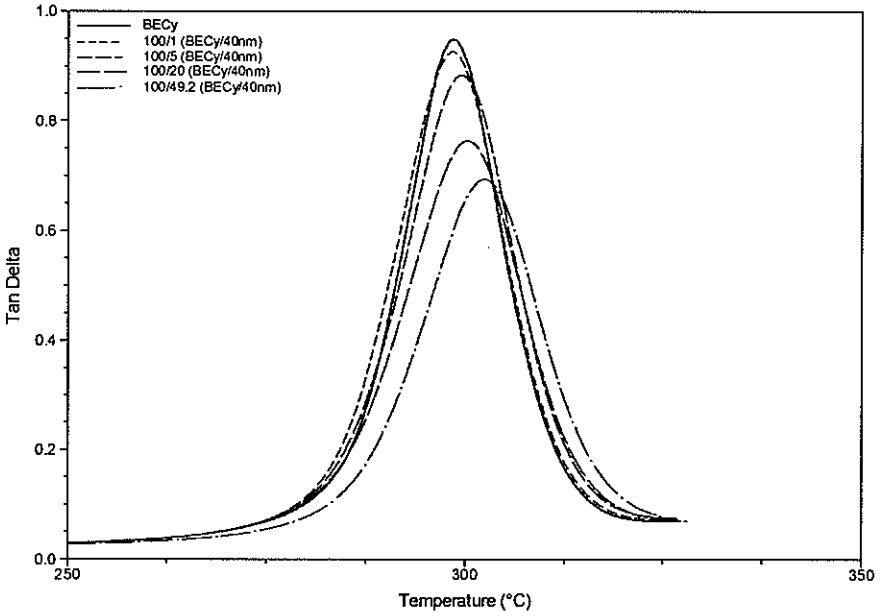

Figure 5-8. Tan delta (damping) as a function of temperature near the glass transition (40 nm).

The effective interfacial thickness of the interphase between the polymer and particle, ΔR, is related to P by

$$P = \left(1 + \frac{\Delta R}{R}\right)^3 \qquad (7)$$

where R is the radius of the particles in question [20,21].

Using Equations 6 and 7, the interfacial thickness, ΔR, was estimated through comparison of the data for each composite with the matrix, yielding estimates of the effective thickness, which are tabulated in Table 5-1.

Table 5-1. Interphase thickness estimation from damping behavior for 12 and 40 nm silica.

phr (12 nm)	Φ_f	ΔR [nm]
0.5	0.003	6.4
1	0.005	7.1
2	0.010	5.4
5	0.026	5.0
6.72	0.034	4.5
Avg. ΔR [nm] for 12 nm:		**5.7**

phr (40 nm)	Φ_f	ΔR [nm]
0.5	0.003	12.3
1	0.005	4.0
2	0.010	13.2
5	0.026	7.3
10	0.050	5.6
20	0.096	4.9
35	0.156	2.7
49.2	0.207	1.6
Avg. ΔR [nm] for 40 nm:		**6.4**

There is a general decreasing function of ΔR with respect to volume fraction, possibly indicating that as volume fraction increases, particle agglomeration is increased, which decreases the available free surface area of the particles to interact with the cyanate ester matrix. For $\phi_f =$

0.005 with the 40 nm composites, ΔR is quite low compared to the surrounding data, but this result was rechecked and there is no apparent explanation for the presence of this outlier.

The presence of a strong interface between the cyanate ester matrix and the fumed silica particles is in agreement with the literature on cyanate ester composites. This is due to the abundant presence of hydroxyl groups on the silica particles' surface. In fact, it has been shown by Liang et al. that Polyhedral Oligomeric Silsesquioxane (POSS) with hydroxyl functionality form covalent bonds with cyanate esters via iminocarbonate groups [27]. Furthermore, hydrogen bonding can occur between the hydroxyl and cyanate groups of the silica and cyanate esters, respectively [27]. Cyanate esters have also been shown to form covalent bonds with substrate hydroxyl groups on other surfaces, such as glass and carbon fibers and metallic substrates [28]. The average ΔR for the 40 nm composites is slightly greater than for the 12 nm composites, but there is a much larger change in ΔR for the 40 nm composites. This may indicate that at low volume fractions, the 40 nm composites have many individual particles or small aggregates, which have a large amount of available surface area, but at large volume fractions, the 40 nm particles are highly agglomerated, decreasing the amount of available surface area. This is consistent with the observations made through TEM, as shown in Figure 5-5 and Figure 5-6. For the 12 nm particles, agglomeration is pronounced at all volume fractions such that the decrease in ΔR with volume fraction is not as substantial.

5.4.3 Glass transition

Figure 5-9 shows the glass transition temperatures for the 12 and 40 nm composites, calculated by three methods: 1) Onset of the drop in storage modulus, 2) Loss modulus peak, and 3) Tan delta peak.

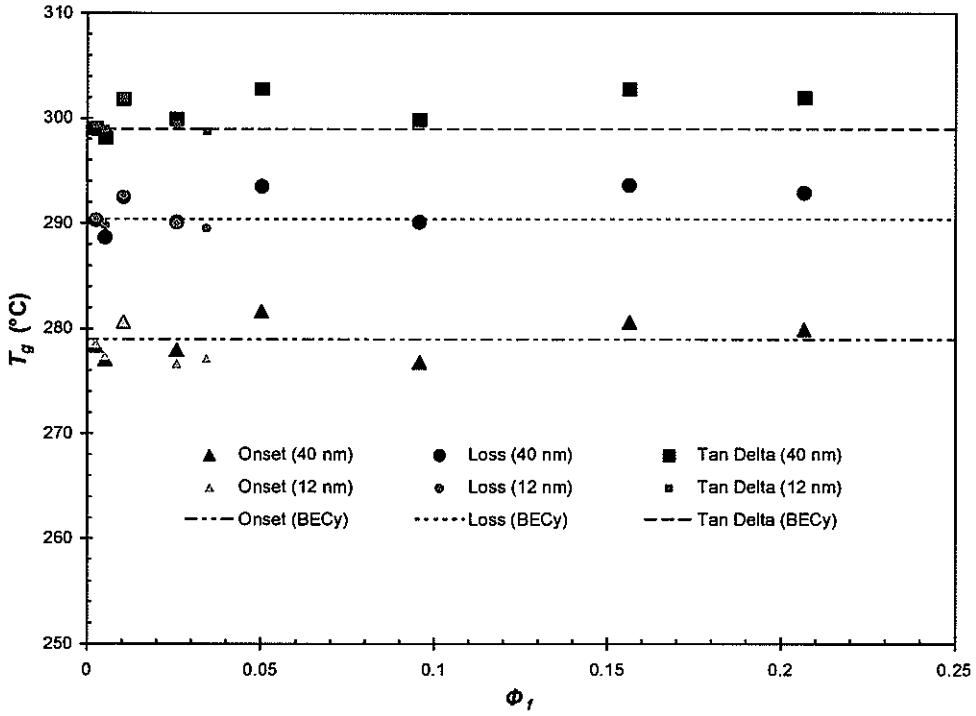

Figure 5-9. T_g versus volume fraction of fumed silica, with horizontal lines indicating the glass transition temperature of the neat BECy resin. Error bars are on same order as symbol size.

It is apparent that there are only very small changes (± < 4 °C) in glass transition temperature for all volume fractions. While a discernable trend is not immediately obvious, it is interesting to note that the T_g's for the 12 and 40 nm samples follow the same trend. This indicates sources of systematic error because the equal volume fraction samples were prepared side by side. While all efforts were made to limit the moisture exposure of the fumed silica between drying and incorporation into the cyanate ester monomer, the relative humidity of the laboratory varied from day to day, from as little as 19% RH to 60% RH. In fact, if only the samples prepared during conditions of less than 20% relative humidity are considered, as shown in Figure 5-10, the T_g increases at each volume fraction.

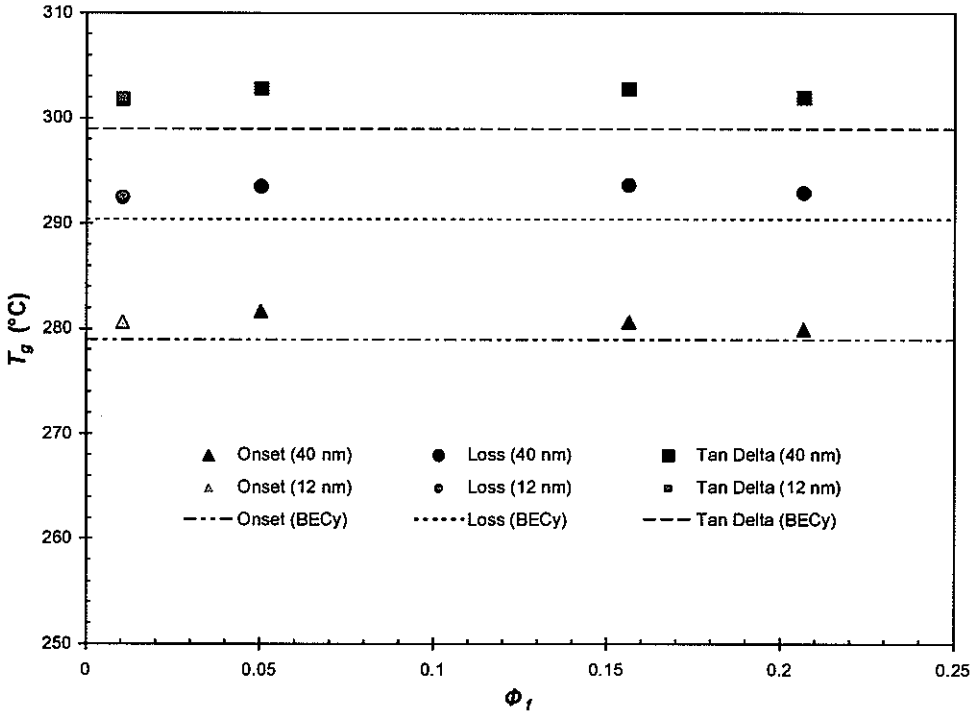

Figure 5-10. T_g versus volume fraction of fumed silica, with horizontal lines indicating the glass transition temperature of the neat BECy resin (Samples prepared in humid conditions were eliminated from this graph).

Our hypothesis was tested by making identical samples on different days. For example, the T_g in 2 phr samples (both 12 and 40 nm) decreased between 2 and 3 °C for a change between 19% and 49% RH. Furthermore, the decrease for the 12 nm samples was larger, which is consistent with the fact that the 12 nm particles have more surface area with which to absorb moisture. It should be noted, however, that other properties, such as modulus and damping, were not affected by the changes in humidity.

To ascertain more information on the effect of the silica nanoparticles on the glass transition temperature of the nanocomposites, a study on the effect of post cure temperature was conducted for a single volume fraction of both 12 and 40 nm particles. The results are shown in Figure 5-11.

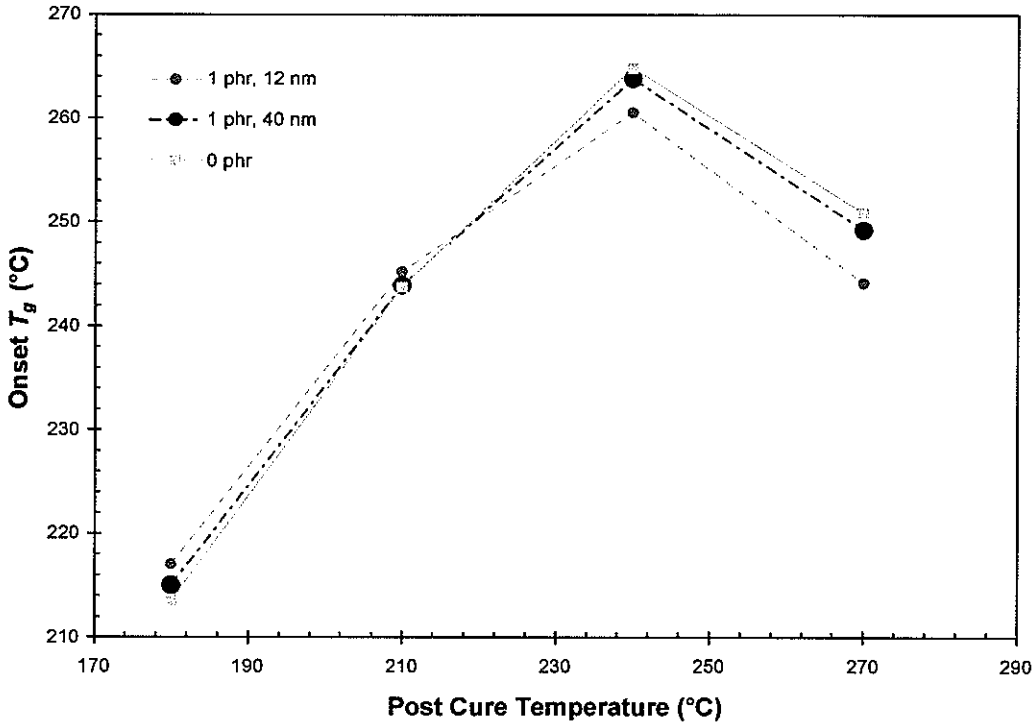

Figure 5-11. T_g vs. post-cure temperature for 1 phr samples.

These results clearly show that at low conversions, the T_g of the nanocomposites is higher, while at high conversions, the T_g is lower than the neat BECy resin. For the highest post-cure temperature, 270 °C, there is a reduction in T_g of all samples including the neat resin, which indicates that thermal degradation is occurring at these temperatures. There are three major factors that affect the glass transition temperature of these nanocomposites. First, the incorporation of the rigid fumed silica into the crosslinked network of cyanate ester serves to decrease segmental motion, which would serve to increase T_g. Second, the incorporation of the fumed silica into the polymer will decrease the overall cross-link density of the resin per unit volume, which would decrease T_g. Third, the fumed silica may add free volume because of disruption in packing of the cyanate ester resin segments, decreasing T_g. For low conversions, the incorporation of fumed silica into the polymer network gives a positive effect on T_g because there

is an excess of unreacted cyanate groups that can link to the fumed silica and decrease large scale segmental motion. For high conversions, however, there is a negative effect on T_g because the increase in T_g due to the first factor is not enough to overcome the decrease in T_g due to a reduction in cross-link density and increase in free volume, as compared to the neat cyanate ester that nears complete conversion.

5.5 Conclusions

Fumed silica particles of varying sizes increased the storage modulus of cyanate ester nanocomposites, according to results from DMA of cured samples. The storage modulus was increased more significantly in the rubbery region, which was consistent with the results of previous studies. The 12 nm particles increased the rubbery storage modulus to a greater degree, indicating the presence of dominant agglomerates, which was confirmed by TEM. The decrease in damping for filled systems was related to the thickness of the interphase between the polymer and particles, and results showed that there was a strong interaction between the particles and cyanate ester polymer. The interfacial thickness for 40 nm samples was higher than that of 12 nm samples for low volume fractions, which was consistent with the fact that there is less agglomeration of 40 nm particles than 12 nm particles, leaving more available surface area. The strong interfacial adhesion between the cyanate ester was attributed to the formation of iminocarbonate linkages during cyclotrimerization. There was little change in glass transition temperature, T_g, for the filled systems, but further analysis showed that moisture absorption of the fumed silica prior to cure, as well as increasing levels of conversion, decreased the T_g of the nanocomposites relative to that of the neat cyanate ester resin.

5.6 Acknowledgements

The authors would like to thank Ben Mac Murray for his help in the preparation of samples. Also, technical guidance from Xia Sheng, Jun Xu, and Prof. Mufit Akinc is greatly appreciated. This material is based upon work supported under a National Science Foundation Graduate Research Fellowship. Additional support from the Strategic Environmental Research and Development Program (SERDP), under the "Environmentally Benign Repair of Composites Using High Temperature Cyanate Ester Nanocomposites" project (Project Number WP-1580) is gratefully acknowledged.

5.7 References

[1] Shimp, D. A., and Craig, Jr., W. M., New Liquid Dicyanate Monomer for Rapid Impregnation of Reinforcing Fibers, *Proceedings of the 34th Annual International SAMPE Symposium*, May 1989, p 1336-1346.

[2] Esslinger, Jr., J. R. and Fruchtnicht O. C., Cyanate Ester Matrix Technology for Improved Thermal Performance of Filament Wound Missile Structures. *SAMPE Journal*, v 40, n 6, 2004, p 9-15.

[3] Mehrkam, P. A. and Cochran, R., Liquid Dicyanate Ester Monomer Resin for Elevated Temperature Composite Repair Applications, *Proceedings of the American Society for Composites*, 1992, p 12-21.

[4] Goertzen, W. K., Kessler, M. R., Thermal and Mechanical Evaluation of Cyanate Ester Composites with Low Temperature Processability, *Composites Part A: Applied Science and Manufacturing*, v 38 n 3, 2007, p 779-784.

[5] Hamerton, I. and Hay, J., Recent Technological Developments in Cyanate Ester Resins. *High Performance Polymers*, v 10, n 2, 1998, p 163-174.

[6] Shimp, D. A., Christenson, J.R., and Ising, S.J., Cyanate Esters – An Emerging Family of Versatile Composite Resins. In: *Proceedings of the 34th Annual International SAMPE Symposium*, May 1989, p 222-233.

[7] Miller, D. G., Improving Rheology Control of Epoxy Hardeners, *Adhesives Age*, v 29, n 5, 1986, p 37-40.

[8] Kang, S., et al., Preparation and characterization of epoxy composites filled with functionalized nanosilica particles obtained via sol-gel process, *Polymer*, v 42, n 3, 2001, p 879-887.

[9] Preghenella, M., Pegoretti, A., and Migliaresi, C., Thermo-mechanical characterization of fumed silica-epoxy nanocomposites, *Polymer*, v 46, n 26, 2005, p 12065-12072

[10] Jana, S. C., and Jain, S., Dispersion of nanofillers in high performance polymers using reactive solvents as processing aids, *Polymer*, v 42, n 16, 2001, p 6897-6905.

[11] Wichmann, M. H. G., Cascione, M., fiedler, B., Quaresimin, M., and Schulte, K., Influence of particle surface treatment on mechanical behavior of fumed silica/epoxy resin nano-composites, *Composite Interfaces*, v 13, n 8-9, 2006, p 699-715.

[12] Torro-Palau, A. M., Fernandez-Garcia, J. C., Orgiles-Barcelo, A. C., Martin-Martinez, J. M., Characterization of polyurethanes containing different silicas, *International Journal of Adhesion and Adhesives*, v 21, n 1, 2001, p 1-9.

[13] Zhou, S., Wu, L., Shen, W., Gu, G., Study on the morphology and tribological properties of acrylic based polyurethane/fumed silica composite coatings, *Journal of Materials Science*, v 39, n 5, 2004, p 1593-1600.

[14] Lippe, R. J., Thixotropy Recovery as a Measure of Sag in Polyester/Silica Systems, *Modern Plastics*, v 54, n 2, 1977, p 62-65.

[15] Dershem, S. M., Derfelt, D. L., Bleed-Resistant Cyanate Ester-Containing Compositions, U.S. Patent, 5646241, 1997.

[16] Craig, Jr., W. M., Bis(4-cyanatophenyl)-1,1-ethane, U.S. Patent, 5162574, 1992.

[17] Goertzen, W. K., Kessler, M. R., Thermal expansion of fumed silica/cyanate ester nanocomposites, unpublished manuscript.

[18] Goertzen, W. K., Kessler, M. R., Rheology and curing kinetics of fumed silica/cyanate ester nanocomposites, unpublished manuscript.

[19] Iisaka, K.; Shibayama, K., Effect of Filler Particle Size on Dynamic Mechanical Properties of Poly(methyl methacrylate), *Journal of Applied Polymer Science*, v 22, n 5, 1978, p 1321-1330.

[20] Goyanes, S. N., Konig, P. G., Marconi, J. D., Dynamic Mechanical Analysis of Particulate-Filled Epoxy Resin, *Journal of Applied Polymer Science*, v 88, n 4, 2003, p 883-892.

[21] Vassileva, E., Friedrich, K., Epoxy/Alumina Nanoparticle Composites. I. Dynamic Mechanical Behavior, *Journal of Applied Polymer Science*, v 89, n 14, 2003, p 3774-3785.

[22] AEROSIL® Product Technical Information, Degussa, Frankfurt, Germany, 2006.

[23] Product Technical Data, CAB-O-SIL® M-5, Cabot Corporation, Billerica, MA, USA, 2000.

[24] Sperling, L. H., *Polymeric Multicomponent Materials: An Introduction*, New York: John Wiley & Sons, 1997.

[25] Halpin, J. C., *Primer on Composite Materials Analysis*, 2nd ed., Lancaster, PA: Technomic Publishing Co., 1992.

[26] Nielsen, L. E., Landel, R. F., *Mechanical Properties of Polymers and Composites*, 2nd edition, New York: Marcel Dekker, 1994.

[27] Liang, K., Li, G., Toghiani, H., Koo, J. H., Pittman, Jr., C. U.., Cyanate ester/Polyhedral Oligomeric Silsesquioxane (POSS) nanocomposites: Synthesis and characterization, *Chemistry of Materials*, v 18, n 2, 2006, p 301-312.

[28] Hamerton, I., *Chemistry and Technology of Cyanate Ester Resins*, London: Chapman and Hall, 1994.

CHAPTER 6: THERMAL EXPANSION OF FUMED SILICA/CYANATE ESTER NANOCOMPOSITES

A paper to be submitted to *Composites Science and Technology*

William K. Goertzen[1,2] and M.R. Kessler[1,3]

6.1 Abstract

The thermal expansion behavior of a cyanate ester matrix reinforced by fumed silica nanoparticles with average primary particle diameters of 12 and 40 nm was investigated using thermomechanical analysis. All nanocomposites showed decreased coefficients of thermal expansion (CTEs) as compared to the neat bisphenol E cyanate ester (BECy) resin, but the 12 nm fumed silica nanocomposites had lower CTEs than the 40 nm nanocomposites for equal volume fractions. The largest decrease in CTE was 27.0 % for 20.7 vol% of 40 nm fumed silica. When compared to applicable theory the best fit of the data was given by Schapery's upper limit and Shi's model. Estimates of the interphase volume fraction and effective thickness surrounding the nanoparticles were made using the results of Shi's model, and the results showed that the interphase volume fraction was larger for the 12 nm fumed silica nanocomposites given an equal fraction of fumed silica. The fact that all 12 nm fumed silica nanocomposites had lower CTEs than the 40 nm counterparts was attributed to the larger interphase volume fraction. The glass transition temperature, T_g, of the nanocomposites from thermomechanical analysis varied only slightly with increasing volume fraction, except for samples prepared under dry conditions, which

---

[1] Graduate student and Assistant Professor, respectively, Department of Materials Science and Engineering, Iowa State University

[2] Primary researcher and author

[3] Author for correspondence

showed small increases in T_g. Thermogravimetric analysis showed that the decomposition of the cyanate ester was unchanged with the addition of the fumed silica.

6.2 Introduction

The coefficient of thermal expansion (CTE) of polymers and polymer composites is an extremely important material property because of the relatively high CTE of polymers compared with other materials. Polymers are often filled with low-CTE or negative-CTE reinforcements in order to reduce the CTE mismatch in parts where polymers are used in conjunction with other materials. Applications include electronic flip-clip underfills, electronic packaging, metal part replacement, coatings, and structural adhesives [1-3].

There have been many studies on the reduction of the CTE of thermosetting polymers with inorganic fillers. The largest amount of literature on this subject concerns epoxies and polyesters, but there have also been many reports on the modification of high-temperature thermosets, such as cyanate esters, polyimides, and bismaleimides. Inorganic fillers used in thermosets include silica, zirconium tungstate, alumina, silicon nitride, aluminum nitride, functional polyhedral oligomer silsesquioxane (POSS), and layered silicates. Wooster et al. has reported on composites of cyanate esters and micron-sized fused silica, showing improved mechanical properties and reduced CTE for high loadings [4-6]. Wippl et al investigated the reinforcement of high temperature thermosets (bismaleimides, polyimides, and cyanate esters) with high loadings of fused silica, silicon nitride, and alumina, and CTEs as low as 15 ppm/°C were reported for volume fractions up to 80% [3]. Wong and Bollampally reinforced epoxy with silica, alumina, and silica-coated aluminum nitride, and reported decreases in CTE of up to 65% with filler contents of 50% by volume [2]. Zirconium tungstate (ZrW_2O_8), a unique ceramic with a strongly negative CTE over a wide temperature range, has shown potential for significant reduction of the CTE of composite materials with polymer matrices, both in micro-particulate and

nano-particulate form [1,7,8]. Shi and coworkers investigated polyester and epoxy matrix composites with ZrW_2O_8 [1], Weyer et al. investigated ZrW_2O_8 with cyanate ester [7], and Sullivan and Lukehart investigated the CTE reduction of micro and nano-particulate ZrW_2O_8/polyimide films [8]. Polyhedral oligomer silsesquioxane (POSS) has also been used for reduction of the CTE of thermosetting polymers. Significant decreases in the CTEs of epoxies and polyimides have been realized through the use of functionalized POSS [9,10]. Finally, layered silicate nanocomposites are another class of materials that can exhibit significant CTE reductions for epoxy and cyanate ester matrices [11-13].

Fumed silica consists of amorphous silicon dioxide particles (between 7 nm and 40 nm in diameter) that are usually sintered together during the flame hydrolysis manufacturing process, yielding aggregates of the primary particles that are about 0.2 to 0.3 μm in diameter [14]. While fumed silica has been used extensively with thermosetting polymers, such as polyesters [15], polyurethanes [16,17], and epoxies [18-22], for the enhancement of processing and mechanical properties, there have been few studies on fumed silica's effect on CTE. Fumed silica should have a significant effect on a polymer's CTE due to the fact that amorphous silicon dioxide has a CTE of only 0.75 ppm/°C [23]. Chung has reported reduction in the thermal expansion of cement-based materials with added fumed silica, in addition to other property enhancements such as increased mechanical properties, sag resistance, and improved filler fiber dispersion [24]. For thermoplastic polymers, Fellahi et al. showed that fumed silica reduced the CTE of rigid PVC, and the use of coupling agents enhanced this effect [25].

The effect of fumed silica on the CTE of cyanate esters has not been reported. Despite the fact that the use of fumed silica with cyanate esters is mentioned in the patent literature for cyanate ester-based adhesives [26,27], there is a lack of literature on the reinforcement of cyanate esters with fumed silica. Other types of silica have been investigated with cyanate esters. While POSS has shown potential for the reduction in CTE of epoxies and polyimides [9,10], the reports

on the use of POSS with cyanate esters did not cover thermal expansion [28,29]. As mentioned above, micron-sized fused silica has been used with success in cyanate esters to reduce CTE [4].

Here we report the effect that particle size and volume fraction of fumed silica have on the thermal expansion behavior, glass transition, and thermal decomposition of a cyanate ester matrix. The CTE data will be compared to applicable theory for composite materials, and conclusions will be made concerning that effect of the polymer-particle interaction. In parallel work, we investigate the effect of particle size and volume fraction on other properties, such as rheology, curing kinetics, and mechanical properties [30,31].

6.3 Experimental

6.3.1 Materials

The BECy monomer used is a commercially available resin from Bryte Technologies (Morgan Hill, CA) called EX-1510. The liquid phase organometallic-based polymerization catalyst (Bryte Technologies, EX-1510-B) was supplied with the resin and was used at the manufacturer's suggested loading of 3 phr (parts per hundred resin). The composition of the product is primarily bis(4-cyanatophenyl)-1,1-ethane monomer (or bisphenol E cyanate ester), which has an extremely low viscosity, 0.09 to 0.12 Pa·s, at room temperature [32].

Hydrophilic fumed silica was supplied by Degussa (Frankfurt, Germany) under the trade names of AEROSIL® 200 and AEROSIL® OX 50 (CAS No.: 112945-52-5, synthetic amorphous, pyrogenic silica, purity $\geq$ 99.8%, true density = 2.2 g/cm^3). AEROSIL® 200 has an average primary particle diameter of 12 nm and a specific surface area of 200 m^2/g [33]. AEROSIL® OX 50 has an average primary particle diameter of 40 nm and a specific surface area of 50 m^2/g [33]. The flame hydrolysis process used to make fumed silica yields mostly aggregates (primary particles sintered together) that are about 0.2 to 0.3 μm in diameter [14].

6.3.2 Specimen manufacturing

BECy monomer/fumed silica suspensions were prepared by adding the fumed silica during mixing of the monomer with a 25 mm diameter high-shear blade at 1000 rpm. For the 12 nm particles, compositions of 0.5, 1, 2, 5, and 6.72 phr were made, with 6.72 phr (3.4 vol%) representing the maximum loading achieved with ease of processing. For the 40 nm particles, the compositions included 0.5, 1, 2, 5, 10, 20, 35, and 49.2 phr (max loading), representing volume fractions of up to 20.7 vol%. Prior to mixing, the fumed silica was dried under vacuum and the BECy monomer was preheated to 60 °C. The partially dispersed suspension was processed using a Fisher Model 100 Sonic Dismembrator with 3.2 mm diameter probe tip for 30 seconds at a frequency of 23 kHz. The power output ranged between 16 and 18 Watts during sonication. After sonication, the suspension was again mixed for 2 minutes at 2000 rpm, followed by an additional 30 seconds of sonication. The temperature of the suspension was maintained between 50 and 65 °C throughout the entire process. A predetermined amount of catalyst was added to the dispersed suspension, corresponding to 3 phr, and mixed at 2000 rpm for 2 minutes, followed by 15 seconds of sonication at the same power level. Finally, the suspensions were poured into high-temperature silicone rubber molds (27 × 48 × 8 mm^3) and degassed at 60 °C for 1 hour under vacuum at 23.4 mmHg, and then placed in a convection oven (preheated to 60 °C) for the final curing process (heat to 180 °C at 1 °C/min, hold for 2 hours, heat to 250 °C at 1 °C/min, hold for 2 hours and cool to ambient at 5 °C/min). Samples were machined from the solid block of material using a diamond blade saw (TechCut 5™ Precision Sectioning Machine with Diamond Wafering Blade, Low-Concentration Diamond Metal Bonded, 6" × .020" × ½", Allied High Tech Products, Inc.). Specimens for thermomechanical analysis (TMA) were machined to 3 × 3 × 6 mm^3, such that top and bottom faces of each specimen were parallel to within 15 μm. Neat BECy control samples without fumed silica were prepared in the same manner as above. All samples were dried at 120 °C under vacuum for 6 hours and kept in a dry environment prior to testing.

6.3.3 Experimental procedure

Thermomechanical testing was completed using a TA Instruments (New Castle, Delaware, USA) TMA (Thermomechanical Analyzer) Q400. Samples were tested in the longest dimension (6 mm height) under a static force of 50 mN through two heating and cooling cycles from 30 °C to 300 °C at a heating rate of 5 °C/min under helium purge at 50 mL/min. For each condition, multiple samples were tested (between 2 and 6) and the data was averaged. For measurements where the standard deviation was more than the size of the symbol used in plots, error bars representing one standard deviation were included.

Thermogravimetric analysis was performed using a TA Instruments (New Castle, Delaware, USA) TGA (Thermogravimetric Analyzer) Q50. Portions of the TMA samples were heated from room temperature to 1000 °C at 20 °C/min under air purge at 60 mL/min.

6.4 Results and discussion

6.4.1 Thermal expansion

Figure 6-1 shows an example of the raw data from the thermomechanical tests and the analysis performed on the data. While the data in the 1st heating phase is dependent on the thermal and mechanical history of the specimen, the 2nd heating phase provides information about the true material behavior only [34]. For this reason, the glass transition temperature, T_g, as well as the CTE were taken from the 2nd heating cycle. The CTE was calculated from the slope of the strain vs. temperature data in the region from 50 °C to 150 °C. The strain is proportional to the dimension change (which is shown in Figure 6-1) by the height of the specimen. Example strain vs. temperature curves for the second heating cycle are shown in Figure 6-2 for the 40 nm nanocomposites at silica loadings of 0 phr (0.0 vol%), 10 phr (5.03 vol%), 35 phr (15.6 vol%), and 49.2 phr (20.7 vol%).

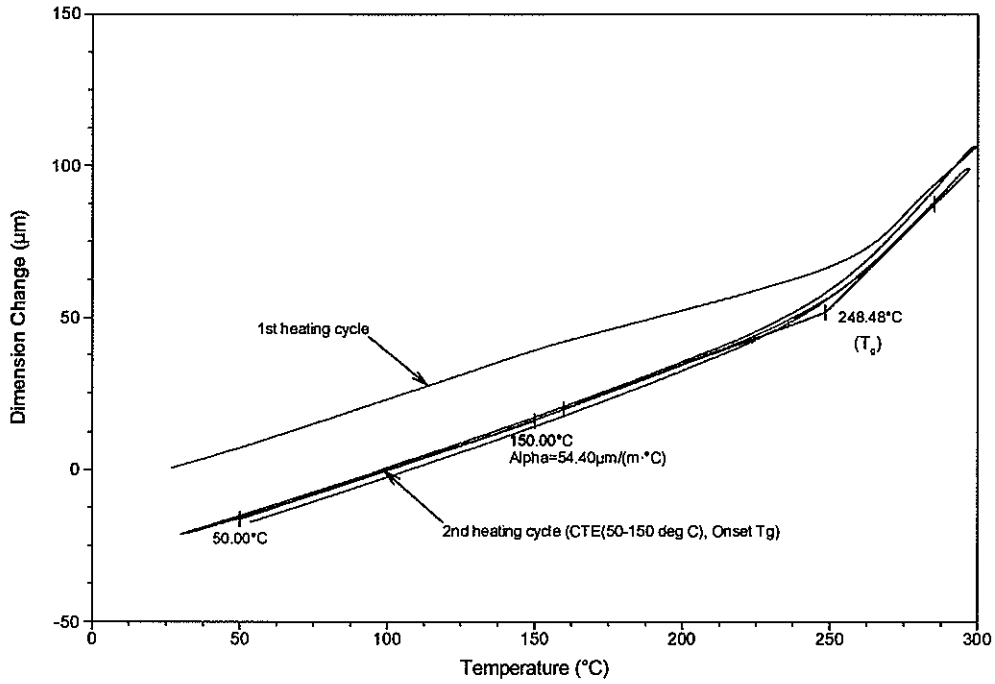

Figure 6-1. Example of raw TMA data with analysis (20 phr, 40 nm shown).

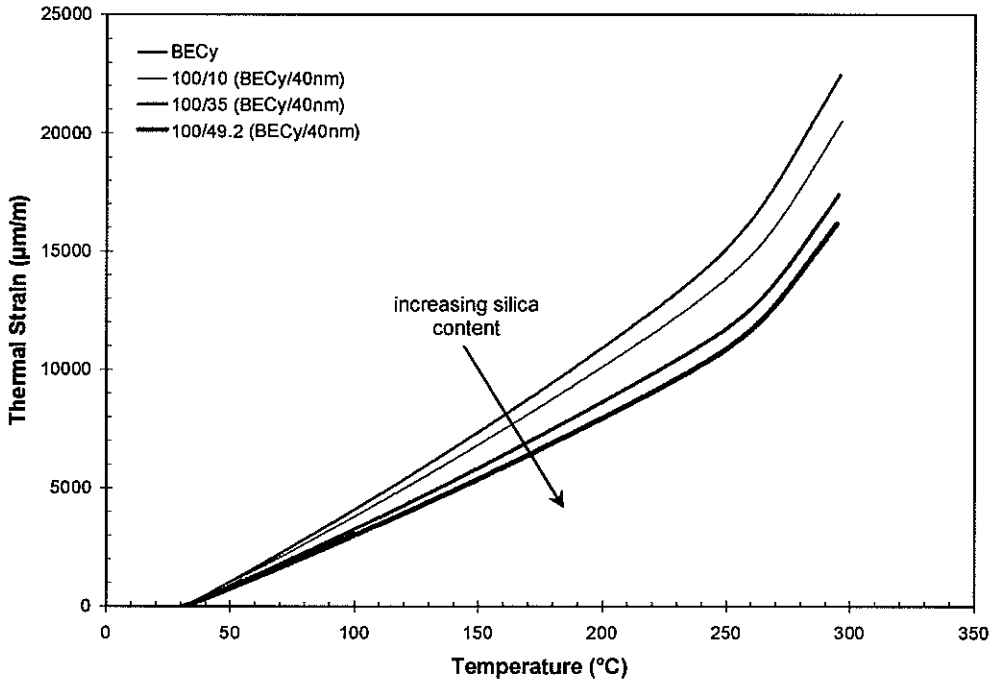

Figure 6-2. Strain vs. temperature for 40 nm cyanate ester nanocomposites.

There is an obvious decrease in thermal strain with increasing volume fraction, ϕ_f. This is due to the influence of the low-CTE fumed silica. The CTE results for each volume fraction of both the 12 and 40 nm fumed silica nanocomposites are shown in Figure 6-3. As expected, the largest decrease in CTE was for the highest loading of 40 nm fumed silica (49.2 phr or 20.7 vol%), which decreased the BECy CTE by 27.0%, from 63.5 to 46.3 ppm/°C.

In Figure 6-3, the experimental CTE data is shown along with model predictions. Among the many different micromechanical models for the isotropic thermal expansion of composites, the simplest is the rule of mixtures (or mixed-law behavior):

$$\alpha_c = \alpha_f \phi_f + \alpha_m \left(1 - \phi_f\right) \quad (1)$$

where α_c, α_m, and α_f are the CTEs of the composite, matrix, and filler respectively, and ϕ_f is the volume fraction of the filler material. The rule of mixtures is an approximation that does not consider the mechanical interaction between the phases. The rule of mixtures approximation yields the most conservative approximation for CTE because of an assumption of a constant stress in the two phases (isostress). In contrast, Turner's model assumes equal dimension change with temperature for all phases, taking into account the interaction between the phases by assuming a constant strain throughout the two phases (isostrain). The CTE of the composite becomes

$$\alpha_c = \frac{\left(1 - \phi_f\right) K_m \alpha_m + \phi_f K_f \alpha_f}{\left(1 - \phi_f\right) K_m + \phi_f K_f} \quad (2)$$

where K_m and K_f are the bulk moduli of the matrix and filler, respectively [2]. In general, Turner's model predicts very low CTE values, and provides a lower limit for CTE. Turner's model is most applicable for unidirectional composites in the fiber direction.

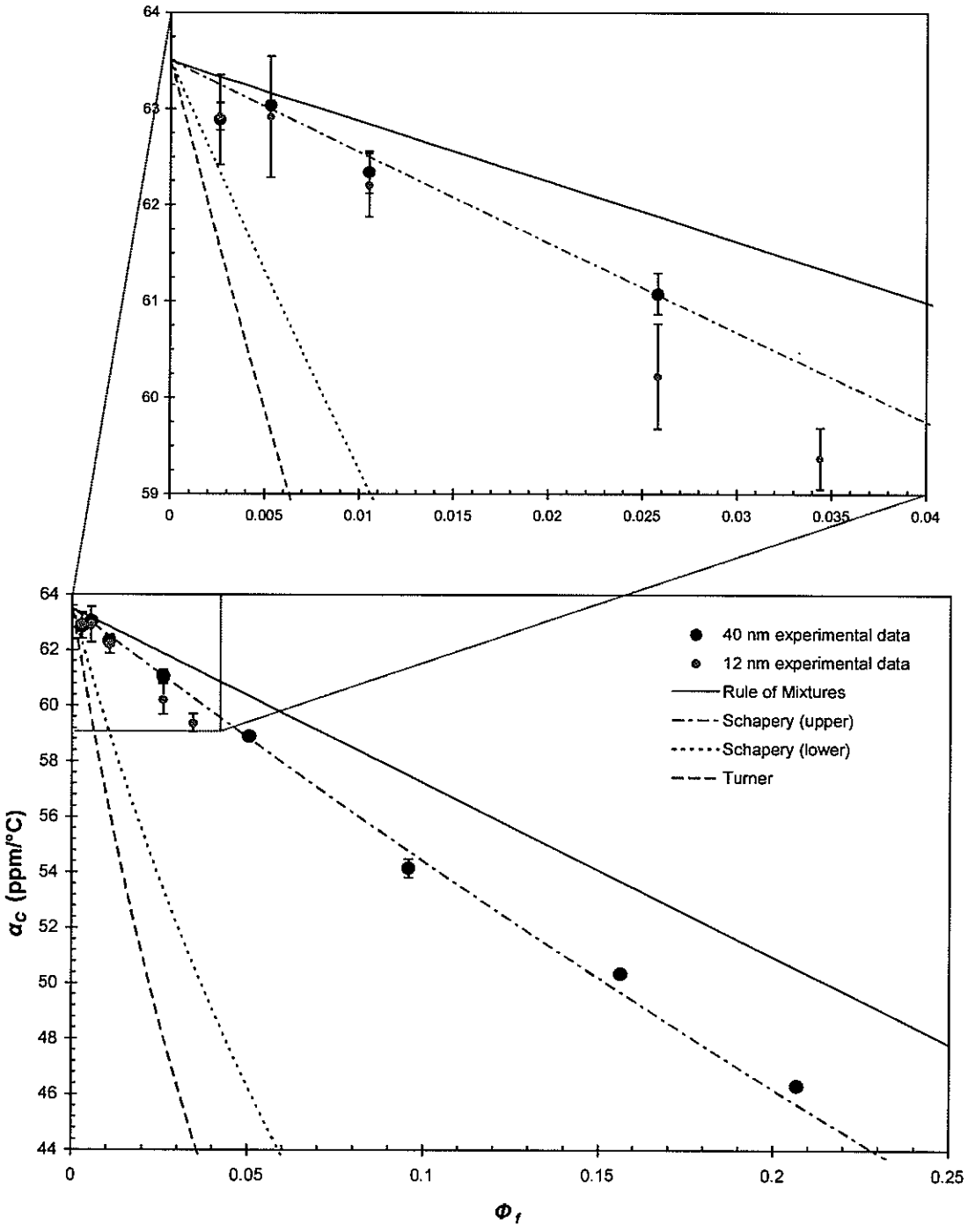

Figure 6-3. Experimental coefficient of thermal expansion vs. volume fraction data for fumed silica nanocomposites, along with model predictions.

Schapery developed equations for the thermal expansion of composites using energy principles, giving upper and lower bounds to the CTE of the composite [35]. The upper and lower bounds for the isotropic CTE of the composite, α_c^u and α_c^l, respectively, are given by

$$\alpha_c^u = \alpha_m + \frac{K_f}{K_c^l}\frac{(K_m - K_c^l)(\alpha_f - \alpha_m)}{(K_m - K_f)} \qquad (3)$$

$$\alpha_c^l = \alpha_m + \frac{K_f}{K_c^u}\frac{(K_m - K_c^u)(\alpha_f - \alpha_m)}{(K_m - K_f)} \qquad (4)$$

where K_c^u and K_c^l are the upper and lower bounds on the bulk modulus of the composite material. These bounds, which are analogous to those derived by Hashin and Shtrikman [2], assume dispersed constituents, and are given by

$$K_c^u = K_f + \frac{1-\phi_f}{\frac{1}{K_m - K_f} + \frac{\phi_f}{K_f + \frac{4}{3}G_f}} \qquad (5)$$

$$K_c^l = K_m + \frac{\phi_f}{\frac{1}{K_f - K_m} + \frac{1-\phi_f}{K_m + \frac{4}{3}G_m}} \qquad (6)$$

where G_m and G_f are the shear moduli of the matrix and filler, respectively. The upper and lower bounds represent assumptions of isostress and isostrain behavior, respectively.

For both sets of data, the rule of mixtures approximation overestimates the CTE for all volume fractions, indicating that there is some strain transfer between the fumed silica and cyanate ester matrix. Schapery's lower limit and Turner's model underestimate the composite CTE for all volume fractions. These models are for an isostrain assumption and are reserved for composites with unidirectional or aligned reinforcement with significant aspect ratios. The

experimental data for 40 nm, however, follows Schapery's upper limit very closely, and the 12 nm data lies slightly below Schapery's upper limit. Schapery's upper limit is likely the most applicable model because it gives nearly identical results to models for particulate reinforced composites, such as those presented by Hashin and Shtrikman, Kerner, and Wang-Kwei [7].

Since the rule of mixtures overestimates the composite CTE for the fumed silica/cyanate ester nanocomposites, there must be an interaction between the two phases that enables strain transfer and alteration of the properties of the matrix in close proximity to the filler. Shi's model is a modification of the rule of mixtures that includes an interphase region between the matrix and filler and is given by

$$\alpha_c = \frac{\alpha_f \phi_f + \alpha_m (1-\phi_f) + K_0 \phi_f (1-\phi_f)(\alpha_f + \alpha_m) + K_0 \phi_f (1-\phi_f) K_1}{1 + K_0 \phi_f (1-\phi_f)} \qquad (7)$$

where K_0 and K_1 are measures of the interphase that are approximated by fitting the model to experimental CTE data [36].

Figure 6-4 shows the experimental CTE data along with fits of the data using Shi's model. For the 40 nm fumed silica nanocomposites, $K_0 = 0.58$ and $K_1 = -4.4$, and for the 12 nm nanocomposites, $K_0 = 1.1$ and $K_1 = -1.4$. From Shi's model, K_0 is related to the volume fraction of the interphase, ϕ_{int}, by

$$\phi_{int} = K_0 \phi_f \phi_m = \phi_f \frac{3\Delta R}{R} \qquad (8)$$

As given by Equation 8, K_0 is also related to the effective thickness of the interphase, ΔR, between the filler and matrix for particles with radius, R [36]. When the constant K_0 is zero, rule of mixtures behavior is assumed; increasingly positive values of K_0 indicate a strong interaction between the filler and matrix [36].

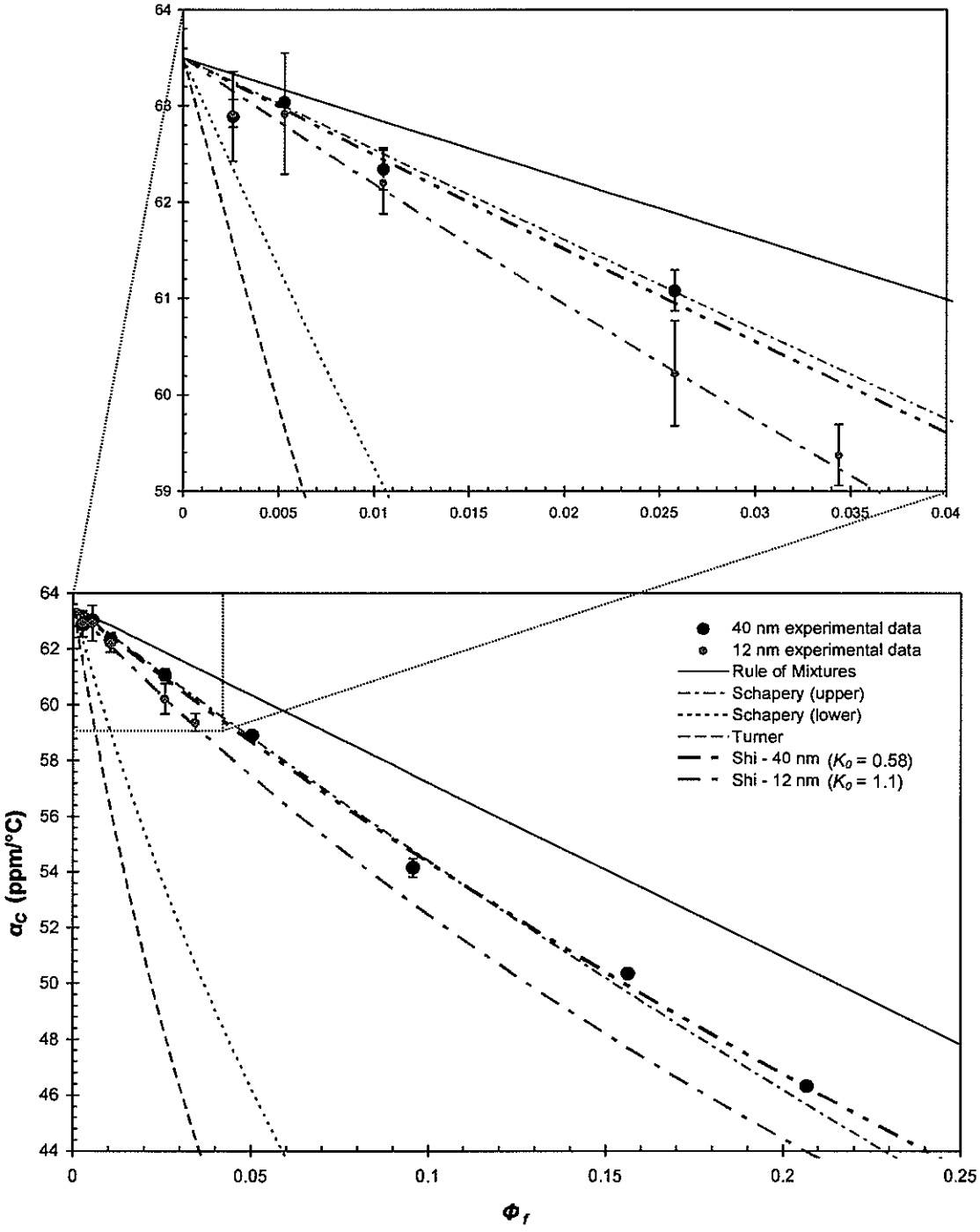

Figure 6-4. Experimental CTE data along with Shi's model fits for 12 and 40 nm nanocomposites.

The constant, K_I, is related to the CTE of the interphase, α_{int}, by

$$\alpha_{\text{int}} = K_{\text{I}} + \alpha_f + \alpha_m - \alpha_c. \qquad (9)$$

such that a large negative value for K_I indicates strong interaction and a lowered CTE for the interphase. Thus, in the case of both the 12 and 40 nm nanocomposites, Shi's model predicts an interaction between the fumed silica and cyanate ester matrix such that predicted CTE's are lower than rule of mixtures behavior would suggest. For the fit of the data using each model, Equation 8 was used to estimate the effective thickness and volume fraction of the interphase between the particles and the matrix. These results are tabulated in Table 6-1.

Table 6-1. Estimated interphase thickness and volume fractions using Shi's model.

phr (12 nm)	Φ_f	Φ_{int}	ΔR [nm]
0.5	0.003	0.003	2.2
1	0.005	0.006	2.2
2	0.010	0.011	2.2
5	0.026	0.027	2.1
6.72	0.034	0.035	2.0
Avg. ΔR [nm] for 12 nm:			**2.1**

phr (40 nm)	Φ_f	Φ_{int}	ΔR [nm]
0.5	0.003	0.002	3.9
1	0.005	0.003	3.8
2	0.010	0.006	3.8
5	0.026	0.014	3.7
10	0.050	0.027	3.6
20	0.096	0.048	3.3
35	0.156	0.070	3.0
49.2	0.207	0.085	2.7
Avg. ΔR [nm] for 40 nm:			**3.5**

According to the predictions, the interphase thickness is greater for the 40 nm fumed silica than for the 12 nm fumed silica. This is consistent with our observations made from dynamic mechanical damping experiments in our parallel work [30], and the difference is attributed to less aggregation of the 40 nm nanoparticles allowing for more free surface area.

However, due to the fact that the 12 nm particles have a greater surface area per volume than the 40 nm particles, the overall interphase volume fraction is higher for the 12 nm nanocomposites. Since the interfacial interaction between the fumed silica and cyanate ester matrix is strong, the 12 nm nanocomposites with more surface area have lower CTE's than the 40 nm nanocomposites for the same volume fraction. The strong interaction between the polymer matrix and fumed silica is attributed to the formation of covalent linkages between the hydroxyl groups of the fumed silica and the cyanate ester matrix [37].

6.4.2 Glass transition

Figure 6-5 shows the glass transition temperatures, T_g's, for the nanocomposites, as calculated from the onset of the increase in dimension change in the 2nd heating cycle of thermomechanical tests.

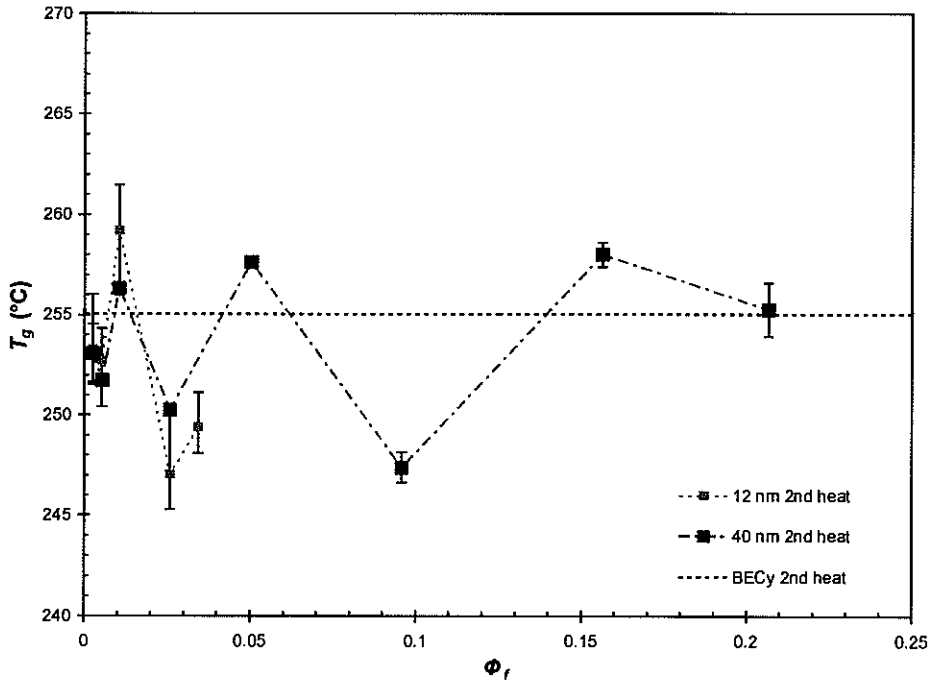

Figure 6-5. TMA glass transition temperature vs. volume fraction for 12 and 40 nanocomposites (the horizontal, dashed line indicates the glass transition temperature of the neat BECy resin).

Initially, it does not appear that there is an obvious trend in the glass transition temperature with increasing volume fraction. However, the T_g's for the 12 and 40 nm samples follow the same trend, which indicates a source of systematic error because the samples with the same volume fraction were prepared at the same time. This error is attributed to the humidity of the laboratory on the day of sample preparation. If only samples prepared on days with a relative humidity of less than 20% are considered, the T_g increases at every volume fraction (see Figure 6-6). This trend was also seen in DMA (dynamic mechanical analysis) glass transition data in our parallel work [30], and our hypothesis was confirmed by preparing identical samples under different environmental conditions and monitoring changes in T_g. It should be noted, however, that further testing showed that the CTE of the composites was not affected by changes in humidity. Additionally, neat BECy resin properties are not affected by environmental humidity because the monomer does not readily absorb moisture.

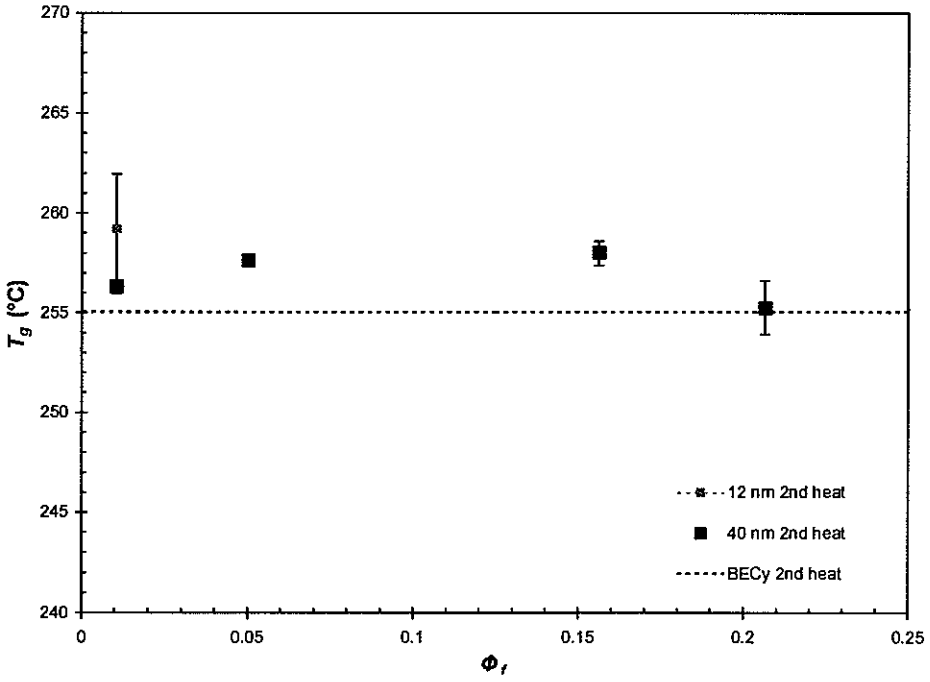

Figure 6-6. TMA glass transition temperatures for samples prepared in dry conditions.

6.4.3 Thermogravimetric analysis

Thermogravimetric data for selected volume fractions of both 12 and 40 nm fumed silica nanocomposites is shown in Figure 6-7.

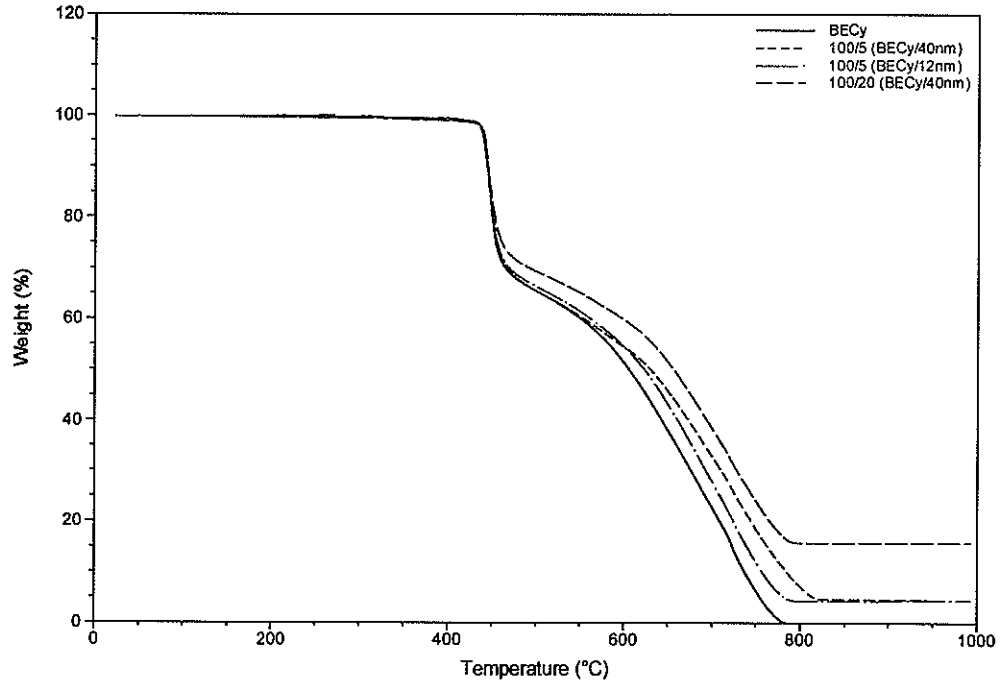

Figure 6-7. Weight loss in air for fumed silica nanocomposites.

From Figure 6-7 it is evident that there is little change in the decomposition of the cyanate ester with the addition of fumed silica. In fact, the initial decomposition at approximately 446 °C is changed by less than 1 °C with the addition of up to 20 phr fumed silica. The oxidation of the matrix at higher temperatures is changed only slightly as well, such that the terminal weight is achieved by 830 °C for all samples. The small difference in the curves of the 40 and 12 nm samples of the same fraction in the temperature range between 600 and 830 °C is not deemed significant due to the fact that there was some variability in the weight loss curves in this region for repeated tests of samples from the identical batches. The final weight for each sample was

compared to the expected value from sample preparation, and agreement was obtained within the limits of experimental error.

6.5 Conclusions

Cyanate esters reinforced with fumed silica particles of two different sizes showed decreased coefficients of thermal expansion (CTEs) as compared to the neat cyanate ester resin. The largest decrease in CTE was for the highest loading of 40 nm fumed silica (20.7 vol%), a composition which decreased the CTE of the BECy by 27.0%, from 63.5 to 46.3 ppm/°C. For all compositions, the CTEs of the nanocomposites were lower than rule of mixtures predictions, indicating an interaction between the fumed silica and cyanate ester. Also, the 12 nm fumed silica nanocomposites had lower CTEs than the 40 nm nanocomposites of the same volume fraction, indicating that the increased surface area of the 12 nm fumed silica was effective in reducing CTE. The best model fit was provided by Schapery's upper limit, as well as a successful fit to the experimental data provided by Shi's model. From Shi's model, estimates of the interphase volume fraction and thickness were made, which indicated that while the thickness of the interphase surrounding the particles was less for the 12 nm nanocomposites than for the 40 nm nanocomposites, the overall volume fraction of interphase was greater for the same volume fraction of fumed silica. The increased volume fraction of immobilized polymer around the nanoparticles was responsible for the further decrease in CTE for the 12 nm nanocomposites, as compared to the 40 nm nanocomposites. The glass transition temperature, T_g, of the nanocomposites was measured using thermomechanical analysis for all compositions, and the initial results showed no apparent trend in the data. However, the variation in T_g was linked to a source of systematic error—the level of humidity in the laboratory during sample preparation. In fact, all samples prepared under dry conditions evidenced at least minor increases in T_g. Thermogravimetric analysis was performed on the nanocomposites, and the results indicated that

the presence of fumed silica imparted only minor changes in the decomposition of the BECy resin.

6.6 Acknowledgements

The authors would like to thank Ben Mac Murray for his help in the preparation of samples. Also, technical guidance from Xia Sheng, Jun Xu, and Prof. Mufit Akinc is greatly appreciated. This material is based upon work supported under a National Science Foundation Graduate Research Fellowship. Additional support from the Strategic Environmental Research and Development Program (SERDP), under the "Environmentally Benign Repair of Composites Using High Temperature Cyanate Ester Nanocomposites" project (Project Number WP-1580) is gratefully acknowledged.

6.7 References

[1] Shi, J. D., Pu, Z. J., et al., Composite materials with adjustable thermal expansion for electronic applications, *Proceedings of the Materials Research Society Symposium*, 1997, p 229-234.

[2] Wong, C. P. and Bollampally, R. S. Thermal conductivity, elastic modulus, and coefficient of thermal expansion of polymer composites filled with ceramic particles for electronic packaging, *Journal of Applied Polymer Science*, v 74, n 14, 1999, p 3396-3403.

[3] Wippl, J., Schmidt, H.-W., and Giesa, R., High temperature thermosets with a low coefficient of thermal expansion , *Macromolecular Materials and Engineering*, v 290, n 7, 2005, p 657-668.

[4] Wooster, T. J., Abrol, S., et al., Thermal, mechanical, and conductivity properties of cyanate ester composites, *Composites Part A: Applied Science and Manufacturing*, v 35, n 1, 2004, p 75-82.

[5] Wooster, T. J., Abrol, S., et al., The effect of particle matrix adhesion on the mechanical properties of silica filled cyanate ester composites, *Macromolecular Materials and Engineering*, v 289, n 10, 2004, p 872-879.

[6] Wooster, T. J., Abrol, S., et al., Polymeric toughening of particle filled cyanate ester composites, *Macromolecular Materials and Engineering*, v 290, n 10, 2005, p 961-969.

[7] Weyer, W. C., Cross, W. M., et al., Achieving dimensional stability using functional fillers, *Proceedings of the 46th AIAA/ASME/ASCE/AHS/ASC Structures, Structural Dynamics and Materials Conference*, v 6, 2004, p 3577-3593.

[8] Sullivan, L. M. and Lukehart, C. M., Zirconium tungstate (ZrW_2O_8)/polyimide nanocomposites exhibiting reduced coefficient of thermal expansion, *Chemistry of Materials*, v 17, n 8, 2005, p 2136-2141.

[9] Huang, J. C., He, C.-B., et al., Polyimide/POSS nanocomposites: Interfacial interaction, thermal properties and mechanical properties, *Polymer*, v 44, n 16, 2003, p 4491-4499.

[10] Sulaiman, S., Brick, C. M., et al., Tailoring the global properties of nanocomposites. Epoxy resins with very low coefficients of thermal expansion, *Macromolecules*, v 39, n 16, 2006, p 5167-5169.

[11] Kim, J.-K., Hu, C., Woo, R., Sham, M.-L., Moisture barrier characteristics of organoclay-epoxy nanocomposites, *Composites Science and Technology*, v 65, n 5, 2005, p 805-813.

[12] Ganguli, S., Dean, D, et al., Mechanical properties of intercalated cyanate ester-layered silicate nanocomposites, *Polymer*, v 44, n 4, 2003, p 1315-1319.

[13] Kim, D. S., Lee, K. M., Mechanical Properties and Structures of Dicyante-Clay Nanocomposites, *Journal of Applied Polymer Science*, v 90, n 10, 2003, p 2629-2633.

[14] Product Technical Data, CAB-O-SIL® M-5, Cabot Corporation, Billerica, MA, USA, 2000.

[15] Lippe, R. J., Thixotropy Recovery as a Measure of Sag in Polyester/Silica Systems, *Modern Plastics*, v 54, n 2, 1977, p 62-65.

[16] Torro-Palau, A. M., Fernandez-Garcia, J. C., Orgiles-Barcelo, A. C., Martin-Martinez, J. M., Characterization of polyurethanes containing different silicas, *International Journal of Adhesion and Adhesives*, v 21, n1, 2001, p 1-9.

[17] Zhou, S., Wu, L., Shen, W., Gu, G., Study on the morphology and tribological properties of acrylic based polyurethane/fumed silica composite coatings, *Journal of Materials Science*, v 39, n 5, 2004, p 1593-1600.

[18] Miller, D. G., Improving Rheology Control of Epoxy Hardeners, *Adhesives Age*, v 29, n 5, 1986, p 37-40.

[19] Kang, S., et al., Preparation and characterization of epoxy composites filled with functionalized nanosilica particles obtained via sol-gel process, *Polymer*, v 42, n 3, 2001, p 879-887.

[20] Preghenella, M., Pegoretti, A., and Migliaresi, C., Thermo-mechanical characterization of fumed silica-epoxy nanocomposites, *Polymer*, v 46, n 26, 2005, p 12065-12072.

[21] Jana, S. C., and Jain, S., Dispersion of nanofillers in high performance polymers using reactive solvents as processing aids, *Polymer*, v 42, n 16, 2001, p 6897-6905.

[22] Wichmann, M. H. G., Cascione, M., fiedler, B., Quaresimin, M., and Schulte, K., Influence of particle surface treatment on mechanical behavior of fumed silica/epoxy resin nano-composites, *Composite Interfaces*, v 13, n 8-9, 2006, p 699-715.

[23] *ASM Engineered Materials Reference Book*, Second Edition, Michael Bauccio, Ed. ASM International, Materials Park, OH, 1994.

[24] Chung, D. D. L., Improving cement-based materials by using silica fume, *Journal of Materials Science*, v 37, n 4, 2002, p 673-682.

[25] Fellahi, S., Boukobbal, S., Boudjenana, F., Study of the Effect of Fumed Silica on Rigid PVC Properties, *Journal of Vinyl Technology*, v 15, n 1, 1993, p 17-21.

[26] Dershem, S. M., Derfelt, D. L., Bleed-Resistant Cyanate Ester-Containing Compositions, U.S. Patent, 5646241, 1997.

[27] Craig, Jr., W. M., Bis(4-cyanatophenyl)-1,1-ethane, U.S. Patent, 5162574, 1992.

[28] Liang, K., Li, G., Toghiani, H., Koo, J. H., Pittman, Jr., C. U.., Cyanate ester/Polyhedral Oligomeric Silsesquioxane (POSS) nanocomposites: Synthesis and characterization, *Chemistry of Materials*, v 18, n 2, 2006, p 301-312.

[29] Liang, K., Toghiani, H., et al., Synthesis, morphology, and viscoelastic properties of cyanate ester/polyhedral oligomeric silsesquioxane nanocomposites, *Journal of Polymer Science, Part A: Polymer Chemistry*, v 43, n 17, 2005, p 3887-3898.

[30] Goertzen, W. K., Kessler, M. R., Dynamic mechanical analysis of fumed silica/cyanate ester nanocomposites, unpublished manuscript.

[31] Goertzen, W. K., Kessler, M. R., Rheology and curing kinetics of fumed silica/cyanate ester nanocomposites, unpublished manuscript.

[32] Shimp, D. A., and Craig, Jr., W. M., New Liquid Dicyanate Monomer for Rapid Impregnation of Reinforcing Fibers, *Proceedings of the 34th Annual International SAMPE Symposium*, 1989, p 1336-1346.

[33] AEROSIL® Product Technical Information, Degussa, Frankfurt, Germany, 2006.

[34] Ehrenstien, G. W., Riedel, G., Trawiel, P., *Thermal Analysis of Plastics: Theory and Practice*, Carl Hanser Verlag: Munich, 2004.

[35] Schapery, R. A., Thermal expansion coefficients of composite materials based on energy principles, J. Composite Materials, v 2, n 3, 1968, p 380-404.

[36] Vo, H. T., Todd, M., Shi, F. G., Shapiro, A. A., and Edwards, M., Towards model-based engineering of underfill materials: CTE modeling, *Microelectronics Journal*, v 32, n 4, 2001, p 331-338.

[37] Liang, K., Li, G., Toghiani, H., Koo, J. H., Pittman, Jr., C. U.., Cyanate ester/Polyhedral Oligomeric Silsesquioxane (POSS) nanocomposites: Synthesis and characterization, *Chemistry of Materials*, v 18, n 2, 2006, p 301-312.

CHAPTER 7: RHEOLOGY AND CURING KINETICS OF FUMED SILICA/CYANATE ESTER NANOCOMPOSITES

A paper to be submitted to *Polymer*

William K. Goertzen,[1,2] Xia Sheng,[1] M.R. Kessler,[3,4] and Mufit Akinc[3]

7.1 Abstract

A low viscosity bisphenol E cyanate ester (BECy) monomer was combined with fumed silica with average primary particle diameters of 12 and 40 nm to form high-temperature adhesives with processability at ambient temperatures. The rheological properties of the uncatalyzed prepolymer suspensions were investigated using steady-state and dynamic rheology, and for silica loadings below 15 vol%, suspensions of both particle sizes exhibited shear thinning and thixotropic behavior. Samples with high silica loadings (>15 vol%) of 40 nm silica also showed intense shear thickening at shear rates above 10 s^{-1}. The relative increase in viscosity with silica volume fraction at low shear rates was greater for the 12 nm silica than the 40 nm silica, which may be attributed to increased surface area and tendency for agglomeration. Thixotropy was most pronounced for the 12 nm silica, but the formation of a gel was slow, indicating that the polar nature of the BECy monomer was responsible for disrupting hydrogen-bonds between silica particles. Rheokinetic evaluation of catalyzed samples showed that increasing silica content reduced gel time and increased gel viscosity, and this effect was most

---

[1] Graduate students, Department of Materials Science and Engineering, Iowa State University

[2] Primary researcher and author

[3] Assistant Professor and Professor, respectively, Department of Materials Science and Engineering, Iowa State University

[4] Author for correspondence

pronounced for the 12 nm silica. Differential scanning calorimetry (DSC) confirmed that the silica does have a minor catalytic effect on the polymerization kinetics, such that the activation energies of the catalyzed suspensions were decreased with increased nanoparticle loading and decreased particle size. This effect is attributed to the abundant presence of hydroxyl groups on the silica surface, which have been shown to react with cyanate esters.

7.2 Introduction

High-temperature thermosetting polymers, such as cyanate esters, bismaleimides, and polyimides, are generally limited in their use to applications that do not require initial processing at ambient temperatures. A unique cyanate ester monomer, bis(4-cyanatophenyl)-1,1-ethane monomer (or bisphenol E cyanate ester), is different from other high-temperature thermosetting polymers in that it is liquid at room temperatures. In fact, the bisphenol E cyanate ester (BECy) exists as a supercooled liquid at room temperature with an extremely low viscosity, 0.09 to 0.12 Pa·s (90 to 120 cP) [1]. The low viscosity of this monomer at room temperature makes it an excellent candidate for many demanding applications [2-4], as it is not only easily processable, but the cured polymer has a high glass transition temperature (approx. 260 °C) and excellent mechanical properties [5,6].

Thermosetting polymers are often modified with rheological additives to alter processing characteristics for end-use applications, and the most common of these is fumed silica. The behavior of fumed silica in commonly used thermosets, such as epoxies [7-11], polyurethanes [12,13], and polyesters [14], has been well studied. Even though it has been documented in the patent literature [15,16] that fumed silica has been used with cyanate esters in industry, there is a lack of literature on the effect that the fumed silica has on the rheology, curing kinetics, thermal, and mechanical properties of cyanate esters. In this work, the rheology and curing kinetics of BECy with both 12 and 40 nm fumed silica is investigated. We discuss the rheological properties

of the uncatalyzed suspensions, as well as curing kinetics by differential scanning calorimetry and rheokinetic experiments. In our parallel work, the dynamic mechanical properties, and thermal expansion behavior of the nanocomposites are discussed [17,18]. These two classes of nanocomposites are under investigation in our research group as processable, high-temperature adhesives for the resin-infusion repair of high-temperature composite materials.

7.3 Experimental

7.3.1 Materials

The BECy monomer used is a commercially available resin from Bryte Technologies (Morgan Hill, CA) called EX-1510, which was used as received, without further purification. The liquid phase organometallic-based polymerization catalyst (Bryte Technologies, EX-1510-B) was supplied with the resin and, for the catalyzed systems, was used at the manufacturer's suggested loading of 3 phr (parts per hundred resin). Hydrophilic fumed silica was supplied by Degussa (Frankfurt, Germany) under the trade names of AEROSIL® 200 and AEROSIL® OX 50 (CAS No.: 112945-52-5, synthetic amorphous, pyrogenic silica, purity $\geq$ 99.8%, true density of 2.2 g/cm^3). AEROSIL® 200 has an average primary particle diameter of 12 nm and a specific surface area of 200 m^2/g [19]. AEROSIL® OX 50 has an average primary particle diameter of 40 nm and a specific surface area of 50 m^2/g [22]. The process used to make fumed silica (vapor phase flame hydrolysis of silicon tetrachloride) yields mostly aggregates (primary particles sintered together) that are about 0.2 to 0.3 μm in diameter [20]. Figure 7-1 a) and Figure 7-1 b) show TEM micrographs of the 12 and 40 nm fumed silica aggregates, respectively. The 40 nm fumed silica has a wider particle size distribution and forms aggregates with a smaller number of particles per aggregate than for the 12 nm fumed silica.

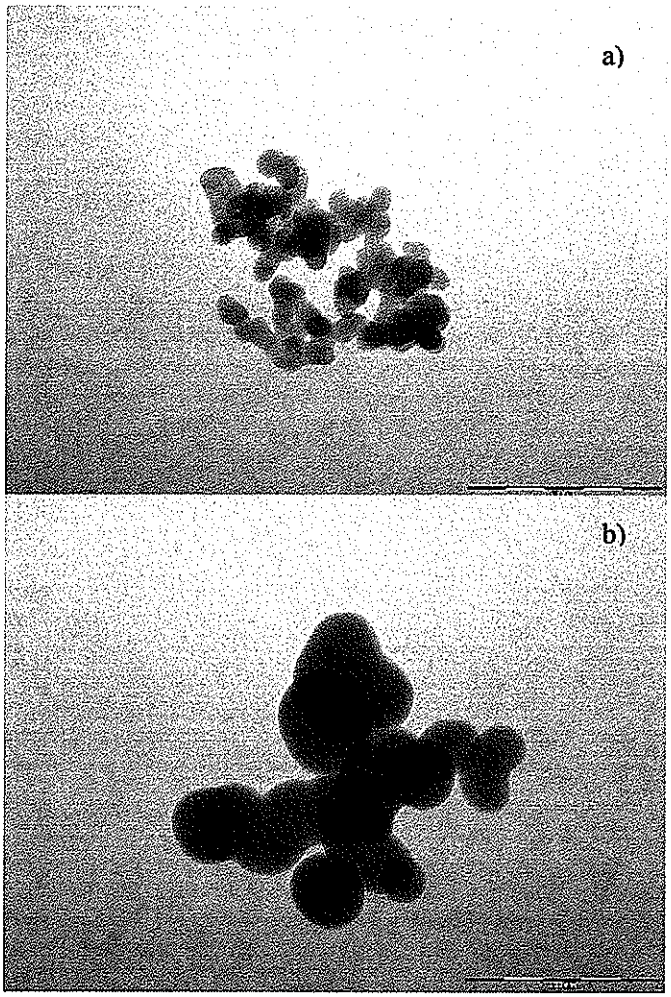

Figure 7-1. TEM micrographs of fumed silica aggregates, a) 12 nm, b) 40 nm (scale bars are 200 nm).

7.3.2 Specimen manufacturing

BECy monomer/fumed silica suspensions were prepared by adding the fumed silica during mixing of the monomer with a 25 mm diameter high-shear blade at 1000 rpm. For the 12 nm particles, compositions of 1, 2, 5, and 6.72 phr were made, with 6.72 phr (3.4 vol%) representing the maximum loading achieved with ease of processing. For the 40 nm particles, the compositions included 2, 5, 10, 20, 30, 35, and 49.2 phr (max loading), representing volume fractions of up to 20.7 vol%. Prior to mixing, the fumed silica was dried under vacuum and the BECy monomer was preheated to 60 °C. The partially dispersed suspension was processed using

a Sonic Dismembrator (Model 100, Fisher Scientific, Hanover Park, IL) with 3.2 mm diameter probe tip for 30 seconds at a frequency of 23 kHz. The power output ranged between 16 and 18 Watts during sonication. After sonication, the suspension was again mixed for 2 minutes at 2000 rpm, followed by an additional 30 seconds of sonication. The temperature of the suspension was maintained between 50 and 65 °C throughout the entire process. Before catalyst addition, a portion of the dispersed suspensions was set aside for rheological evaluation. For the remaining material, catalyst was added to the suspension at a level of 3 phr and mixed at 2000 rpm for 2 minutes, followed by 15 seconds of sonication at the same power level. Finally, the suspensions were poured into high-temperature silicone rubber molds ($27 \times 48 \times 8$ mm^3) and degassed at 60 °C for 1 hour under vacuum at 23.4 mmHg. The catalyzed suspensions were immediately moved to a freezer at -13 °C and stored in sealed containers for subsequent rheokinetic testing and differential scanning calorimetry. Neat BECy control samples without silica were also prepared in the same manner as above.

7.3.3 Experimental procedure

Uncatalyzed BECy/silica suspensions were tested for rheological properties using a TA Instruments (New Castle, Delaware, USA) AR2000ex stress-controlled rheometer with a forced gas environmental test chamber, utilizing a parallel plate geometry (25 mm diameter disposable aluminum). A gap of 0.5 mm was used, and the temperature was maintained at 22.5 °C ±0.3 °C. A sample volume of 0.25 mL was transferred to the parallel plates using a 1 mL syringe. A stepped steady state flow test was conducted for each sample from 0.1 to 100 s^{-1} (5 points per decade), allowing for equilibrium to be reached at each shear rate.

Additional oscillatory experiments were used to monitor changes in viscosity with time. In these thixotropy recovery experiments, a pre-conditioning shear of 100 s^{-1} was initially applied, followed by short oscillatory stress iterations at 0.1 Pa (0.1 Hz) in two-minute intervals, allowing

for the sample to rest in between. The environmental chamber was purged with air and maintained at a temperature of 30 °C.

Catalyzed BECy/fumed silica suspensions were tested at an isotherm of 130 °C using the AR2000ex rheometer in stress control at an amplitude of 1000 Pa and 1 Hz, with the 25 mm diameter disposable parallel plates and 0.5 mm gap. The suspensions were applied to the geometry in the same manner as above, and a one-minute equilibrium period was allowed for each sample to reach the test temperature before collecting data. The catalyzed suspensions were prepared in hermetic pans and tested using a TA Instruments (New Castle, Delaware, USA) Q2000 DSC (Differential Scanning Calorimeter) at constant heating rates of 5, 7, 10, 15, and 20 °C/min under helium purge from room temperature to 350 °C. Uncatalyzed suspensions were tested at a heating rate of 1 °C/min under helium purge from room temperature to 350 °C. Separate thermogravimetric analysis experiments revealed that the weight loss was less than 0.4 wt% during this heating cycle.

7.4 Results and discussion

7.4.1 Suspension rheology

Figure 7-2 and Figure 7-3 show viscosity vs. shear rate data (0.1 to 100 s^{-1}) for uncatalyzed BECy/silica suspensions at room temperature, for 12 and 40 nm particles, respectively. For the shear rate range from 0.1 to 10 s^{-1}, all BECy/silica compositions show pseudo-plastic or "shear thinning" behavior, characteristic of an apparent decrease in viscosity with shear rate, while the neat BECy resin exhibits near Newtonian flow. Figure 7-4 and Figure 7-5 show the viscosity data on a log-normal scale for this range (0.1 to 10 s^{-1}) only. The pseudo-plastic behavior is amplified with increasing silica content. Additionally, viscosity is higher and the shear thinning is most pronounced for the 12 nm silica, which has higher surface area.

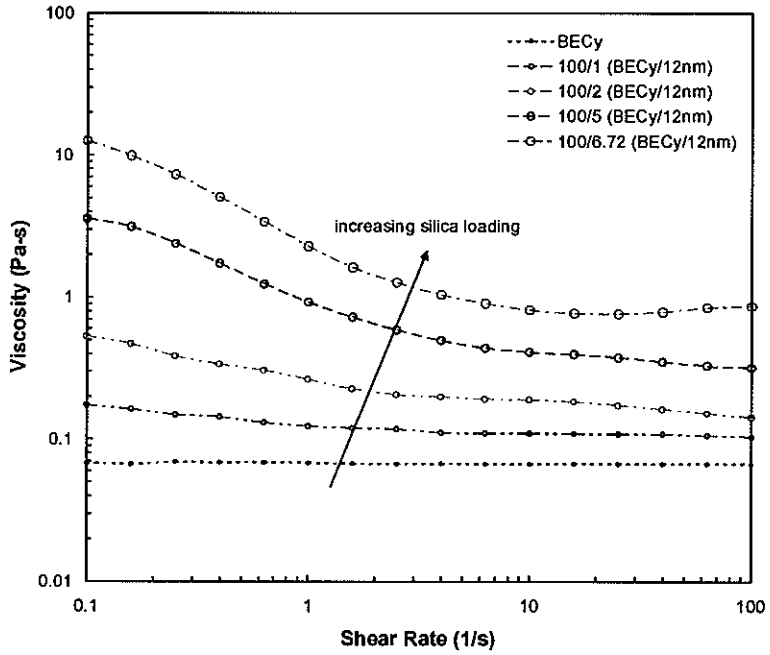

Figure 7-2. Viscosity vs. shear rate for 12 nm fumed silica suspensions (0.1 to 100 s^{-1}).

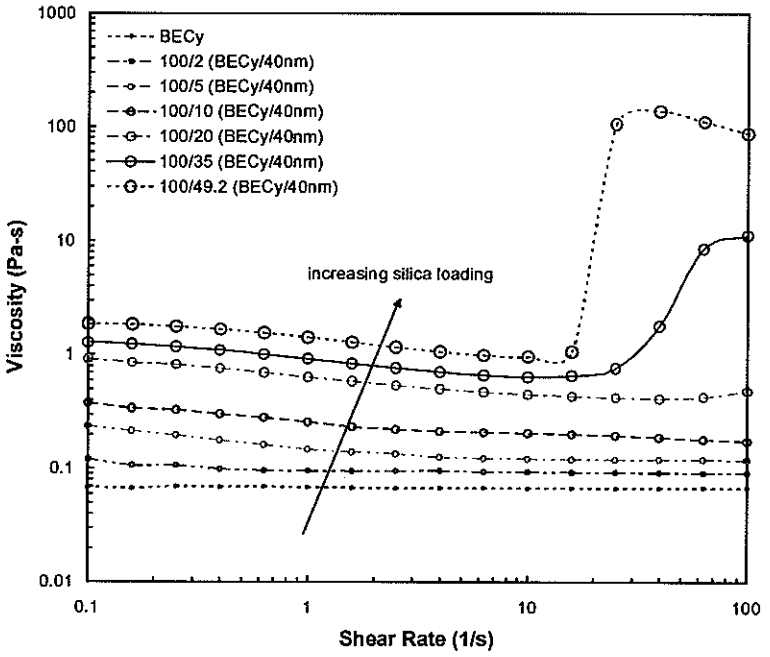

Figure 7-3. Viscosity vs. shear rate for 40 nm fumed silica suspensions (0.1 to 100 s^{-1}).

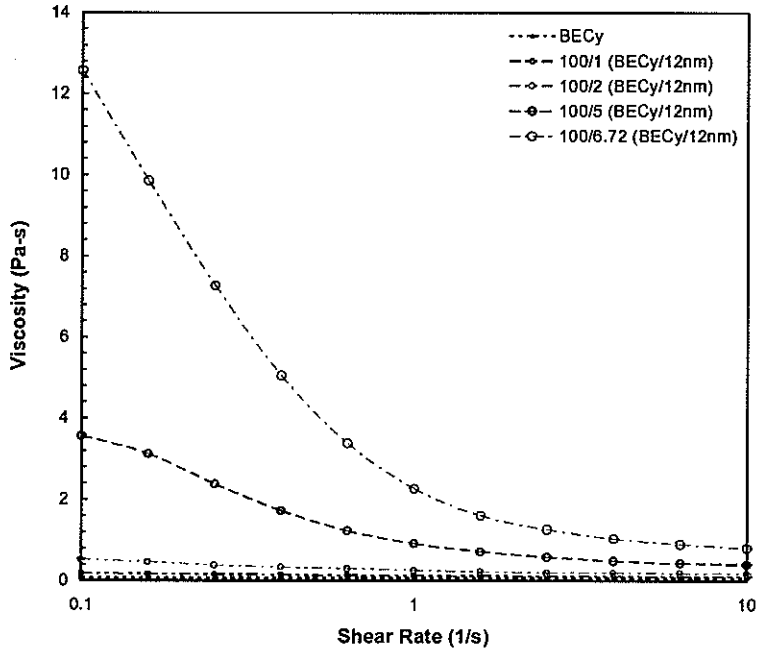

Figure 7-4. Viscosity vs. shear rate for 12 nm suspensions (log-normal, < 10 s^{-1}).

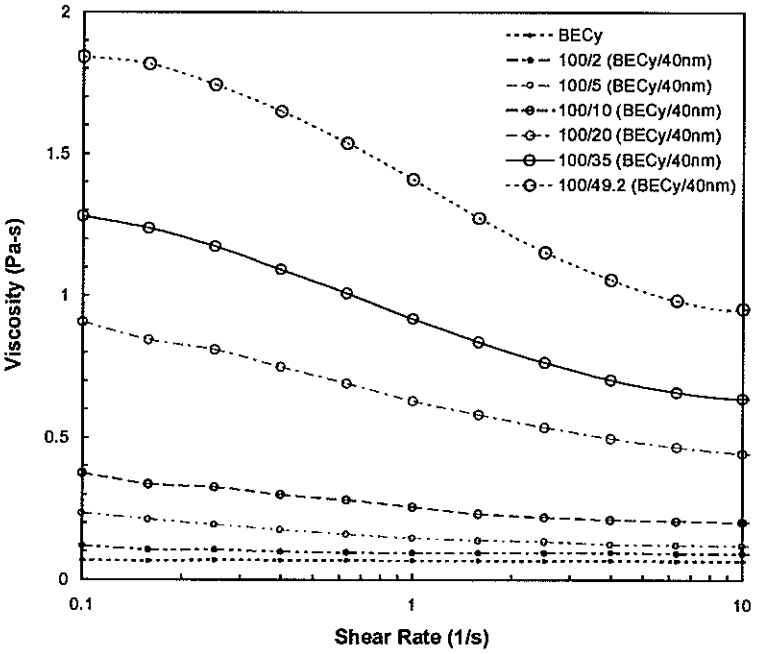

Figure 7-5. Viscosity vs. shear rate for 40 nm suspensions (log-normal, < 10 s^{-1}).

The primary mechanism for the pseudo-plastic or shear thinning nature of hydrophilic fumed silica suspensions is well-known, and is attributed to the formation of hydrogen bonds between hydroxyl groups of neighboring particles [21]. The hydrogen bonds form under low shear and are broken under high applied shear. The effect is most pronounced for weakly hydrogen-bonding liquids, which do not form as many bonds at the particle-liquid interface. This allows a complete network of hydrogen-bonds to be formed between particles, resulting in a gel. For strongly hydrogen-bonding liquids, a stable sol is formed because of the interference of the liquid in the formation of a complete network of hydrogen-bonds between particles [21]. The polar cyanate groups in the BECy monomer should have an affinity to the hydroxyl groups of the silica, which would disrupt the formation of a complete network between the silica particles. In fact, other work on cyanate ester nanocomposites has shown that hydrogen bonding can occur between the hydroxyl and cyanate groups of silica and cyanate esters, respectively [27].

Another factor may be at work in the rheological behavior of these suspensions: physical entanglement and agglomeration of fumed silica particles and aggregates. In our parallel work, TEM analysis of cured nanocomposites showed that the 12 nm silica had a greater degree of agglomeration than the 40 nm silica [17]. The agglomeration of the silica aggregates would create pockets of immobilized and/or trapped monomer, which raise the effective volume fraction of fumed silica [22]. Similar observations by Li and Akinc were noted for nano-alumina dispersions in water [23]. The larger tendency of the 12 nm silica to agglomerate would explain the higher viscosity of these suspensions compared to the 40 nm silica suspensions of the same volume fraction. This mechanism could also be responsible for shear thinning because the shearing of the suspensions would help to break up the agglomerates, decreasing the effective volume fraction and thus the viscosity of the suspension [22].

In the highest volume fractions of the 40 nm silica nanocomposites (49.2 phr or 20.7 vol% and 35 phr or 15.6 vol%), a shear thickening effect was observed above 10 s^{-1}, which raises

the apparent viscosity of the suspensions by as much as two orders of magnitude (see Figure 7-3). There is also a very slight increase in viscosity above 20 s^{-1} in the highest volume fraction of the 12 nm silica (6.72 phr or 3.44 vol%), but the magnitude of this change is much less and may not be significant. According to the literature, there are two conditions that must be satisfied for shear thickening to occur in suspensions: 1) the volume fraction of the filler must be very high, and 2) the suspension must be "nonflocculated" (free of agglomeration) [24]. The shear thickening of a suspension is attributed to the formation of particle clusters that raise the effective volume fraction of the suspension [24], a mechanism that is brought about at a critical shear stress where particles that were kept apart at low stresses are driven together at high stresses [25]. For more polar liquids with fumed silica, the shear thickening mechanism is more pronounced because of hydrogen-bonding between the liquid and silica, which reduces agglomeration [24]. For fumed silica particles in BECy, 40 nm silica particles show a lower degree of agglomeration compared to the 12 nm (see Figure 7-6 and Figure 7-7) [17]. This phenomenon may also be due in part to the fact that the aggregates of fumed silica would have a higher probability of entanglement at high shear than perfectly spherical particles of the same size. Raghavan and Khan reported shear thickening for 14 nm fumed silica suspensions in propylene glycol for loadings of only 3 to 10 wt%, but work by Bender and Wagner [26] and Lee and Wagner [27] on colloidal suspensions of spherical silica showed shear thickening only for compositions exceeding 50 vol%.

A standard way to compare levels of pseudoplasticity in fumed silica suspensions is to calculate the shear thinning index (STI) of the suspension by dividing the viscosity at a low shear rate by the viscosity at a high shear rate [7,14,22]. In Table 7-1, the STI's are tabulated for the 12 and 40 nm fumed silica suspensions, comparing the viscosities at 1 and 10 s^{-1}.

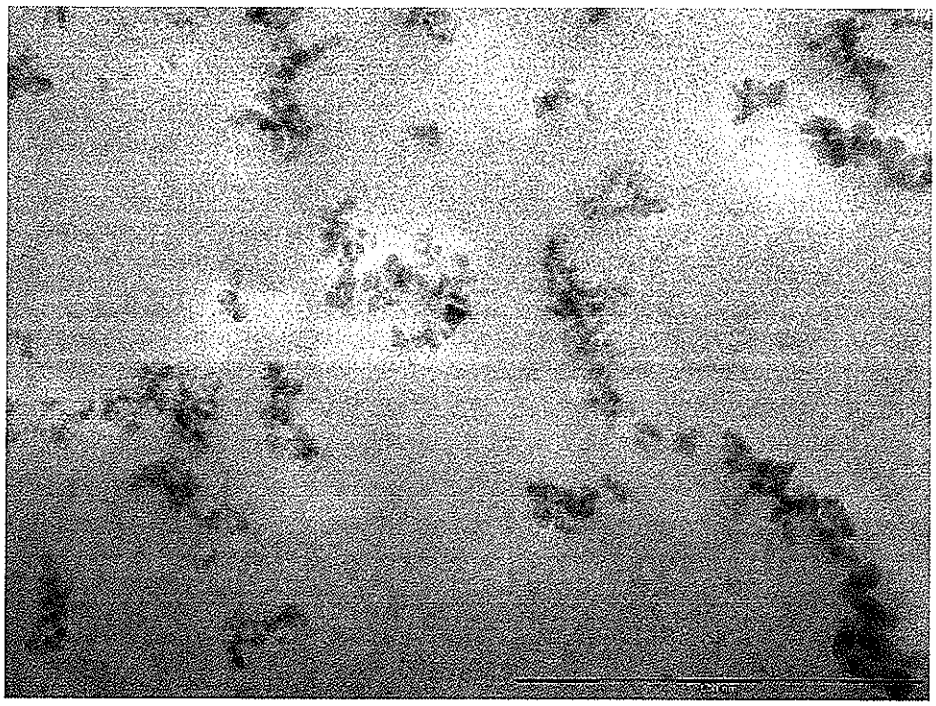

Figure 7-6. 12 nm fumed silica (5 phr, 2.58 vol%) in polymerized BECy matrix (Scale bar is 500 nm).

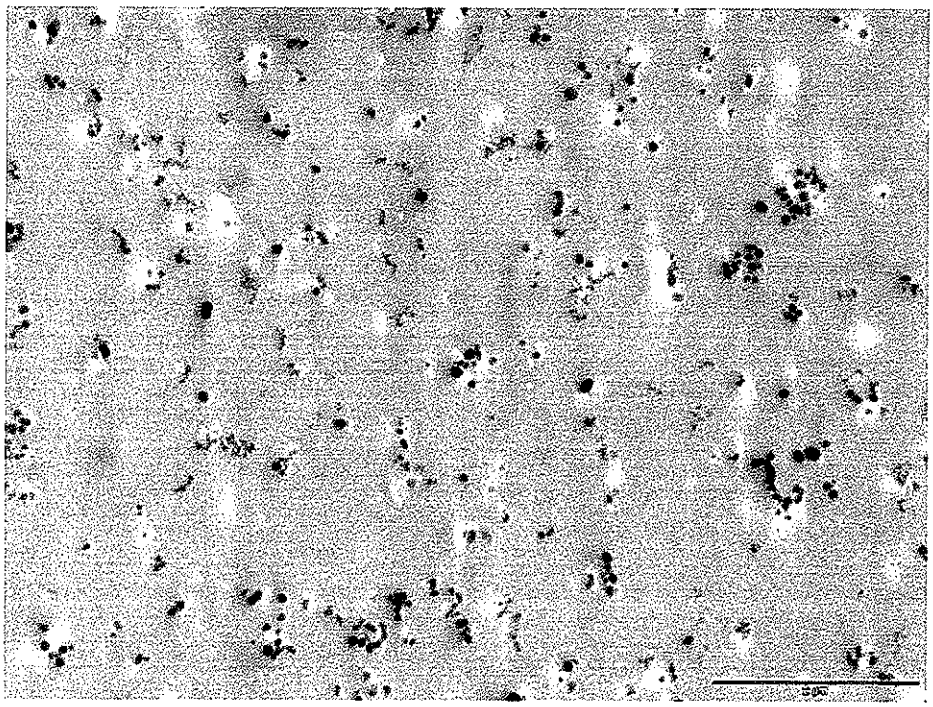

Figure 7-7. 40 nm fumed silica (5 phr, 2.58 vol%) in polymerized BECy matrix (Scale bar is 2 μm).

Table 7-1. Shear thinning index (STI) values for 12 and 40 nm BECy/silica suspensions, from viscosity at 1 and 10 s^{-1}.

phr	Size (nm)	vol%	STI
1	12	0.53	1.12
2	12	1.05	1.40
5	12	2.58	2.23
6.72	12	3.44	2.80
2	40	1.05	1.02
5	40	2.58	1.22
10	40	5.03	1.26
20	40	9.58	1.42
35	40	15.6	1.44
49.2	40	20.7	1.48

The STI's for the 12 nm silica suspensions are higher than that of the 40 nm silica suspensions. In fact, the STI for 2 phr of 12 nm is about the same at 20 phr of 40 nm silica. It can be concluded that the 12 nm silica nanocomposites exhibit greater degrees of pseudoplasticity for equal volume fractions.

Further testing of the fumed silica suspensions showed thixotropic behavior. Thixotropy is a rheological term that literally means, "sensitive to touching" [28]. Thixotropy implies shear thinning (although shear thinning does not imply thixotropy). Unlike time-independent non-Newtonian behavior, however, thixotropy is a transient property, such that changes do not occur instantaneously but over time [28]. In our systems, we observed decreases in viscosity over time with applied shear, as well as increases in viscosity over time with little or no applied shear.

In general, the characterization of thixotropy is difficult due to the many factors that affect its behavior, such as 1) shear history, 2) dispersion state, 3) temperature, and 4) age of suspension [14,22]. Attempts were made to fully characterize the changes in thixotropy recovery with volume fraction and particle size using transient test methods, but the results were somewhat unpredictable due to the large number of factors that affect the thixotropic behavior of fumed silica suspensions. To qualitatively illustrate some of our observations, Figure 7-8 shows the

results of thixotropy recovery tests on highly loaded BECy/silica suspensions. The suspensions were monitored with time for changes in viscosity and viscoelastic properties using periodic dynamic oscillation (0.1 Hz) at a very low stress (0.1 Pa), immediately following an initial pre-shear of 100 s^{-1} for one minute, a procedure similar to one used previously for exhaustive investigations into thixotropy recovery of fumed silica in polyester resins [14].

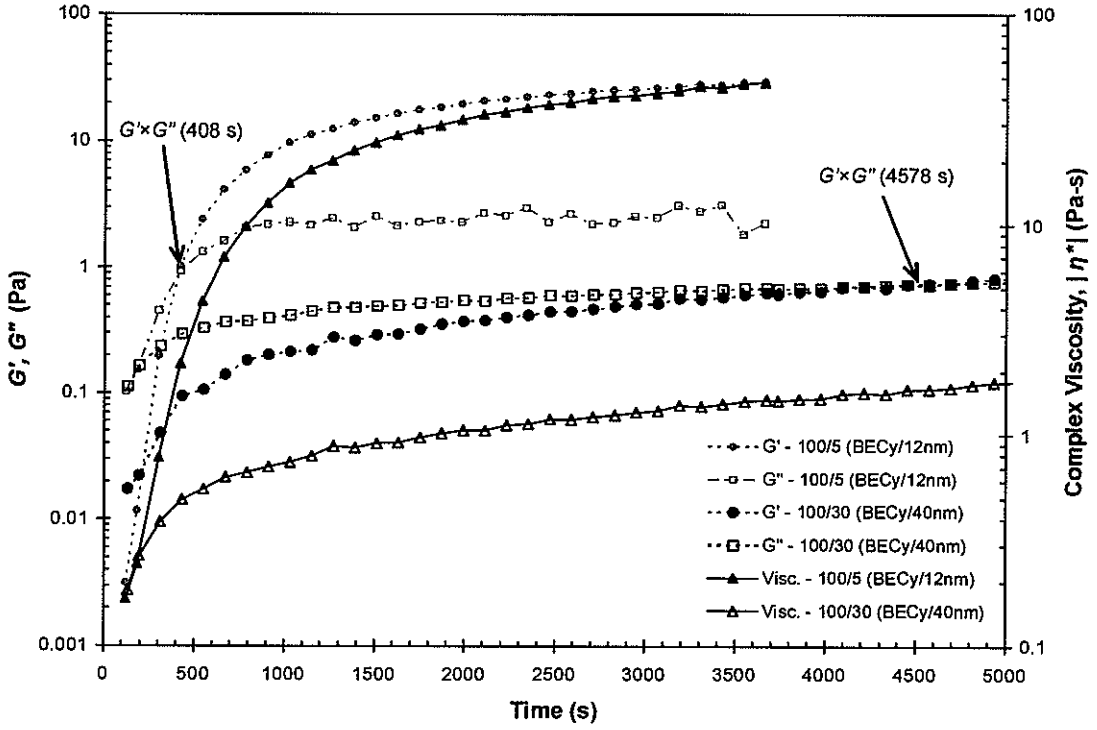

Figure 7-8. Thixotropy recovery as a function of time (0.1 Pa, data taken at 2 min intervals).

The shear storage modulus, G', represents the elastic component of the response, the shear loss modulus, G'', represents the viscous component, and the viscosity is the dynamic viscosity (also called complex viscosity, $|\eta^*|$). For the 12 nm sample at a loading of 5 phr (2.58 vol%), the complex viscosity increases quickly after the initial pre-shear, and G' is equal to G'' at 408 s (or 6.8 min). The $G'\times G''$ point is loosely defined as the gel point, indicating that a network has formed and the material's response is dominated by elastic behavior. The complex viscosity

and elastic component continue to rise, and after one hour, the viscosity has reached about 48 Pa-s. For a much higher loading (30 phr or 13.7 vol%) of the 40 nm silica, the rise in complex viscosity is much less pronounced. After two hours, the viscosity increased only from about 0.17 Pa-s to 1.79 Pa-s. There is a weak crossover between G' and G'', indicating the presence of a gel, but it takes 76.3 minutes (4578 s) for this to occur. According to the literature on fumed silica in non-polar liquids, a suspension should gel within 30 to 120 seconds for the fumed silica to be completely effective as a rheology control agent (raise viscosity substantially, eliminate sag, and control settling) [14,20]. For the BECy/silica suspensions, the thixotropy recovery phenomenon is slower. This is due to hydrogen-bonding between the polar BECy monomer and fumed silica, which will lessen the thixotropic effect, as seen in other polar liquids [7,21]. However, since some concentrations of the suspensions eventually form gels, it is possible that some hydrogen-bonding is occurring between the fumed silica aggregates, especially for the 12 nm silica, which has a faster gel time and greater level of thixotropy than the 40 nm silica in BECy monomer.

However, the thixotropy recovery may be due to formation of agglomerates, not hydrogen-bonding, or it may be a combination of the two. At rest, the dispersed silica will agglomerate over time, leading to immobilized monomer, which may contribute to recovery by raising the effective volume fraction, and thus viscosity. This is the primary mechanism for thixotropy in treated (hydrophobic) fumed silica, which does not hydrogen-bond [22], but may be appropriate in the present study because of the polar nature of the BECy monomer used. However, it is not possible to differentiate between these two mechanisms within the limited scope of the present study because of the complexity of the interactions between the particles, aggregates, agglomerates, and monomer.

7.4.2 Rheokinetic evaluation

Dynamic oscillatory rheology was used to monitor changes in the rheological properties of catalyzed cyanate ester nanocomposites during isothermal cure. Here, we refer to this as "rheokinetic evaluation," but it can also be termed "chemorheology" [29]. Figure 7-9 shows dynamic mechanical properties of the catalyzed 12 nm fumed silica/BECy suspensions as they cure at an isotherm of 130 °C. The gelation point was taken at the point where G' is equal to G'' (G'×G'' crossover), which is representative of the point where the prepolymer forms a crosslinked network [30,31] and the macroscopic response of the material is viscoelastic, dominated by an elastic behavior [29].

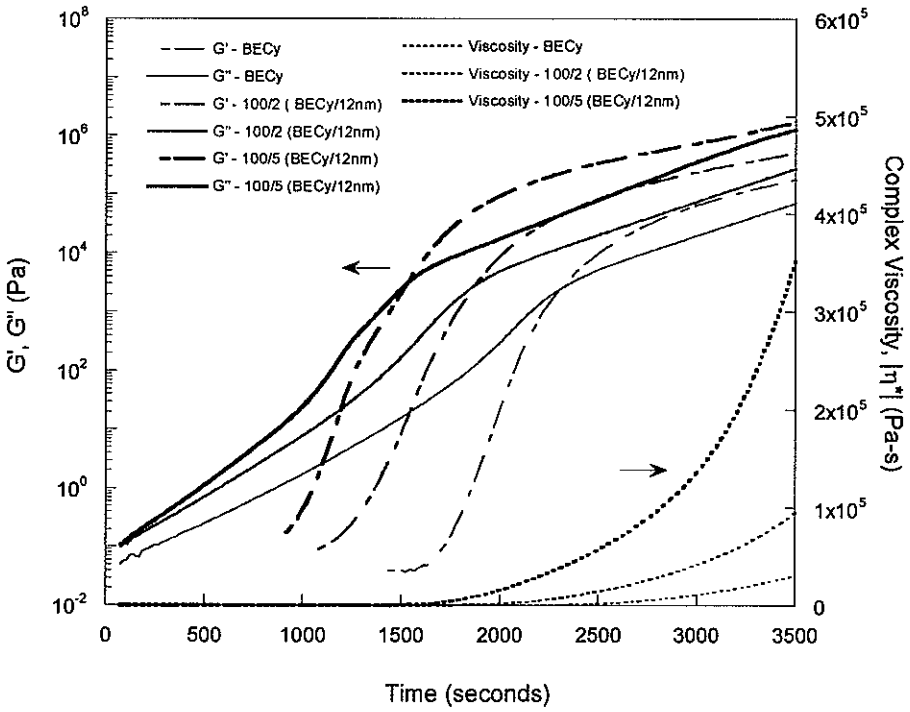

Figure 7-9. Rheological properties of 12 nm fumed silica nanocomposites during cure at 130 °C.

Figure 7-10 shows the rheokinetic evaluation of the 40 nm fumed silica nanocomposites at 130 °C. For both the 12 and 40 nm nanocomposites, the gel time is reduced with increasing silica content. This may be due to two factors: 1) side reactions between the hydroxyl

functionality of the silica and the cyanate ester, and 2) the influence of the fumed silica on the rheological properties of the prepolymer suspensions. Both factors will reduce the gel time with increasing fumed silica loading, the former by increasing the reaction rate, and the latter by giving the material an increasingly elastic response.

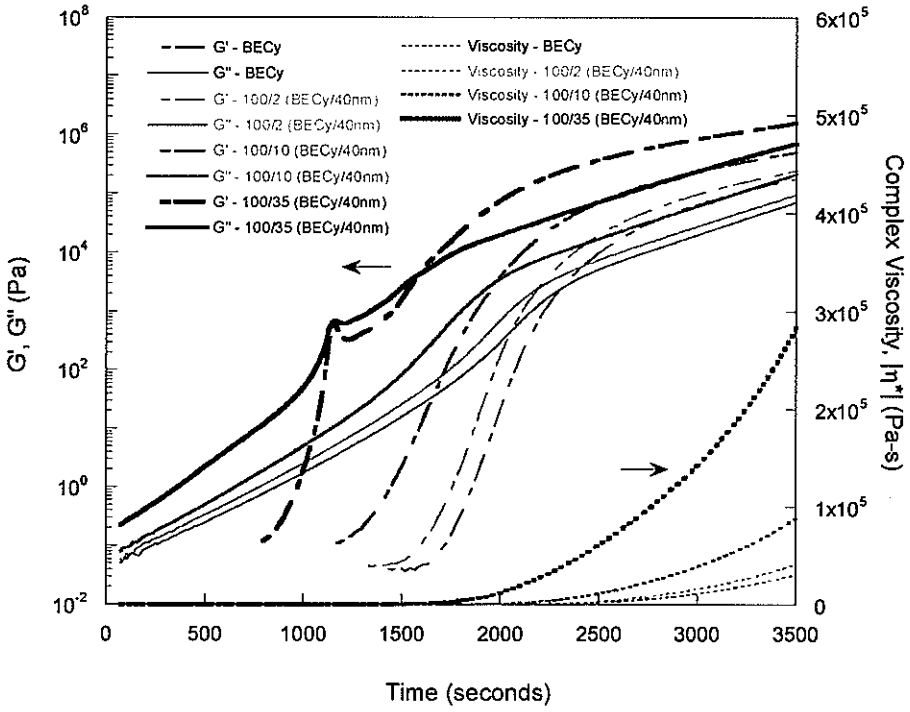

Figure 7-10. Rheological properties of 40 nm fumed silica nanocomposites during cure at 130 °C.

There was an interesting feature in the G' and G'' curves for the highly loaded (35 phr or 15.6 vol%) 40 nm fumed silica sample: a quick increase and subsequent decrease in both parameters around 1100 seconds. This is attributed to the shear thickening of highly loaded 40 nm fumed silica/BECy suspensions that was described in Section 7.4.1. Overall, however, the 40 nm fumed silica nanocomposites exhibit a similar response to the 12 nm fumed silica nanocomposites, but the gel times are slightly longer, and the viscosity at gel is slightly lower. Figure 7-11 shows a comparison in the rheokinetics of 12 and 40 nm fumed silica samples at a loading of 2 phr (1.05 vol%).

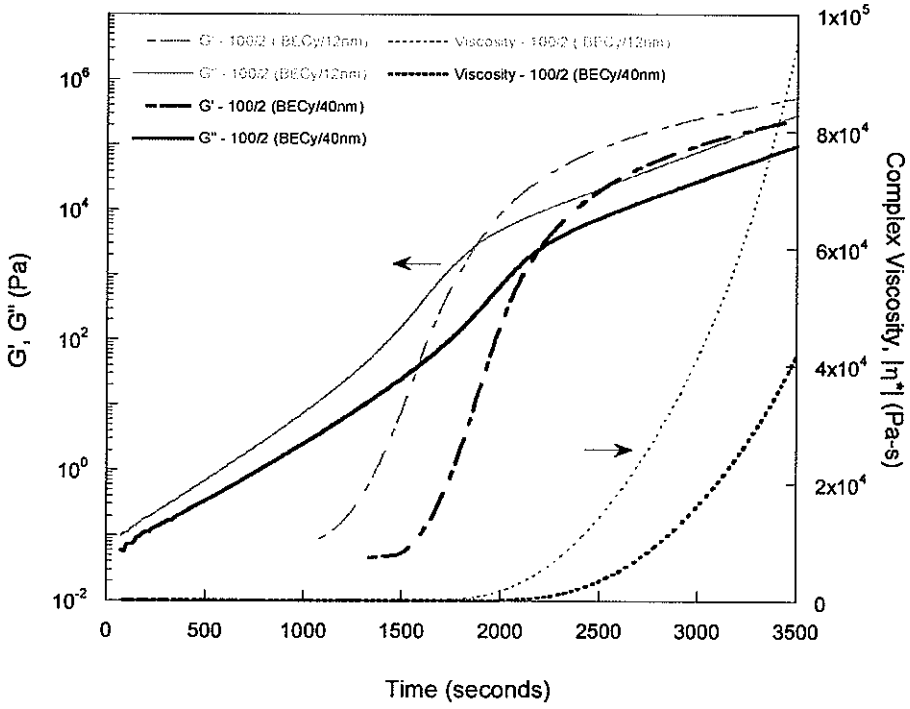

Figure 7-11. Rheokinetics comparison for 2 phr (1.05 vol%) 12 and 40 nm fumed silica nanocomposites.

Table 7-2 compares gel time and properties at gel and 1000 seconds after gel. For a given volume fraction, the 12 nm silica gives a faster gel time, higher G' and $|\eta^*|$ at gel, and higher G' and $|\eta^*|$ 1000 seconds after gel than the 40 nm silica. This may be due to changes in the reaction rate and/or rheological properties brought about by the silica.

Table 7-2. Gel times and properties at gel and 1000 s after gel.

Sample			Gel Point			1000 s after Gel	
phr	vol%	Size (nm)	Time (s)	G' (Pa)	$\|\eta^*\|$ (Pa-s)	G' (Pa)	$\|\eta^*\|$ (Pa-s)
0	0.00	-	2307	2422	550	1.28E+05	2.16E+04
2	1.05	12	1872	2843	633	1.98E+05	3.27E+04
5	2.58	12	1530	3109	695	3.72E+05	6.09E+04
2	1.05	40	2193	2485	559	1.41E+05	2.42E+04
10	5.03	40	1983	3264	734	1.92E+05	3.13E+04
35	15.60	40	1579	4041	919	4.42E+05	7.19E+04

7.4.3 Differential scanning calorimetry

In order to separate the effect that the fumed silica has on the reaction kinetics from the rheology of the suspensions, differential scanning calorimetry (DSC) was used to evaluate curing kinetics of the fumed silica/BECy nanocomposites. Using dynamic scans at multiple heating rates, the position of the peak of the exotherm for each scan can be compared to give the activation energy, E_a, of the reaction. Using Kissinger's model, which assumes that the maximum reaction rate occurs at the exotherm peak, the activation energy, E_a, is related to the heating rate, β, and the peak exotherm temperature, T_p, by

$$\ln\left(\frac{\beta}{T_p^2}\right) = \ln\left(\frac{AR}{E_a}\right) - \frac{E_a}{RT_p} \qquad (1)$$

where A is a pre-exponential factor [32]. Thus, the slope of a plot of $\ln(\beta/T_p^2)$ vs. $1/T_p$ is proportional to the activation energy. Figure 7-12 shows this plot, comparing the data for the neat BECy resin to both the 12 and 40 nm fumed silica nanocomposites.

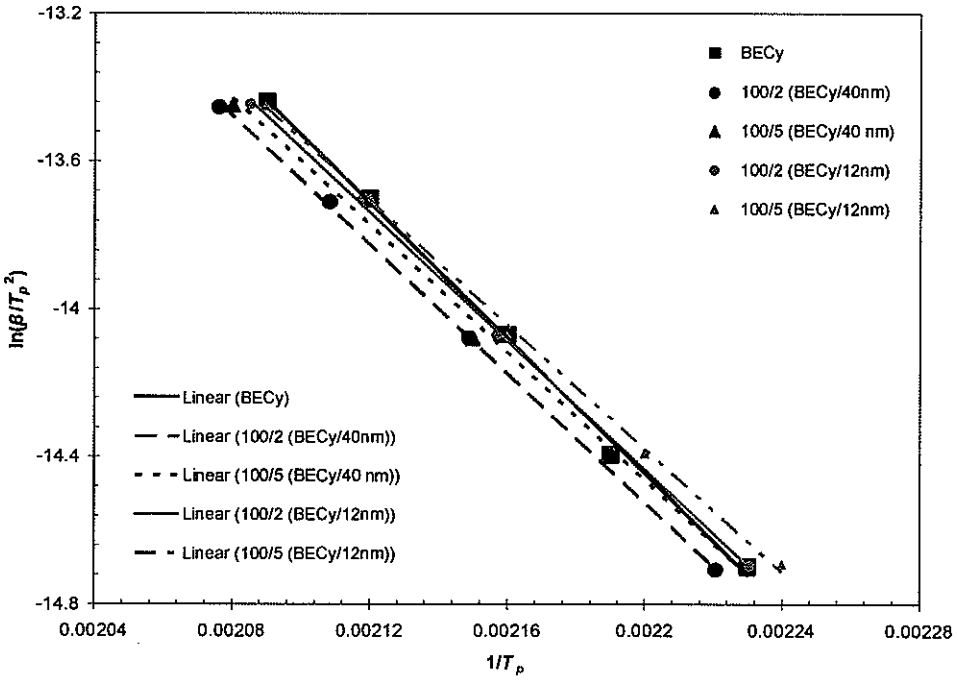

Figure 7-12. Plot of $\ln(\beta/T_p^2)$ vs. $1/T_p$, where the slope is proportional to the activation energy, E_a.

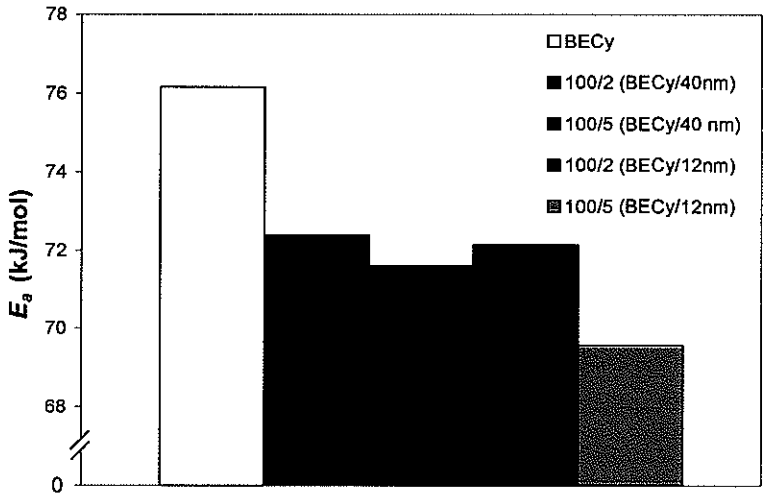

Figure 7-13. Activation energies for catalyzed 12 and 40 nm fumed silica/BECy from DSC.

Figure 7-13 shows the activation energies calculated from Figure 7-12. There are relatively small differences in the activation energies for each system, such that the largest variation is only 6.6 kJ/mol for 5 phr (4.63 wt%, 2.58 vol%) of 12 nm fumed silica. This represents a decrease of less than 9%, which is much less than the 65% decrease in activation energy observed by Ganguli et al. for 5.0 wt% loading in cyanate ester layered silicate nanocomposites [30]. The small changes in activation energy are consistent with the small changes in glass transition temperature observed in the cured nanocomposites presented in our other work [17]. However, there is an observable trend showing decreasing activation energy with increasing filler content and surface area. Both of these factors increase the amount of hydroxyl groups available for reaction with the cyanate ester. The presence of an interaction between cyanate esters and the fumed silica is confirmed by literature on cyanate ester composites. Liang et al. showed that Polyhedral Oligomeric Silsesquioxane (POSS) with hydroxyl functionality form covalent bonds with cyanate esters via iminocarbonate groups [33]. The fumed silica particles have hydroxyl groups present on their surface, and it is asserted that the mechanism for the interaction of the fumed silica is the same. Cyanate esters have also been

shown to form covalent bonds with substrate hydroxyl groups on other surfaces, such as glass and carbon fibers and metallic substrates [34].

In order to further investigate whether the hydroxyl groups of the fumed silica have an interaction with the cyanate ester, tests were done on uncatalyzed suspensions at a slow heating rate of 1 °C/min. This was done to assure that the reaction was controlled, because without catalyst the reaction can still occur, but the peak temperature is raised to over 250 °C, compared to around 180 °C for the catalyzed reaction. Figure 7-14 (a) shows these tests for 2 phr (1.05 vol%) of 12 and 40 nm silica, and the exotherm peak temperatures are noted in Figure 7-14 (b).

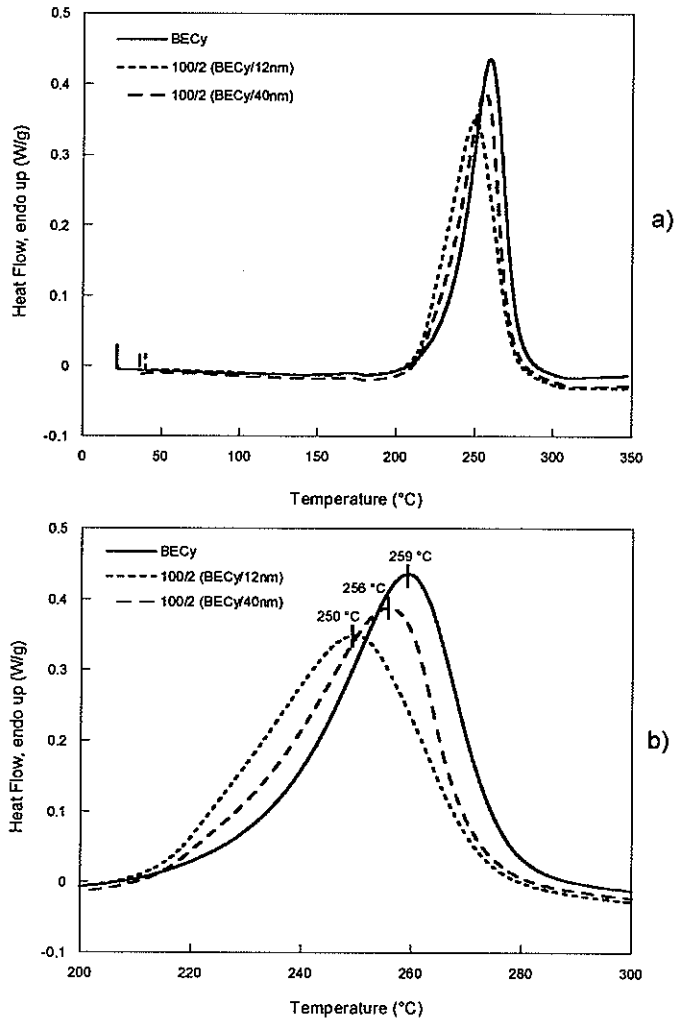

Figure 7-14. DSC of uncatalyzed BECy/silica suspensions, a) all data, b) close-up of peaks.

The presence of the 40 nm silica at 2 phr decreases the peak temperature by about 3 °C and the 12 nm silica at the same loading decreases the peak temperature by about 9 °C, as compared to the neat BECy resin. This confirms that the fumed silica does have a slight catalytic effect on the curing kinetics of the BECy resin, a conclusion that is consistent with the literature. It is well documented that active hydrogen additions, such as water and phenol, have a catalytic effect on the polymerization of cyanate esters [35].

7.5 Conclusions

Suspensions of a low viscosity cyanate ester monomer and fumed silica particles with average primary particle diameters of 12 and 40 nm were prepared and evaluated for their rheological properties and curing kinetics. Uncatalyzed prepolymer suspensions showed shear thinning from steady-state rheology, and dynamic rheology gave evidence of thixotropic behavior. For high loadings of the 40 nm silica (15.6 and 20.7 vol%), an intense shear thickening was observed above shear rates of 10 s^{-1}. All 12 and 40 nm suspensions showed shear thinning behavior at shear rates below 10 s^{-1}. Shear thinning increased with increasing silica loading and decreasing particle size, and was attributed to hydrogen-bonding between silica aggregates and agglomeration of silica. The polar nature of the BECy monomer was responsible for disruptions of hydrogen bonding between silica particles, which resulted in a slow recovery of thixotropy after shearing. Rheokinetic evaluation of catalyzed samples at an isotherm of 130 °C showed that increasing fumed silica content reduced gel time and increased gel viscosity. This effect was most pronounced for the 12 nm silica, and was attributed to both rheological and cure kinetic factors. Tests using differential scanning calorimetry of both catalyzed and uncatalyzed suspensions showed that the silica does have a minor catalytic effect on the polymerization kinetics. This was evidenced by the fact that the catalyzed suspensions showed a slight decrease in activation energy (of up to 9%) with increased nanoparticle loading and surface area (smaller

particle size). Also, uncatalyzed suspensions showed decreased exotherm peak temperatures, as compared to the neat cyanate ester. The catalyzing effect of the fumed silica on the cyanate ester was attributed to the fact that hydroxyl groups, which are present on the fumed silica, have been shown to react with cyanate esters, forming iminocarbonate linkages.

7.6 Acknowledgements

The authors would like to thank Ben Mac Murray for his help in the preparation of samples. Also, technical advice from Jun Xu is greatly appreciated. This material is based upon work supported under a National Science Foundation Graduate Research Fellowship. Additional support from the Strategic Environmental Research and Development Program (SERDP), under the "Environmentally Benign Repair of Composites Using High Temperature Cyanate Ester Nanocomposites" project (Project Number WP-1580) is gratefully acknowledged.

7.7 References

[1] Shimp, D. A., and Craig, Jr., W. M., New Liquid Dicyanate Monomer for Rapid Impregnation of Reinforcing Fibers, *Proceedings of the 34th Annual International SAMPE Symposium*, 1989, p 1336-1346.

[2] Esslinger, Jr., J. R. and Fruchtnicht O. C., Cyanate Ester Matrix Technology for Improved Thermal Performance of Filament Wound Missile Structures. *SAMPE Journal*, v 40, n 6, 2004, p 9-15.

[3] Mehrkam, P. A. and Cochran, R., Liquid Dicyanate Ester Monomer Resin for Elevated Temperature Composite Repair Applications, *Proceedings of the American Society for Composites*, 1992, p 12-21.

[4] Goertzen, W. K., Kessler, M. R., Thermal and Mechanical Evaluation of Cyanate Ester Composites with Low Temperature Processability, *Composites Part A: Applied Science and Manufacturing*, v 38, n 3, 2007, p 779-784.

[5] Hamerton, I. and Hay, J., Recent Technological Developments in Cyanate Ester Resins. *High Performance Polymers*, v 10, n 2, 1998, p 163-174.

[6] Shimp, D. A., Christenson, J.R., and Ising, S.J., Cyanate Esters – An Emerging Family of Versatile Composite Resins. In: *Proceedings of the 34th Annual International SAMPE Symposium*, 1989. p 222-233.

[7] Miller, D. G., Improving Rheology Control of Epoxy Hardeners, *Adhesives Age*, v 29, n 5, 1986, p 37-40.

[8] Kang, S., et al., Preparation and characterization of epoxy composites filled with functionalized nanosilica particles obtained via sol-gel process, *Polymer*, v 42, n 3, 2001, p 879-887.

[9] Preghenella, M., Pegoretti, A., and Migliaresi, C., Thermo-mechanical characterization of fumed silica-epoxy nanocomposites, *Polymer*, v 46, n 26, 2005, p 12065-12072.

[10] Jana, S. C., and Jain, S., Dispersion of nanofillers in high performance polymers using reactive solvents as processing aids, *Polymer*, v 42, n 16, 2001, p 6897-6905.

[11] Wichmann, M. H. G., Cascione, M., fiedler, B., Quaresimin, M., and Schulte, K., Influence of particle surface treatment on mechanical behavior of fumed silica/epoxy resin nano-composites, *Composite Interfaces*, v 13, n 8-9, 2006, p 699-715.

[12] Torro-Palau, A. M., Fernandez-Garcia, J. C., Orgiles-Barcelo, A. C., Martin-Martinez, J. M., Characterization of polyurethanes containing different silicas, *International Journal of Adhesion and Adhesives*, v 21, n 1, 2001, p 1-9.

[13] Zhou, S., Wu, L., Shen, W., Gu, G., Study on the morphology and tribological properties of acrylic based polyurethane/fumed silica composite coatings, *Journal of Materials Science*, v 39, n 5, 2004, p 1593-1600.

[14] Lippe, R. J., Thixotropy Recovery as a Measure of Sag in Polyester/Silica Systems, *Modern Plastics*, v 54, n 2, 1977, p 62-65.

[15] Dershem, S. M., Derfelt, D. L., Bleed-Resistant Cyanate Ester-Containing Compositions, U.S. Patent, 5646241, 1997.

[16] Craig, Jr., W. M., Bis(4-cyanatophenyl)-1,1-ethane, U.S. Patent, 5162574, 1992.

[17] Goertzen, W. K., Kessler, M. R., Dynamic mechanical analysis of fumed silica/cyanate ester nanocomposites, unpublished manuscript.

[18] Goertzen, W. K., Kessler, M. R., Thermal expansion of fumed silica/cyanate ester nanocomposites, unpublished manuscript.

[19] AEROSIL® Product Technical Information, Degussa, Frankfurt, Germany, 2006.

[20] Product Technical Data, CAB-O-SIL® M-5, Cabot Corporation, Billerica, MA, USA, 2000.

[21] Raghavan, S., Walls, H. J., and Khan, S. A., Rheology of Silica Dispersions in Organic Liquids: New Evidence for Solvation Forces Dictated by Hydrogen Bonding, *Langmuir*, v 16, n 21, Oct, 2000, p 7920-793.

[22] Wen, J., Bryant, D., Fumed Silica Controls Rheology of Adhesives and Sealants, reprinted from August 1999 issue of *Adhesives and Sealants Industry* by Cabot Corporation, Billerica, MA, USA.

[23] Li, C., Akinc, M., Role of bound water on the viscosity of nanometric alumina suspensions, Journal of the American Ceramic Society, v 88, n 6, 2005, p 1445-1454.

[24] Raghavan, S. R., Khan, S. A., Shear-Thickening Repsonse of Fumed Silica Suspensions under Steady and Oscillatory Shear, *Journal of Colloid and Interface Science*, v 185, 1997, p 57-67.

[25] Smith, W. E., Zukoski, C. F., Flow Properties of Hard Structured Particle Suspensions, *Journal of Rheology*, v 48, n 6, 2004, p 1375-1388.

[26] Bender, J., Wagner, N. J., Reversible shear thickening in monodisperse and bidisperse colloidal dispersions, *Journal of Rheology*, v 40, n 5, 1996, p 899-916.

[27] Lee, Y. S., Wagner, N. J., Dynamic properties of shear thickening colloidal suspensions, *Rheological Acta*, v 42, 2003, p 199-208.

[28] Malkin, A. Y., Isayev, A. I., *Rheology: Concepts, Methods, & Applications*, Toronto: ChemTech Publishing, 2006.

[29] Yousefi, A., Lafleur, P. G., Gauvin, R., Kinetic Studies of Thermoset Cure Reactions: A Review, *Polymer Composites*, v 18, n 2, 1997, p 157-168.

[30] Ganguli, S., Dean, D., et al., Chemorheology of cyanate ester - Organically layered silicate nanocomposites, *Polymer*, v 44, n 22, Oct 3, 2003, p 6901-6911.

[31] Simon, S. L. and Gillham, J. K., Cure kinetics of a thermosetting liquid dicyanate ester monomer/high-T_g polycyanurate material, *Journal of Applied Polymer Science*, v 47, n 3, Jan 15, 1993, p 461-485.

[32] Kissinger, H. E., Reaction Kinetics in Differential Thermal Analysis, *Analytical Chemistry*, v 29, 1957, p 1702-1706.

[33] Liang, K., Li, G., Toghiani, H., Koo, J. H., Pittman, Jr., C. U.., Cyanate ester/Polyhedral Oligomeric Silsesquioxane (POSS) nanocomposites: Synthesis and characterization, *Chemistry of Materials*, v 18, n 2, Jan 24, 2006, p 301-312.

[34] Shimp, D. A., *Technologically Driven Applications for Cyanate Ester Resins*, In: Chemistry and Technology of Cyanate Ester Resins (Hamerton, I.), London: Chapman and Hall, 1994.

[35] Pascault, J. P. Galy, J., Mechin, F., *Additives and Modifiers for Cyanate Ester Resins*, In: Chemistry and Technology of Cyanate Ester Resins (Hamerton, I.), London: Chapman and Hall, 1994.

CHAPTER 8: GENERAL CONCLUSIONS

8.1 General discussion

Carbon/epoxy composites for structural pipe repair were evaluated for their thermal and mechanical properties using dynamic mechanical analysis, creep testing, and thermal expansion testing. Use-temperature limits were set for the repair system based on glass transition temperature data. The upper limit for the carbon/epoxy was set at 53 °C, which is the highest temperature at which the T_g exceeds the cure temperature by at least 20 °C. Long-term creep behavior was predicted using novel accelerated creep characterization methods. Little room temperature creep was observed, and the principle of time-temperature superposition held for creep data at multiple isotherms. The stress required to induce failure at 50 years was 84% UTS at 30 °C and 42% UTS at 50 °C. Thus, the modulus of the composite would reduce by approximately 16% at 30 °C for 50 years, and 58% at 50 °C for 30 years. The thermal expansion behavior of the composite and matrix material was evaluated using both the strain gage method and thermomechanical analysis. The results for both test methods were in agreement, except for situations where the substrate modulus was low enough that strain gage reinforcement of the material was an issue. The CTE's of the composite ranged from 3.4 to 17.5 ppm/°C and the epoxy matrix CTE was between 70 and 73 ppm/°C.

Continuous carbon fiber/cyanate ester composites were evaluated for their thermal and mechanical properties, with special consideration to low-temperature processability using wet-layup. The bisphenol E cyanate ester (BECy) was used as a reactive diluent in a high-T_g cyanate ester to form a modified matrix material with a viscosity appropriate for the wet-layup application of a high-temperature overwrap pipe repair at low temperatures. Between 25 and 45 wt% of the BECy monomer was needed to produce a viscosity of the prepolymer blend that was suitable for ambient temperature processing. Results showed that the benefit of enhanced low-temperature

processability achieved with these cyanate ester blends is only achieved at the expense of significant decreases in thermal properties, when compared to the T_g of cyanate esters with poor low-temperature processability. Also, the amount of catalyst used presented a trade off because high levels of catalyst reduce the overall T_g, but they enhance the curing process (less resin flow during cure), and they reduce the drop in T_g with increasing post cure temperature. The resin composition also had an effect on CTE, such that the systems with the higher compositions of the BECy resin and lower catalyst amounts had lower CTE's. It is concluded that for blends of these resins, the lowest composition of the BECy monomer that is necessary to alter processing should be used in order to maintain thermal properties.

Fumed/silica cyanate ester nanocomposites using two sizes (12 and 40 nm) of fumed silica were characterized for the thermal, mechanical, and rheological properties. These nanocomposites were identified as a candidate for three applications: 1) primer and filler adhesive for initial bond coat in high-temperature pipe repair, 2) adhesive for resin-infusion repair of high-temperature aerospace composites, and 3) starting material for development of three-phase composites including additional reinforcements, such as short fibers of various types and micron-sized particulates. Dynamic mechanical analysis (DMA) was used to determine mechanical properties and glass transition temperatures. It was shown that increasing fumed silica content increased storage modulus significantly in both the glassy and rubbery regions. For compositions containing 20.7 vol% of 40 nm fumed silica, there was a 75% increase in storage modulus at 30 °C (glassy state) and a 231% increase in storage modulus at 30 °C above T_g (rubbery state). The decreased damping behavior of the nanocomposites was used to estimate the interaction between the fumed silica and cyanate ester. The effective thickness of the interphase was as high as 13.2 nm for the 40 nm fumed silica and 7.1 nm for the 12 nm fumed silica.

The T_g of the nanocomposites from both DMA and thermomechanical analysis (TMA) was changed only slightly, with small increases observed for compositions of dry fumed silica.

The small increase was most pronounced for low cyanate ester conversions. From TMA, the CTE's of nanocomposites showed a decrease that was greater than that which is predicted by the rule of mixtures. In fact, a decrease in CTE of 27.0 % (from 63.5 to 46.3 ppm/°C) was observed for 20.7 vol% of 40 nm fumed silica. The 12 nm fumed silica, however, produced even lower CTE's than the 40 nm fumed silica for equal volumes. When compared to applicable models, the experimental data agreed well with Schapery's upper limit, and was fit well by Shi's model. From Shi's model, estimates of the interphase thickness and volume fraction were made, which indicated a larger volume fraction (although smaller thickness) of the interphase for the 12 nm fumed silica. This gave an explanation for the lower CTE of the 12 nm fumed silica nanocomposites.

The rheological evaluation of fumed silica/BECy suspensions showed that shear thinning and thixotropy was characteristic, although recovery of viscosity was somewhat slow due to interactions between the polar cyanate groups and the hydroxyl groups of the fumed silica. This limited the hydrogen-bonding between the neighboring fumed silica particles and aggregates. An interesting property was observed in high loadings (>15 vol%) of 40 nm fumed silica: shear thickening. At shear rates above 10 s^{-1}, a relative increase in viscosity of up to 2 orders of magnitude was observed. This phenomenon was due to the excellent dispersion of the 40 nm fumed silica at a high volume fraction, but was pronounced by the aggregate nature of the fumed silica particles that is present from the manufacturing process, which accelerates the formation of hydroclusters during high shear.

The curing kinetics of the BECy resin with incorporated fumed silica were evaluated, and DSC results showed that increasing fumed silica content and surface area decreased the activation energy. Also, rheokinetic evaluation showed faster gel times and higher viscosity and modulus at gel. The interaction between the hydroxyl groups of the fumed silica and the cyanate ester is attributed to this change in curing kinetics. Cyanate esters form iminocarbonate linkages with

hydroxyl functionalities, which increase the reaction rate. However, this effect was small, such that decreases in activation energy for up to 2.58 vol% were no more than 9 %. This explains the fact that only small differences in T_g are observed.

Throughout this work, the properties of the nanocomposites were discussed as they relate to the morphology of the nanocomposites. Overall, TEM showed that the 12 nm fumed silica, with high surface energy, more readily formed agglomerates and networks than the 40 nm fumed silica. The 40 nm fumed silica showed excellent dispersion, with some individual particles existing in the cured polymer in addition to the aggregates and smaller agglomerates. The aggregated nature of the fumed silica, which is made through a flame hydrolysis process, gives materials unique properties, especially rheological properties, and this was no exception for BECy. This factor allowed loadings of up to 20.7 vol% for the 40 nm silica, but only 3.44 vol% for the 12 nm silica. The polar nature of the BECy monomer, which reduces fumed silica hydrogen-bonding, was also a major factor in determining rheological properties.

For the repair applications in question, the fumed silica/cyanate ester nanocomposites possess many of the necessary properties. Processing, which is a key issue in all applications, was enhanced with nearly all compositions, with the exception of the highly loaded 40 nm composites that exhibited intense shear thickening. All samples showed the desired shear thickening and thixotropic behavior. This will allow for the prepolymer to flow when applied to or pumped into the repair site, but stay in place during cure. Depending on the exact viscosity that is needed for resin infusion, it may be necessary to use low volume fractions of fumed silica.

Importantly, the high T_g of the BECy was not changed significantly with the addition of fumed silica, which allows for the material to continue to be applicable for high-temperature applications. The DMA data shows that the T_g of the cured nanocomposites exceeds the final cure temperature, a criterion that is important for in-situ repairs. Also, the catalytic effect of fumed silica on the cyanate ester curing process may be desirable. For structural applications, the

nanocomposites exhibit enhanced modulus and decreased thermal expansion, which are both desirable. For applications where additional enhancement of modulus or decrease in CTE is needed, the thixotropic nature of the fumed silica will allow for the incorporation of additional filler materials.

8.2 Recommendations for future research

There are several additional types of characterization that would be beneficial for determining the suitability of the fumed silica/cyanate ester nanocomposites for high-temperature structural repair applications. Adhesion is obviously an important property in these applications, so surface tension measurements and lap shear testing (or other adhesive test method) are recommended. For resin infusion repair of composites, the substrate would be an aerospace structural composite (carbon/epoxy or BMI/epoxy panels) and for pipe repair the substrate would be metallic. Additionally, further mechanical characterization (such as fracture testing, tensile testing, and creep testing) would be beneficial. The effect of environmental factors (such as humidity and the presence of contaminants) on properties would also be useful for determining properties for materials used in less than ideal conditions. Additionally, a full cure kinetic model would be beneficial for determining cure schedules, and further work to determine the effect that shear history, dispersion state, temperature, and aging have on thixotropy would be of interest. Aging of the material is an important concern if this material is transferred to a commercial product and given a shelf life.

For the fumed silica nanocomposites, changes in the composition of the composites may make it possible to further tailor the properties of the composites. Work may be pursued on the effect of different surface functionalities, such as amine, which has shown to be successful in other cyanate ester nanocomposites [1,2]. Nitrile groups may be another choice, but have shown limited interaction with cyanate esters in POSS nanocomposites [1]. Another option may be to

incorporate multiple sizes of fumed silica particles or fumed silica and micron-sized fused silica (spherical) into the nanocomposites, a strategy which has proved to be effective for marked property enhancement as compared to a single size of silica in PTFE [3]. This would add complexity to the system, but may be of interest. Other types of three-phase composites may be developed, which utilize larger-sized fillers that would otherwise settle out of the cyanate ester during storage or cure. Fumed silica is used in other materials to keep components from settling or phase separating, and the initial work shown in Appendix D indicates that it is also possible for this system. The incorporation of a third phase with larger size would allow higher volume fractions and more property control without large increases in viscosity. Finally, fumed silica could be replaced with other fumed metal oxides or nanoparticles with desirable properties. These desirable properties may include, but are not limited to: low density, high modulus, and low CTE.

Finally, for all structural repair applications, full-scale testing of the repair should be conducted in order to determine the feasibility of making repairs with materials that have been shown to possess the right combination of properties. These tests can be time consuming and expensive, but will give valuable information and possible ways the materials can be further improved. For all test setups, care should be taken to ensure that the correct cure schedule is used for the repair because the properties of the cyanate ester are dependent on conversion and thermal history. Testing may not only include the effects of loading and geometry, but also of temperature, thermal cycling, and other environmental factors.

8.3 References

[1] Liang, K., Toghiani, H., Li, G., Pittman Jr., C. U., Synthesis, Morphology, and Viscoelastic Properties of Cyanate Ester/Polyhedral Oligomeric Silsesquioxane Nanocomposites, *Journal of Polymer Science: Part A: Polymer Chemistry*, v 43, 2005, p 3887-3898.

[2] Fang, Z., Wang, J., Gu, A., Structure and Properties of Multiwalled Carbon Nanotubes/Cyanate Ester Composites, *Polymer Engineering and Science*, v 46, n 5, 2006, 670-679.

[3] Huang, S.-I., Chen, T.-H., Chen, H., Study on the Composites of Two Size Silica in PTFE, *Journal of Reinforced Plastics and Composites*, v 25, n 10, 2006, p 1053-1058.

APPENDIX A: THERMAL EXPANSION OF CARBON/EPOXY COMPOSITES FOR STRUCTURAL PIPELINE REPAIR

A.1 Introduction

The discussion included in this appendix is unpublished work that complements the data presented in Chapters 2 and 3. Due to mismatches in the coefficients of thermal expansion of the pipe and repair materials, stresses can develop in the repair system when the application temperature is different than the operational temperature of the pipe or when temperatures fluctuate. A woven carbon fiber/epoxy matrix composite material system used for pipeline repair has been evaluated for its thermal expansion properties through the strain gage method and thermomechanical analysis (TMA). The CTEs are determined so that predictions can be made concerning the magnitude of thermal stresses that are generated due to CTE mismatch.

A.2 Experimental

A.2.1 Materials

The composite specimens were constructed using bi-directional woven carbon fiber reinforcement. This reinforcement was plain weave fabric consisting of 12K tow in the warp direction and 3K tow in the fill direction. The 12K indicates that there are approximately 12,000 carbon filaments (fibers) in each bundle (tow), while 3K indicates approximately 3,000 filaments per tow. The fabric is fairly coarse, with 4 tows/inch in the warp direction and 8 tows/inch in the fill direction. The matrix material was a two-part epoxy system developed by Citadel Technologies™, called the Standard Wet-Out system. The particular epoxy used is a diglycidyl ether of bisphenol-A (DBEGA) type epoxy cured with an aliphatic amine hardener.

A.2.2 Specimen manufacturing

The epoxy matrix was formulated by mixing the two-part Standard Wet-Out system supplied by Citadel Technologies™ using a resin-to-hardener ratio of 2.65:1. The plain weave carbon fabric, also supplied by Citadel Technologies™, was impregnated with the epoxy prepolymer using a paintbrush. Composite panels 12 in x 10 in were fabricated by hand layup with one or two plies. The layup was done in a Teflon release spray coated pan and a Plexiglas caul plate (sprayed with a Teflon release spray) was placed on the top of panel with less than 0.5 psi of pressure. The Plexiglas was laid down in such a way as to remove the air bubbles from the epoxy and create a uniform surface on the top of the specimen sheet. The panels were cured at room temperature for at least 24 hours. The thickness per ply of the composite panels is similar to the thickness per ply of the composite overwrap system used to repair damaged pipelines and pipework. The fiber volume fraction of the composite was measured to be between 35% and 40%, using both the TGA burnoff and matrix digestion methods in accordance with ASTM D 3171 [1]. Once the panels were cured, they were machined into specimens with widths of 8-11 mm and lengths of approximately 45 mm for DMA testing and creep flexural testing. For strain gage thermal expansion testing, the specimens were machined to 50 mm square. For TMA thermal expansion testing, specimens were 8 mm x 8 mm. The thickness of the specimens for each type of testing was approximately 1 mm.

A.2.3 Experimental procedure

Thermal expansion testing was done by the strain gage method and thermomechanical analysis (TMA). For the strain gage measurements, a Vishay Micro-Measurements P-3500 Strain Indicator and Budd Instruments Switch and Balance were used along with Micro-Measurements CEA-06-250UT-350 biaxial strain gages. The specimens were placed in Yamato DX-600 oven with a fused quartz reference (Esco Products, CTE = 0.59 ppm/°C). A heating and cooling rate of

5 °C/min was used from 25 to 150 °C. For TMA testing, a DuPont TMA 943 was used under nitrogen purge at 5 °C/min from 25 to 150 °C.

A.3 Results and discussion

For the woven carbon fiber composite material, the CTE was determined for both the axial (12K fiber direction) and transverse (3K fiber direction) directions. Table A-1 shows the resulting CTE (α) data from both the strain gage method and thermomechanical analysis (TMA) methods. The lower limit for the sensitivity of the TMA method was 5 ppm/°C.

Table A-1. CTE data for the carbon/epoxy composite for pipeline repair.

Test	α_{12K} [ppm/°C]		α_{3K} [ppm/°C]		α_{Epoxy} [ppm/°C]	
Method	$< T_g$	$> T_g$	$< T_g$	$> T_g$	$< T_g$	$> T_g$
Strain Gage	3.4 ± 0.04	3.8 ± 0.51	17.5 ± 0.69	11.5* ± 0.44	72.7* ± 3.4	27.7* ± 1.2
TMA	<5	<5	12.0 ± 1.5	8.0 ± 0.7	70.7 ± 0.05	170.9 ± 4.7

*Suspect values due to strain gage reinforcement effect

From the strain gage data, it appears that the CTE of the epoxy matrix actually decreases to approximately one-third of its original value below the T_g. It is a commonly known and well documented fact that the CTE of polymeric materials above their T_g is larger than the CTE below the T_g [2]. The apparent drop in CTE above T_g for the epoxy matrix is actually a measurement error that can be attributed to the reinforcement effect of strain gages on low modulus materials (less than 7 GPa ($1 \cdot 10^6$ psi)), such as plastics [3-6]. The errors associated with local and global reinforcement of the test specimen by the gage can be significant, especially when the specimen has a small relative thickness [5,6]. Errors ranging from 10 to 42 percent for gages installed on plastics have been reported, with the magnitude of the error being negative [5,6].

Due to the reinforcement effect, the apparent strain measured is actually less than the actual strain in the material. Table A-2 shows approximate DMA storage modulus (E') values for the composite and epoxy matrix above and below the glass transition.

Table A-2. Storage moduli for the epoxy composite and matrix materials above and below T_g.

E'_{12K} (GPa)		E'_{3K} (GPa)		E'_{Epoxy} (GPa)	
$< T_g$	$> T_g$	$< T_g$	$> T_g$	$< T_g$	$> T_g$
40	15	10	4	2	0.005

From Table A-2, it is evident that the CTE measurements are suspect for the following cases: above the T_g for the 3K composite direction and above and below the T_g for the epoxy matrix. However, only the data for the epoxy matrix above its T_g does not follow the general trend of the TMA CTE data. Above T_g, the stiffness of the epoxy reduces by several orders of magnitude, rendering the strain measurement impossible because the strain gage is much stiffer than the polymer. The fact that the CTE specimens had a relatively small thickness (approx. 1 mm) also contributed to the strain gage reinforcement problem. For the epoxy matrix material below the T_g and the composite in the 3K direction, the stiffness is on the same order of magnitude as the lower limit suggested in the literature (7 GPa), so the errors are reduced.

The measured epoxy matrix CTE of 73 ppm/°C below the T_g is a reasonable value, which is in the range of 45 to 100 ppm/°C found in the literature [7]. Although this range is wide, one reference reported a CTE of 62.7 ppm/°C for a similar epoxy measured using the strain gage method [8]. This reference also reported a non-linearity in the thermal strain response of the epoxy near the material's T_g, but with a slight increase in CTE above the T_g. However, the researchers used a 5 mm thick specimen, which would reduce the global strain gage reinforcement effect, and thus also reduce the reduction in apparent strain.

The strain gage CTE results for the composite below the T_g should be generally accurate due to the fact that the stiffness of the composite below the T_g in both directions is significant. In fact, the TMA and strain data for the composite in both directions and in both temperature regions follow the same general trend. The results agree with a simple explanation of the physical phenomenon. The carbon fiber has a CTE that is slightly negative, while the epoxy matrix material has a large, positive CTE. Since there is a larger fiber content in the 12K direction than

in the 3K, the influence of the fiber properties is greater, causing the CTE in the 12K direction to be significantly lower than the CTE in the 3K direction. For the region above the T_g, the CTE in the 12K direction increases slightly, which may be due to the fact that the larger CTE of the matrix causes the overall composite CTE to increase. However, the increase is so small that the uncertainty intervals for the CTE measurement in both regions actually overlap. For the 3K direction above the T_g, the trend is more clear, with a significant decrease in CTE for data from both the strain gage and TMA methods. The decrease in CTE above T_g may be due to the viscoelastic nature of the epoxy matrix. The intense relaxation of the matrix causes a decrease in stiffness by over two orders of magnitude, allowing the stiff carbon fibers to have a greater influence on the overall CTE of the composite. A similar phenomenon was observed by Shrotriya et al. for woven glass/epoxy composites [9].

A.4 Conclusions

Steel has CTE values ranging between 11.3 and 17.8 ppm/°C, depending on the type [7]. While the CTE values of the carbon fiber/epoxy matrix material tested are similar to the steel in the 3K, the CTE of the material in the 12K direction is significantly less than that of the steel. The lower CTE of the composite allows for the overwrap repair to achieve a tighter fit on the steel pipe in the hoop (12K) direction when the pipe temperature increases from a lower installation temperature. While the tighter fit would further constrain the steel, the stress in the composite overwrap would increase. For cases where the installation temperature is higher than the operational temperature, the stress in the composite overwrap would decrease due to the greater shrinkage of the steel, and the constraint of the steel would be reduced. However, the interface between the steel substrate and the initial epoxy matrix primer layer should be considered due to the fact that the large CTE of the epoxy matrix causes large thermal expansion mismatch.

A.5 References

[1] ASTM Standard D 3171-99, *Standard Test Methods for Constituent Content of Composite Materials*, American Society for Testing and Materials, West Conshohocken, PA, 2004.

[2] Rudin, A., *Polymer Science and Engineering*, 2nd ed., Academic Press, 1999.

[3] Sullivan, J. L., Creep Testing of Composites, *Manual on Experimental Methods for Mechanical Testing of Composites*. 2nd Ed., 2004.

[4] Perry, C. C., The Resistance Strain Gage Revisited, *Experimental Mechanics*, 24(4): 286-299, 1984.

[5] Measurement of Thermal Expansion Coefficients Using Strain Gages, *Report TN-513*, Micro-Measurements Group, Raleigh, NC, Feb. 1987.

[6] Perry, C. C., Strain Gage Reinforcement Effects on Low-Modulus Materials, *Experimental Techniques*, 9(5): 25-27, 1985.

[7] Avallone, E. and Baumeister, T., *Mark's Standard Handbook for Mechanical Engineers*, 10th Ed., McGraw-Hill, 1996.

[8] Kim, Y. K. and Daniel, I. M., Determination of the relaxation modulus of polymers and composites, *International SAMPE Symposium and Exhibition Proceedings*, 45(II): 1613-1626, 2000.

[9] Shrotriya, P., Sottos, N.R., Skipor, A.F., Residual stress development during relamination of woven composite circuit boards, *Journal of Composite Materials*, v 35, n 10, 2001, p 905-927.

APPENDIX B: THERMAL EXPANSION AND PROCESSING OF WOVEN CARBON FIBER/CYANATE ESTER COMPOSITES

B.1 Introduction

The discussion included in this appendix is unpublished work that complements the data presented in Chapter 4. Here, the effect that blend ratio and catalyst composition have on the thermal expansion of the neat cyanate ester polymer are presented. Also, the effect of cure schedule on woven carbon fiber/cyanate ester composite panels is discussed. Both the thermal expansion and processing results are discussed as they relate to use of cyanate esters for high-temperature pipe repair.

B.2 Experimental

B.2.1 Materials

Two prepolymer blends of Bryte Technologies' (Morgan Hill, CA) EX-1510 and EX-1551-1 resins were used as the matrix in composite specimens for DMA. EX-1510 has intermediate thermal stability (post cured T_g of up to 260°C), and is a low viscosity liquid at room temperature. From NMR analysis, it was determined that the EX-1510 consists mainly of bisphenol E cyanate ester (BECy) monomer. EX-1551-1 is a higher viscosity resin that produces a polymer with excellent thermal stability (post cured T_g of up to 318°C). From NMR analysis, it was determined that the EX-1551-1 is primarily a bisphenol A cyanate ester monomer with a small novolac cyanate ester prepolymer component. A liquid phase organometallic-based polymerization catalyst (Bryte Technologies, EX-1551-1B) was also used as a component in the prepolymer blend, in varying ratios. The composite specimens were constructed using plane weave bi-directional woven carbon fiber reinforcement with 12K tow in the warp direction and 3K tow in the fill direction.

B.2.2 Specimen manufacturing

Two prepolymer blends were used in the test specimens: (1) 75% by weight of EX-1551 and 25% by weight of EX-1510 (denoted as "75/25") and (2) 55% weight of EX-1551 and 45% by weight of EX-1510 (denoted as "55/45"). The catalyst was mixed with the prepolymer blends in catalyst/resin weight ratios of 0.0%, 1.5%, and 3.0% (each prepolymer/catalyst system will be denoted by the prepolymer blend ratio followed by the catalyst ratio, i.e. 75/25-1.5%).

For the thermal expansion specimens, mixed resin was poured into 60 mm diameter steel cylinders coated with release spray in order to achieve a pool thickness of approximately 8 mm. The filled cylinders were cured using the same initial cure schedule as the composite panels, but with no post cure (82°C for 24 hours, followed by 3 hours at 177°C). The resulting neat resin discs were machined into cubes approximately 8 × 8 × 8 mm^3 using a diamond blade saw, ensuring that the two sides perpendicular to the test direction were parallel within 25 μm.

To make the composite panels, two pieces of 12K × 3K woven carbon fiber fabric, each 20 cm × 20 cm, were thoroughly wetted with the prepolymer/catalyst mixture, and placed between two sheets of Teflon® (ranging in thickness between 0.5 and 1.0 mm) on a steel pan. A 25 cm × 30 cm glass caul plate was placed on top of the top sheet of Teflon®, followed by a third sheet of Teflon® and steel bars for added weight. The weight of the steel bars was controlled such that the pressure on the glass caul plate was approximately 690 Pa (0.1 psi). The entire setup was placed in a laboratory oven and cured for either a one-stage or two-stage cycle. For a single stage, the cure was conducted at 177 °C (350 °F) for 3 hours. For the two stage cycle, the second stage was also conducted at 177 °C (350 °F) for 3 hours, but the first stage was conducted at a lower temperature, 82 °C (180 °F), for 24 hours in order to achieve a better surface finish on the panel through a slight B-stage, which initiates partial polymerization and lowers resin flow during the 177 °C (350 °F) cure cycle. Sections for evaluation were cut from the cured panels

into specimens 10 mm wide and 45 mm long. A diamond blade saw was used to make each cut. The average thickness of the panels and specimens was approximately 1 mm.

B.2.3 Experimental procedure

Thermal expansion testing of neat resin samples (75/25-0.0%, 75/25-3.0%, 55/45-0.0%, and 55/45-3.0%) was done by TMA. Linear displacement was measured as the temperature was increased at 5°C/min from 25°C to 350°C in a nitrogen atmosphere. Each specimen was annealed above its T_g prior to testing to relieve residual thermal stresses. The coefficients of thermal expansion (CTEs) for four systems (75/25-3.0%, 75/25-0.0%, 55/45-3.0%, and 55/45-0.0%) were determined from the slope of the displacement vs. temperature curve in the temperature regions below and above the T_g of the material.

B.3 Results and discussion

B.3.1 Thermal expansion

The results of the thermal expansion testing by TMA are shown in Table B-1.

Table B-1. Cyanate ester average CTEs in the regions below and above T_g

Resin	CTE (ppm/°C)	
System	Below T_g	Above T_g
75/25-0.0%	57.9	147.9
75/25-3.0%	62.6	146.6
55/45-0.0%	54.6	144.0
55/45-3.0%	61.9	136.9

For all samples, the systems with a lower content of catalyst displayed a lower CTE for the region below T_g. Additionally, the samples with a higher content of EX-1510 (55/45) had slightly lower CTEs. The lower CTE of the cyanate ester compared to the epoxy used in Appendix A (70 to 72 ppm/°C) will allow for slightly lower CTE values for the woven carbon fiber composites than those presented in Appendix A (Table A-1).

B.3.2 Processing

Initial attempts at manufacturing composite panels resulted in specimens with voids left from the flow out of resin from the woven carbon fiber fabric during cure. Figure B-1 shows sections from panels with different cure cycles and compositions.

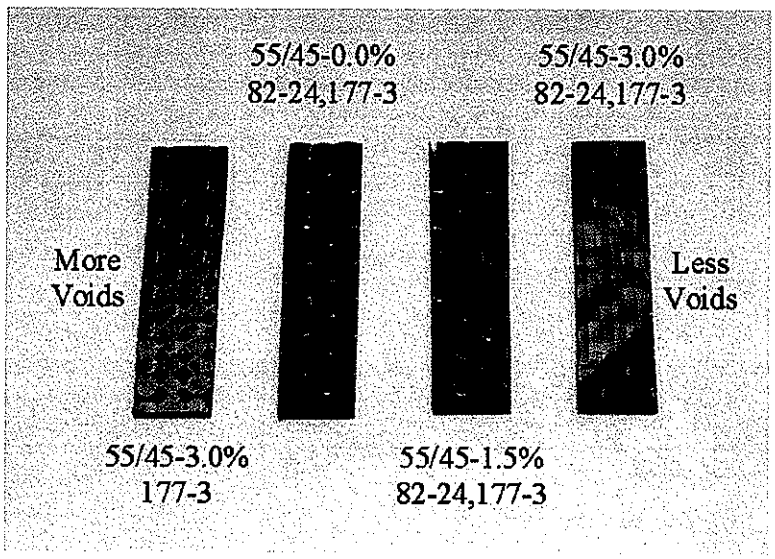

Figure B-1. DMA specimens showing varying levels of resin flow during cure.

The resin content is denoted by the blend, followed by the catalyst content in percent. The cure cycle is denoted by the cure temperature in degrees C, followed by a dash and the hours at that temperature; separate stages are shown following a comma. For example, 82-24,177-3 stands for 24 hours at 82 °C followed by 3 hours at 177 °C. The specimen on the left had the largest void content and the specimen on the right had the lowest void content. The least resin flow out during cure was seen when the highest level of catalyst was used with a 24-hour B-stage at 82 °C. A large amount of resin flow out of the reinforcement was experienced for the specimen on the left side, which was heated directly to 177 °C at 5 °C/min.

Curing the cyanate esters rapidly results in a large decrease in viscosity when the temperature is high and gelation has not occurred yet. Gel formation then occurs at a very low

viscosity followed by rapid viscosity increase. Curing at lower temperatures, or in this case, using a primary step at 82 °C, allows for gradual increases in viscosity up to the point of gelation, such that the viscosity never decreases to the level it would if a fast cure cycle is used. A larger amount of catalyst increases the gradual polymerization at the 82 °C step, allowing for fewer voids with increasing levels of catalyst. As a result, appropriate cure cycles should be used for repair applications in order to avoid defects in the composite overwrap repair.

B.4 Conclusions

The CTE of each composition with varying blend and catalyst ratios varied slightly such that samples with lower catalyst amounts and higher contents of the BECy monomer (EX-1510) gave lower CTEs. The CTE of the cyanate ester is lower than the CTE of epoxy, so there will be reduced CTEs in the woven carbon fiber composites as compared to those presented in Appendix A. This will allow for decreased CTE mismatch with the pipe for the 3K direction and between the neat resin and pipe, but will slightly increase CTE mismatch for the 12K direction (hoop direction of pipe) because the composite CTE is lower than that of the pipe.

In order to create void-free repairs, a B-stage should be conducted during installation. It should be noted that the B-stage does not affect the final T_g of the composite, but it will add complexity to the repair installation. If a faster cure cycle must be used, a rheological additive, such as fumed silica, should be used (see Chapter 7). The thixotropic behavior fumed silica/cyanate ester suspensions will allow for the resin to flow when applied to the fabric or pipe surface (high shear), but have a high "at-rest" viscosity that will reduce resin flow-out during cure (low shear). Additionally, the incorporation of fumed silica to the cyanate ester will improve other properties (see Chapters 5 and 6).

APPENDIX C: TEM OF FUMED SILICA/CYANATE ESTER NANOCOMPOSITES

This section presents TEM micrographs for the fumed silica/cyanate ester nanocomposites based on both the 12 and 40 nm particles. These images were taken by Tracey Pepper at the Microscopy and NanoImaging Facility (formerly Bessey Microscopy Facility) at Iowa State University. Microtome of the sample blocks were also performed there. The appendix is organized as follows: 1) Images of the fumed silica particles by themselves; these were dispersed in water, the solution placed on the grid, and the water allowed to evaporate. 2) At least two micrographs are presented for each composition. This page includes an example micrograph showing the wide distribution of particle sizes and agglomerates in the 40 nm silica.

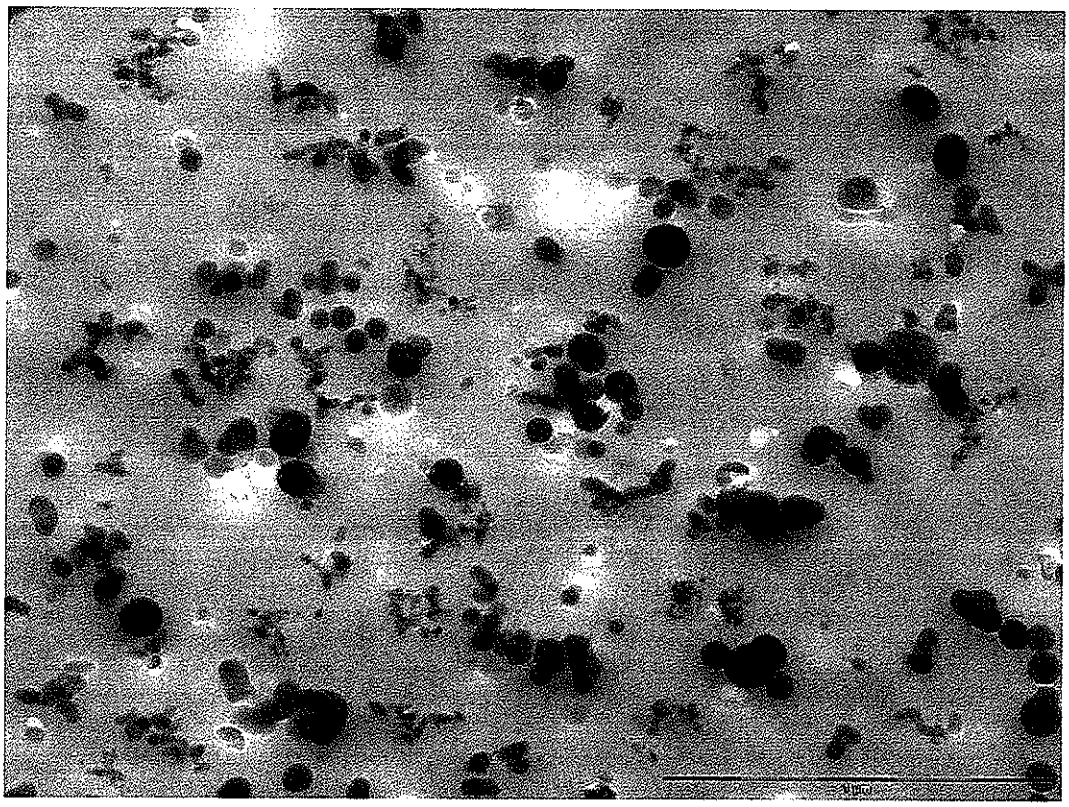

Figure C-1. 40 nm fumed silica (20 phr, 9.58 vol%) in BECy matrix. Scale bar is 1 μm. This example image shows the wide particle size distribution and the tendency for the smaller particles to form aggregates with a greater number of particles.

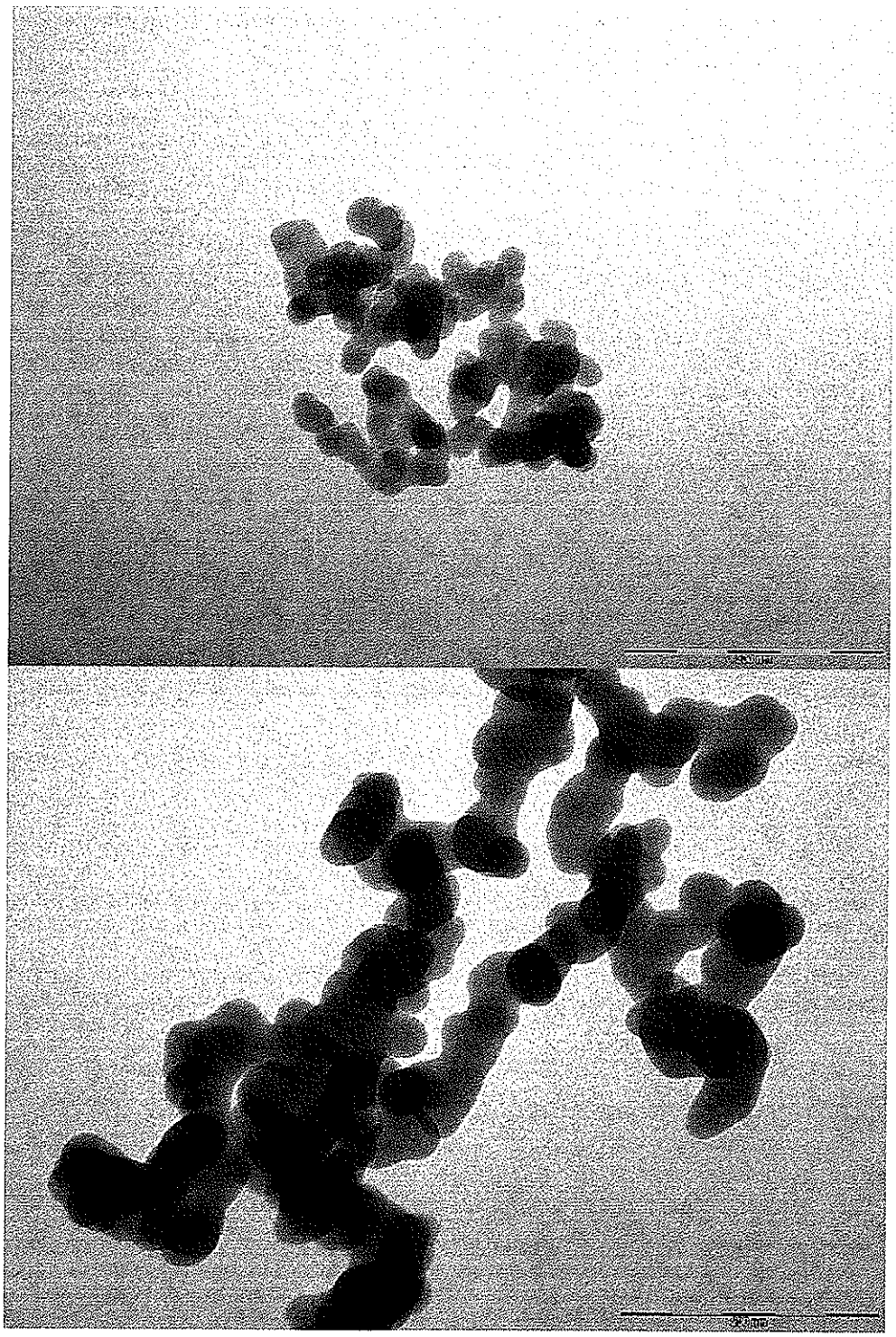

Figure C-2. 12 nm fumed silica aggregate on TEM grid without matrix (small aggregate, top, and large aggregate, bottom). Scale bar is 200 nm, both top and bottom.

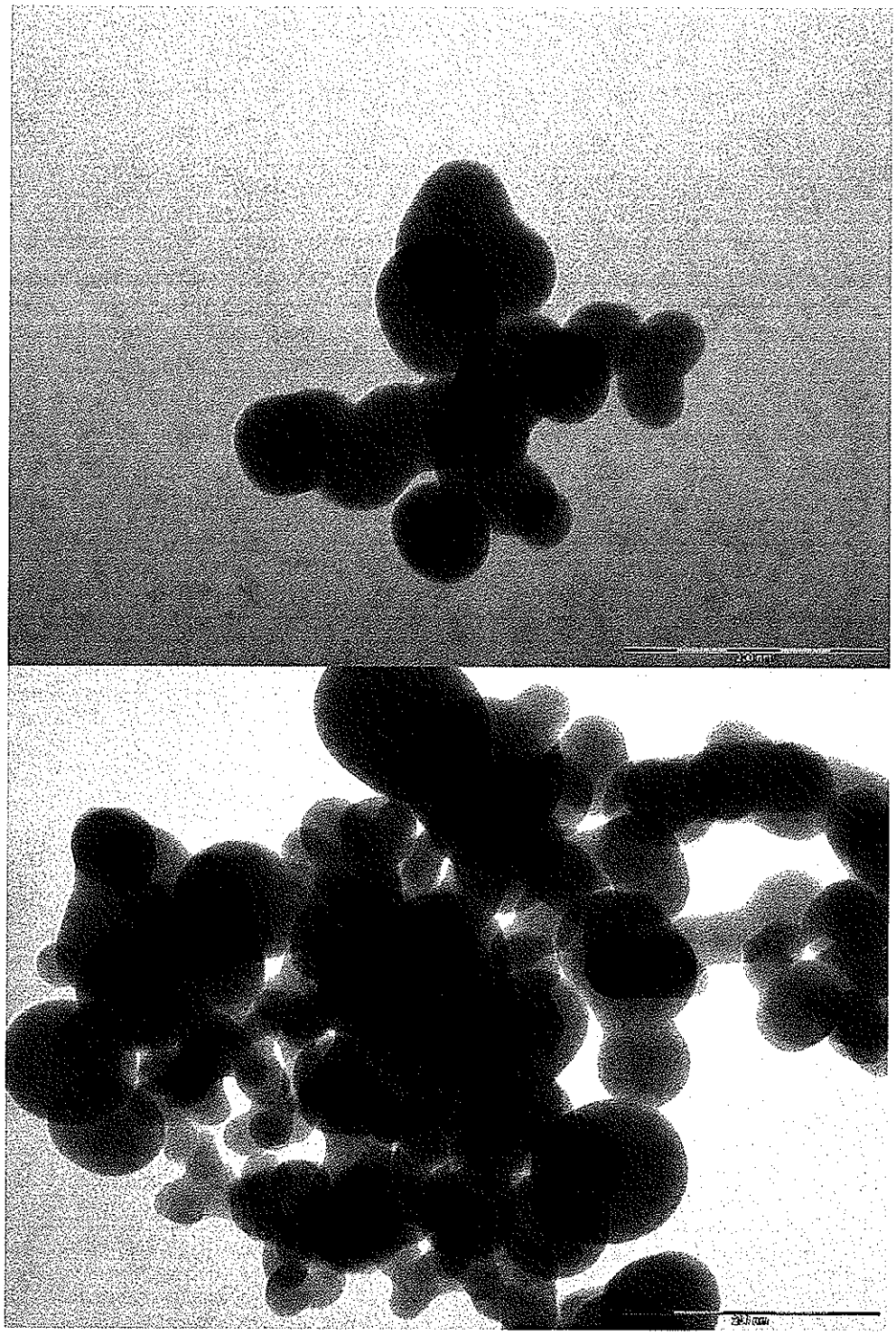

Figure C-3. 40 nm fumed silica aggregate on TEM grid without matrix (small aggregate, top, and large aggregate, bottom). Scale bar is 200 nm, both top and bottom.

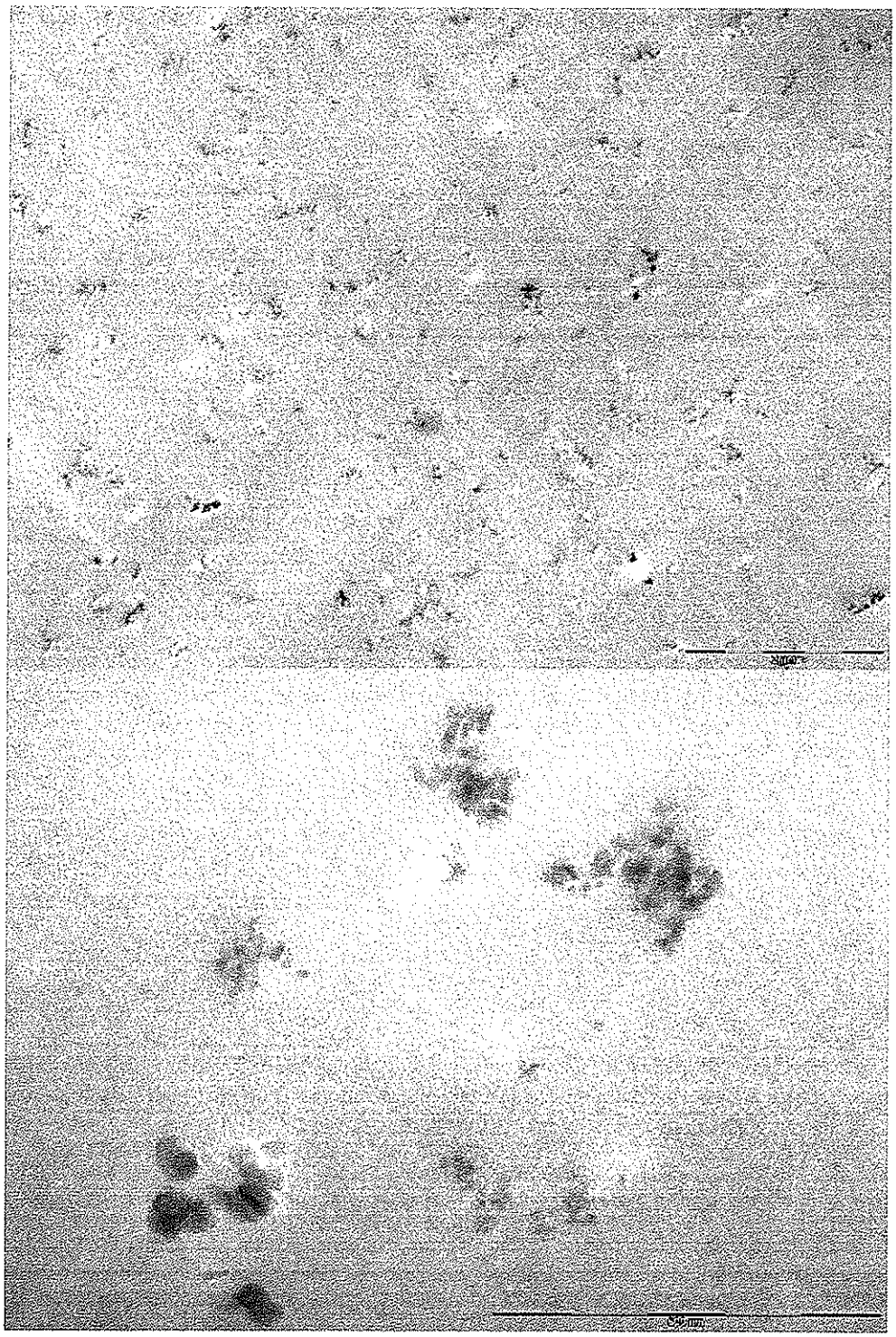

Figure C-4. 12 nm fumed silica (1 phr, 0.53 vol%) in BECy matrix.

Scale bar is 2 μm (top) and 500 nm (bottom).

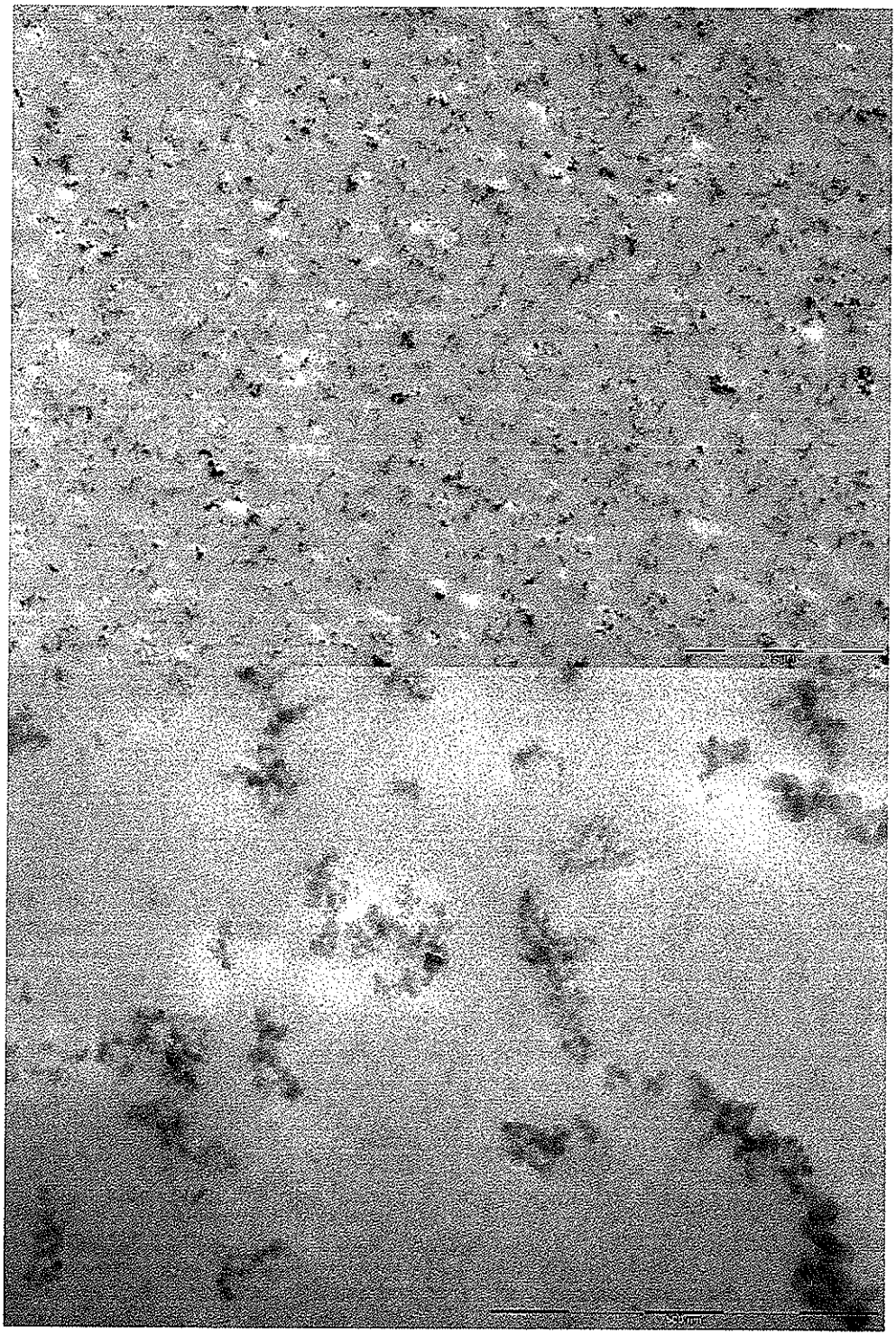

Figure C-5. 12 nm fumed silica (5 phr, 2.58 vol%) in BECy matrix.
Scale bar is 2 μm (top) and 500 nm (bottom).

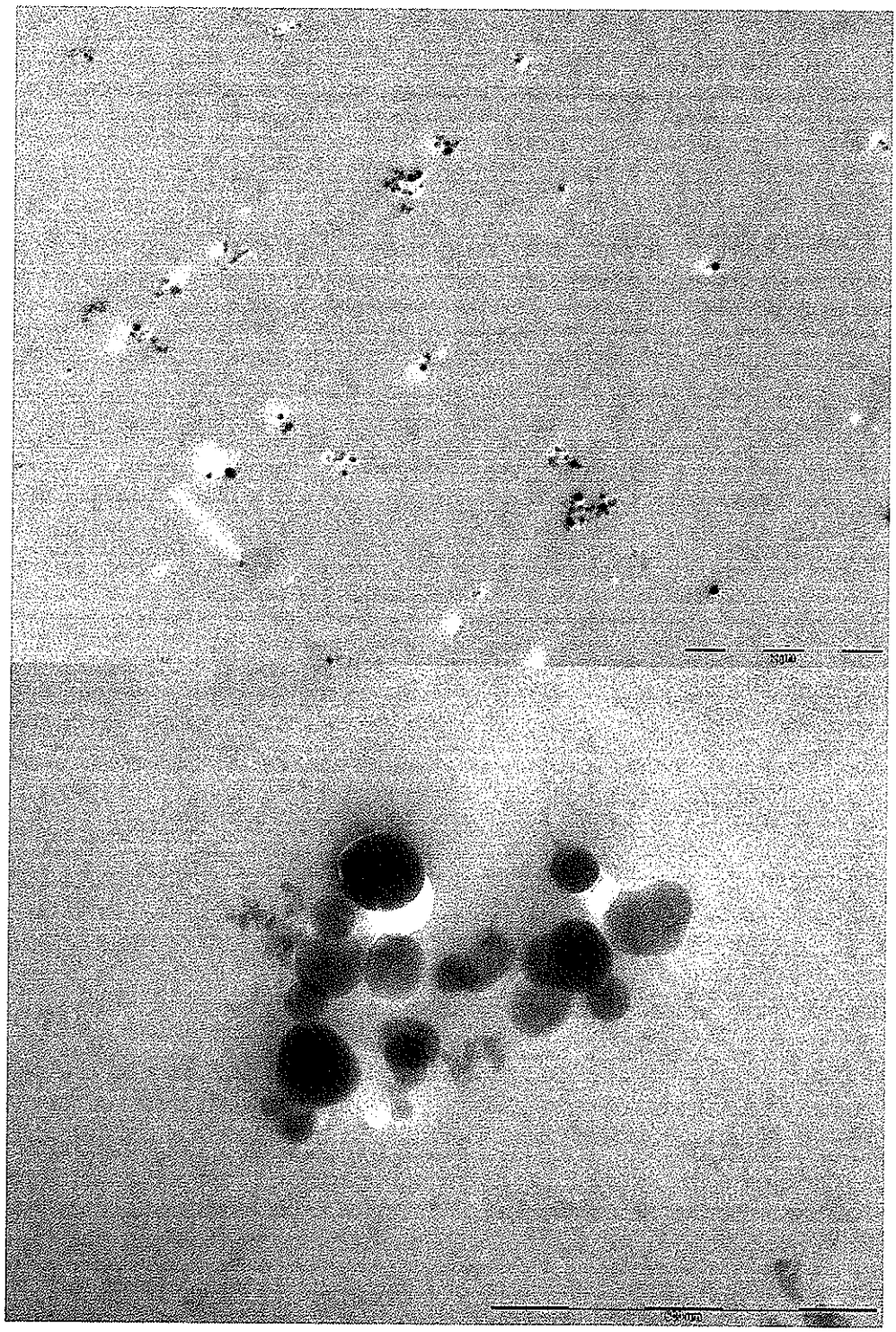

Figure C-6. 40 nm fumed silica (1 phr, 0.53 vol%) in BECy matrix.
Scale bar is 2 μm (top) and 500 nm (bottom).

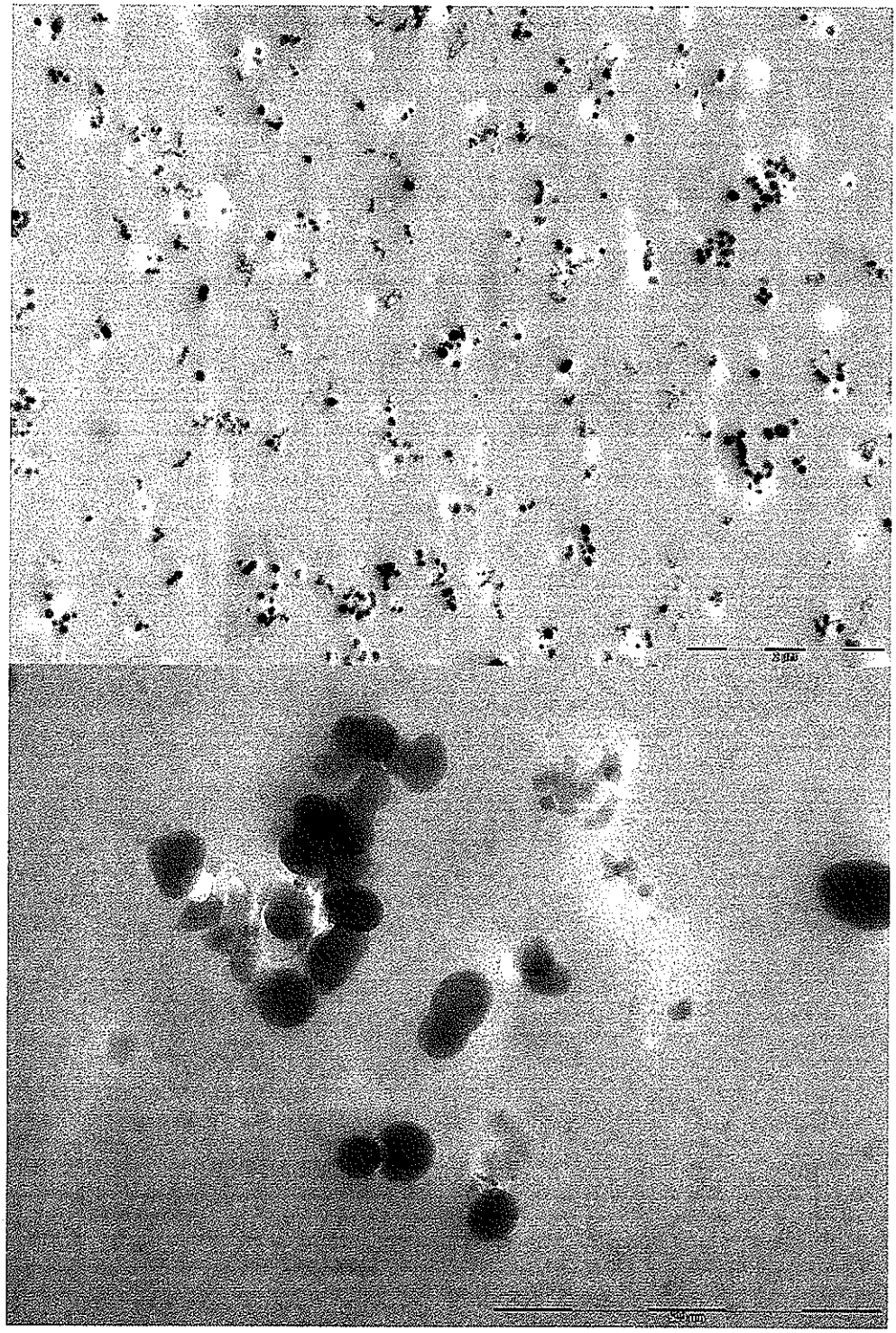

Figure C-7. 40 nm fumed silica (5 phr, 2.58 vol%) in BECy matrix.
Scale bar is 2 μm (top) and 500 nm (bottom).

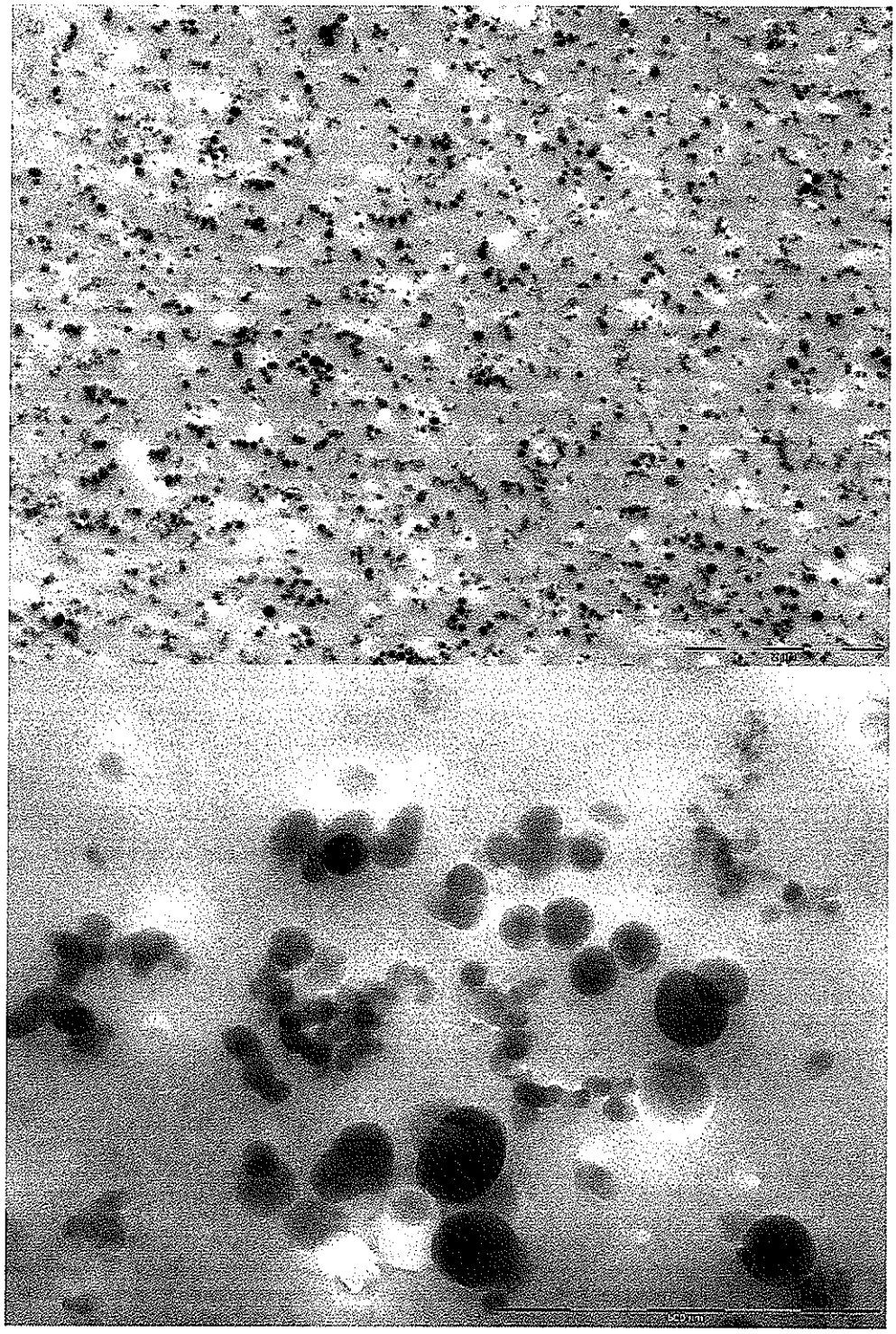

Figure C-8. 40 nm fumed silica (20 phr, 9.58 vol%) in BECy matrix.

Scale bar is 2 μm (top) and 500 nm (bottom).

APPENDIX D: THERMAL-MECHANICAL PROPERITES OF SHORT CARBON FIBER/FUMED SILICA/CYANATE ESTER COMPOSITE MATERIALS

D.1 Introduction

Settling and phase separation can be a problem in cyanate ester adhesives because of the high density of fillers and the low density of the BECy monomer. This problem is also complicated because the already low viscosity of the BECy during storage is even lower during the initial stages of cure before gelation has occurred. Fumed silica has been used in many systems to reduce phase separation and settling [1,2]. This work covers initial investigations into three-phase composite materials that use the fumed silica/cyanate ester nanocomposites of Chapters 5, 6, and 7 as the basis for paste adhesives with decreased thermal expansion and enhanced mechanical properties. In this appendix, short carbon fibers are investigated with fumed silica/cyanate ester, and the thermal-mechanical properties are characterized for a loading of 20 vol%.

D.2 Short carbon fiber composites

Short carbon fibers (SCFs) are a scrap material from the production of continuous fiber reinforcements. This 7 μm diameter waste product can be milled to a variety of lengths for various applications. Not only are SCFs a cheap and widely available commodity, but CTE reduction with SCFs is well documented. Studies of SCFs with epoxies are common, but SCFs have not been used with cyanate esters. Short carbon fibers have long been used as a modifier for thermoplastics, and there has been extensive use of short carbon fibers in epoxies [3-5]. For the reduction of composite CTE, short carbon fibers in epoxy reduced the CTE of the composite from 60 ppm/°C to less than 10 ppm/°C for loadings of up to 45% by volume [5].

D.3 Experimental

D.3.1 Materials

The BECy monomer from Bryte Technologies (Morgan Hill, CA), EX-1510, was used as the matrix material. The supplied catalyst from Bryte Technologies was used in all samples at a 3% loading by weight. Polyacrylonitrile (PAN)-based milled carbon fiber (Fortafil 341, CAS No.: 07440-44-0) was supplied by Toho Carbon Fibers, Inc., Rockwood, TN (a subsidiary of Toho Tenax Co., Ltd.). This product is a loose, black, powdery material comprised of unsized 7 μm diameter fibers with lengths ranging from 75 to 150 μm. Hydrophilic fumed silica was supplied by Degussa (Frankfurt, Germany) under the trade name of AEROSIL® 200 (CAS No.: 112945-52-5, synthetic amorphous, pyrogenic silica, purity ≥ 99.8%). AEROSIL® 200 has an average primary particle diameter of 12 nm and a specific surface area of 200 m^2/g [6].

D.3.2 Specimen manufacturing

BECy monomer/fumed silica suspensions of 5 phr (parts per hundred resin) were prepared using the procedure outlined in Section 7.3.2, except sonication of the suspensions was eliminated. After catalyst addition, the short carbon fiber was added while mixing with a high shear blade (25 mm diameter) at 2000 rpm for 10 minutes. Carbon fiber was then added in a stepwise fashion until the desired composition, 20 vol%, was reached (based on the total volume with fumed silica and a SCF density of 1.74 g/cm^3). The suspensions were poured into high-temperature silicone rubber molds (27 × 48 × 8 mm^3) and degassed at 60 °C for 1 hour under vacuum at 23.4mmHg, and then placed in a convection oven (preheated to 60 °C) for the final curing process (heat to 180 °C at 1 °C/min, hold for 2 hours, heat to 250 °C at 1 °C/min, hold for 2 hours and cool to ambient at 5 °C/min). Samples were machined from the solid block of material using a diamond blade saw (TechCut 5™ Precision Sectioning Machine with Diamond

Wafering Blade, Low-Concentration Diamond Metal Bonded, 6" × .020" × ½", Allied High Tech Products, Inc.). Specimens for thermomechanical analysis (TMA) were machined to 3 × 3 × 6 mm^3, such that top and bottom faces of each specimen were parallel to within 15 μm. Specimens for dynamic mechanical analysis (DMA) were machined to 23 × 6 × 1.6 mm^3, such that the thickness of each specimen varied by less than 15 μm over its length. Neat BECy control samples without fumed silica were prepared in the same manner as above. All samples were dried at 120 °C under vacuum for 6 hours and kept in a dry environment prior to testing.

Initial prepolymer samples made using the as-received milled carbon fiber product were very "clumpy." This was attributed to agglomeration of fibers into small "balls," which occurs during manufacturing and storage. The described mixing strategies were not sufficient to break up these clumps of fibers. In order to solve this problem, the as-received product was forced through a No. 100 (150 μm) Cole-Parmer U.S.A. Standard Test Sieve prior to addition to the prepolymer. This change nearly eliminated the inhomogeneity in the prepolymer and polymer samples.

D.3.3 Experimental procedure

DMA samples were tested using a TA Instruments (New Castle, Delaware, USA) DMA (Dynamic Mechanical Analyzer) Q800 with LN_2 GCA (Gas Cooling Accessory) from 30 °C to 330 °C at a heating rate of 3 °C/min. A constant amplitude of 20 μm at 1 Hz was applied throughout the test, with a static load tracking at 150% of the dynamic force. A low-friction three-point bending fixture with a length of 20 mm was utilized for each test. Thermomechanical testing was completed using a TA Instruments (New Castle, Delaware, USA) TMA (Thermomechanical Analyzer) Q400. Samples were tested in the longest dimension (6 mm height) under a static force of 50 mN through two heating and cooling cycles from 30 °C to 300 °C at a heating rate of 5 °C/min under helium purge at 50 mL/min.

D.4 Results and discussion

The results from DMA testing are shown in Figure D-1 for a loading of 20 vol% of short carbon fiber combined with fumed silica/BECy at a loading of 5 phr.

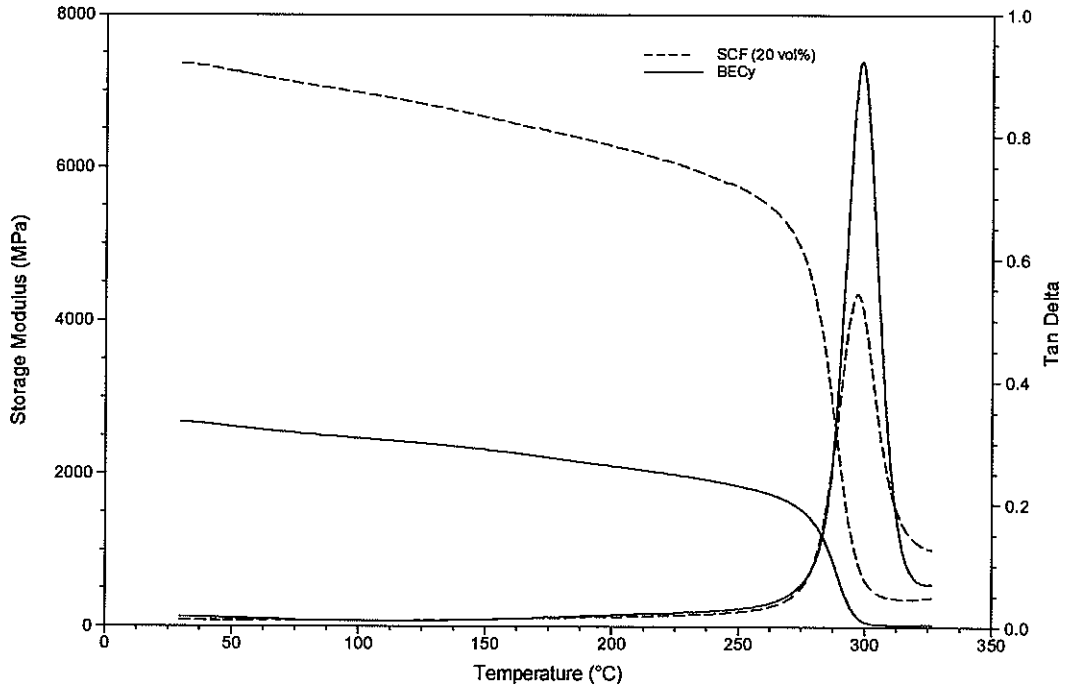

Figure D-1. DMA curves for 20 vol% SCF in 100/5 (BECy/12nm).

The addition of short carbon fiber addition at 20 vol% raises the modulus from 2.70 GPa for BECy to 7.36 GPa at 30 °C (the modulus of the 5 phr 12 nm fumed silica nanocomposite is 3.04 GPa). This represents an increase in modulus of 173%. The increase in modulus is due to the high modulus graphite fibers (110 GPa), which have a significant aspect ratio (approx. 20). Additionally, there is no decrease in T_g for this composite. The short carbon fiber is unsized, so the surface would be similar to fumed silica in that it would have hydroxyl groups for covalent bonding with the cyanate ester. There is also a large decrease in the maximum tan delta peak (41%).

The CTE of the composite is reduced significantly as well. TMA curves for the BECy and SCF composite are shown in Figure D-2.

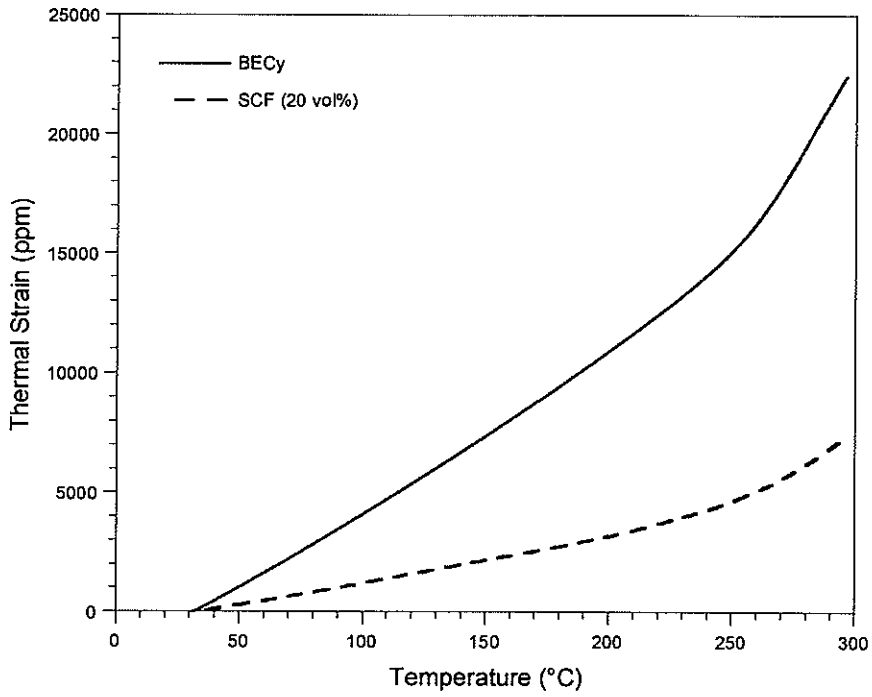

Figure D-2. TMA curves for 20 vol% SCF in 100/5 (BECy/12nm), showing sample variability.

The CTE of the SCF sample was reduced from 63.5 ppm/°C to 19.1 ppm/°C. This represents a decrease of 70%. The test on this sample was repeated several times and all results were within 2 ppm/°C. If model predictions are made using 60.4 ppm/°C as the matrix CTE (CTE of 5 phr 12 nm fumed silica/BECy nanocomposite), Turner's model would predict 9.4 ppm/°C, Schapery's lower limit, 15.0 ppm/°C, and Schapery's upper limit, 43.2 ppm/°C. Thus, the point falls within Schapery's limits, lying closer to the lower bound. This agrees with the physical situation due to the fact that the large aspect ratio of the fibers will allow for more strain transfer than in the case of spherical particles. Thus, this demonstrates the feasibility of making three-phase composites with the fumed silica/cyanate ester nanocomposites that have enhanced thermal and mechanical properties.

D.5 Conclusions

Three-phase composites based on fumed silica/cyanate ester nanocomposites and short carbon fiber were demonstrated for feasibility. Without fumed silica, complete phase separation was observed, but with fumed silica, useable composites were manufactured. The composites exhibited significant enhancements in modulus and significant reduction in CTE, without sacrificing thermal properties. This procedure can be used to create other three-phase composites based on BECy, using large-sized particles, fiber, or plates. This method may be especially useful for fillers with high specific gravities.

D.6 References

[1] Wen, J., Bryant, D., Fumed Silica Controls Rheology of Adhesives and Sealants, reprinted from August 1999 issue of *Adhesives and Sealants Industry* by Cabot Corporation, Billerica, MA, USA.

[2] Product Technical Data, CAB-O-SIL® M-5, Cabot Corporation, Billerica, MA, USA.

[3] Kaynak, C., Orgun, O., and Tincer, T., Matrix and interface modification of short carbon fiber-reinforced epoxy, *Polymer Testing*, v 24, n 4, June, 2005, p 455-462.

[4] Gong, X., Dynamic mechanical behavior of random-in-plane short fiber-reinforced epoxy resin composites, *Polymers for Advanced Technologies*, v 7, n 2, Feb, 1996, p 141-145.

[5] Jeong, M. Y. and Lee, D. G., Development of the ferrule for optical fiber connectors with short fiber polymer composites, *Journal of Materials Processing Technology*, v 63, n 1-3, Jan, 1997, p 375-378.

[6] AEROSIL® Product Technical Information, Degussa, Frankfurt, Germany, August 2006.